

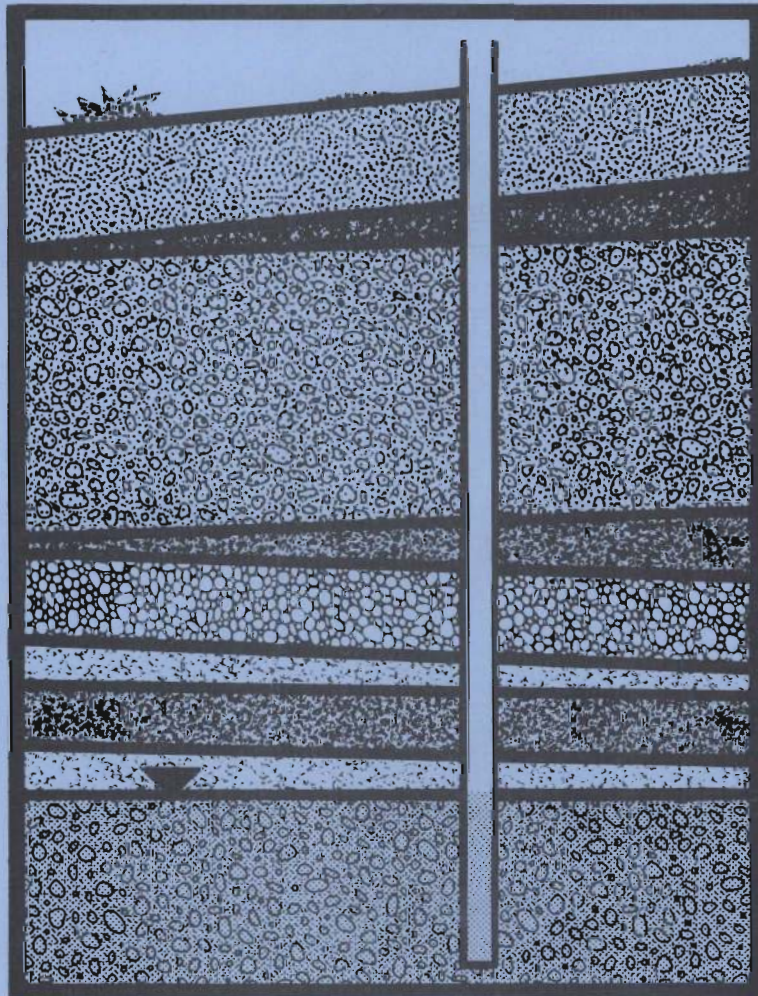
2F

PNL-2949

UC-70

13-14

Geohydrology and Ground-Water Quality Beneath the 300 Area, Hanford Site, Washington



June 1979

Prepared for the U.S. Department of Energy
under Contract EY-76-C-06-1830

Pacific Northwest Laboratory
Operated for the U.S. Department of Energy
by Battelle Memorial Institute



PNL-2949

NOTICE

This report was prepared as an account of work sponsored by the United States Government. Neither the United States nor the Department of Energy, nor any of their employees, nor any of their contractors, subcontractors, or their employees, makes any warranty, express or implied, or assumes any legal liability or responsibility for the accuracy, completeness or usefulness of any information, apparatus, product or process disclosed, or represents that its use would not infringe privately owned rights.

The views, opinions and conclusions contained in this report are those of the contractor and do not necessarily represent those of the United States Government or the United States Department of Energy.

PACIFIC NORTHWEST LABORATORY
operated by
BATTELLE
for the
UNITED STATES DEPARTMENT OF ENERGY
Under Contract EY-76-C-06-1830

Printed in the United States of America
Available from
National Technical Information Service
United States Department of Commerce
5285 Port Royal Road
Springfield, Virginia 22151

Price: Printed Copy \$ ____*; Microfiche \$3.00

*Pages	NTIS Selling Price
001-025	\$4.00
026-050	\$4.50
051-075	\$5.25
076-100	\$6.00
101-125	\$6.50
126-150	\$7.25
151-175	\$8.00
176-200	\$9.00
201-225	\$9.25
226-250	\$9.50
251-275	\$10.75
276-300	\$11.00



Pacific Northwest Laboratories

P. O. Box 999

Richland, Washington 99352

Telephone (509) 375-3678

Telex ~~926345~~ 15-2874

October 31, 1979

Recipients of PNL-2949

Dear Recipients:

RE: Geohydrology and Ground-Water Quality Beneath the 300 Area,
Hanford Site, Washington, Pacific Northwest Laboratory,
Richland, WA, June, 1979

Please make the following changes in your copy of the subject report:

Page 1-2, line 3: Change "Phase 1" to "the investigative phase."

Page 2-1, line 8: Change "Pool was" to "Pool (the Columbia
River at Richland and the 300 Area) was . ."

Page 4-2, upper cross-section: Change RINGOLD INFORMATION to
RINGOLD FORMATION

Page 6-4, line 2: Change $q \hat{n} < 0$ to $q \bullet \hat{n} < 0$

Page 6-6, equation 6.9: Change the first integral sign $\int \Gamma_{ij}$
to $\oint \Gamma_{ij}$

Page 6-8, line 13: Change $= q_{ij}$ to $= q_{ij}n$

Page 7-4, below the left-hand figure, insert an '(a)'. Below the
right-hand figure, insert a '(b)'.

Page 7-8, Table 7.1, last line: Change left-left to lower-left.

Page 8-2, Equation 8.1: Change $\frac{\partial p}{\partial t} k$ to $\frac{\partial \rho k}{\partial t}$

Page 8-6, line 12: Change $-Nm + N$ to $-N < m < +N$

Page 8-7, Equation 8.8: Change $p(m,N) (\Delta x/2\ell)$ to $p(m,N) \bullet (\Delta x/2\ell)$

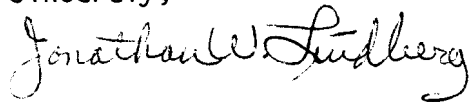
Page 8-11, Section 8.1.9, line 11: Change $\frac{D}{H} \nabla H \nabla \rho^k$ to $\frac{D}{H} \nabla H \bullet \nabla \rho^k$

Replace Table 9.1 with the attached Table 9.1.

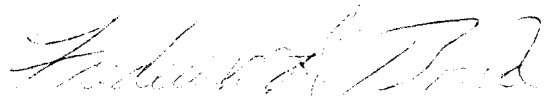
Replace Table 9.2 with the attached Table 9.2.

Add the additional references which are attached.

Sincerely,



J. W. Lindberg
Scientist
Environmental Assessment Section
Water and Land Resources Department



F. W. Bond
Research Engineer
Hydrologic Systems Section
Water and Land Resources Department

JWL/FWB:mj

Attachments:3

PNL-2949
UC-70

3 3679 00053 1683

GEOHYDROLOGY AND GROUND-WATER QUALITY
BENEATH THE 300 AREA, HANFORD SITE,
WASHINGTON

J. W. Lindberg
F. W. Bond

June 1979

Prepared for the U.S. Department of Energy
Under Contract EY-76-C-06-1830

Pacific Northwest Laboratory
Richland, Washington 99352

CONTENTS

FIGURES	vi
TABLES	ix
1.0 INTRODUCTION	1-1
2.0 SUMMARY AND CONCLUSIONS	2-1
3.0 DATA COLLECTION	3-1
3.1 COMPILATION OF EXISTING DATA	3-1
3.2 300 AREA PROCESSES IMPACTING GROUND-WATER SYSTEM	3-1
3.3 COLLECTION OF NEW 300 AREA DATA THROUGH THE 1977 CALENDAR YEAR	3-1
4.0 RESULTS AND INTREPRETATIONS OF DATA	4-1
4.1 GEOLOGIC SETTING	4-1
4.1.1 Stratigraphy	4-1
4.1.1.1 Columbia River Basalt Group.	4-1
4.1.1.2 The Ringold Formation	4-1
4.1.1.3 Glaciofluvial Deposits	4-5
4.1.1.4 Eolian Sands and Silts	4-8
4.1.2 Structure	4-8
4.2 HYDROLOGIC SETTING	4-9
4.3 PREVIOUS 300 AREA PROCESSES	4-12
4.4 UNPLANNED RELEASES	4-18
4.5 300 AREA GROUND-WATER SYSTEM DURING STUDY	4-19
5.0 QUALITY ASSURANCE OF GROUND-WATER QUALITY ANALYSES	5-1
6.0 THE VARIABLE THICKNESS TRANSIENT (VTT) GROUND-WATER FLOW MODEL	6-1
6.1 THE BOUSSINESQ EQUATION	6-2
6.1.1 Boundary and Initial Conditions for the Boussinesq Equation	6-3
6.1.2 Boussinesq Equation Assumptions	6-5

6.2	NUMERICAL FORMULATION OF THE SYSTEM EQUATIONS	6-5
6.3	CALCULATION PROCEDURE	6-10
6.4	DATA REQUIREMENTS	6-10
7.0	DEVELOPMENT OF THE 300 AREA VTT GROUND-WATER MODEL	7-1
7.1	MODELING CONDITIONS	7-1
	7.1.1 Boundary Conditions and Finite Difference Grid	7-1
	7.1.2 Initial Conditions	7-3
7.2	DATA INPUT TO THE MODEL	7-5
	7.2.1 Recharge and Discharge	7-5
	7.2.2 Transmissivity	7-9
	7.2.3 Aquifer Top	7-9
	7.2.4 Aquifer Bottom	7-10
	7.2.5 Storage Coefficient	7-10
7.3	MODEL CALIBRATION AND VERIFICATION	7-10
7.4	VTT MODEL RESULTS	7-13
7.5	MODEL APPLICATION	7-20
8.0	THE MULTICOMPONENT MASS TRANSFER (MMT) MODEL	8-1
8.1	THEORETICAL DEVELOPMENT OF THE MODEL - THE DIRECT SIMULATION APPROACH	8-1
	8.1.1 Numerical Implimentation Algorithm	8-2
	8.1.2 Particles of Mass	8-3
	8.1.3 Advective Transport	8-4
	8.1.4 Dispersive Transport	8-5
	8.1.5 Total Particle Movement	8-9
	8.1.6 Concentration Distribution	8-10
	8.1.7 Source/Sink Terms	8-10
	8.1.8 Boundary Conditions	8-11
	8.1.9 Assumptions for Vertically Averaged Version	8-11
8.2	DATA REQUIREMENTS	8-11
9.0	DEVELOPMENT OF MMT MODEL FOR THE 300 AREA	9-1
9.1	MMT DATA REQUIREMENTS	9-1

9.1.1	Boundary and Flow Data	9-1
9.1.2	Important Contaminants	9-1
9.1.3	Initial Concentrations and Sources	9-1
9.1.4	Contaminant Related Data	9-2
9.2	CALIBRATION AND VALIDATION	9-2
9.3	MMT TEST CASE	9-2
9.3.1	MMT Transport Simulation Results	9-3
10.0	REFERENCES	10-1
APPENDIX:	ELEVATION-VERSUS-TIME HYDROGRAPH PLOTS FOR THE 29	
	OBSERVATION WELLS IN THE 300 AREA	A-1

FIGURES

1.1	Hanford Site Location Map	1-2
3.1	300 Area Well Location Map	3-2
4.1	Geologic Cross Sections of 300 Area	4-2
4.2	Location of Geologic Cross Sections shown in Figure 4.1	4-3
4.3	Hanford Site Water-Table Map	4-11
4.4	Location of 300 Area Wells, Burial Ground, Buildings, Ponds, and Trenches	4-13
4.5	Concentration of Uranium in the Unconfined Aquifer Under the 300 Area in January 1977	4-15
4.6	Concentration of Alpha Emitters in the Unconfined Aquifer Under the 300 Area in January 1977	4-16
4.7	Concentration of Beta Emitters in the Unconfined Aquifer Under the 300 Area in January 1977	4-17
4.8	300 Area Water-Table Map, July 1, 1977	4-20
4.9	Temperatures in the Unconfined Aquifer Under the 300 Area, February 16, 1977	4-21
4.10	Temperature in the Unconfined Aquifer Under the 300 Area, September 1, 1977	4-22
4.11	300 Area Water-Table Map, May 20, 1977	4-24
4.12	300 Area Water-Table Map, May 27, 1977	4-25
4.13	300 Area Water-Table Map, June 3, 1977	4-26
4.14	300 Area Water-Table Map, June 10, 1977	4-27
4.15	Temperatures in the Unconfined Aquifer Under the 300 Area, June 3, 1977	4-28
4.16	300 Area Water-Table Map, February 16, 1977	4-30
4.17	300 Area Water-Table Map, July 15, 1977	4-31

4.18	Calcium Concentration in the Unconfined Aquifer Under the 300 Area During May 1977	4-32
4.19	Magnesium Concentration in the Unconfined Aquifer Under the 300 Area in January 1977	4-33
4.20	Sodium Concentration in the Unconfined Aquifer Under the 300 Area in March 1977	4-34
4.21	Bicarbonate Concentration in the Unconfined Aquifer Under the 300 Area in January 1977	4-35
4.22	Sulfate Concentration in the Unconfined Aquifer Under the 300 Area in January 1977	4-36
4.23	Nitrate Concentration in the Unconfined Aquifer Under the 300 Area in January 1977	4-37
4.24	Fluoride Concentration in the Unconfined Aquifer Under the 300 Area in February 1977	4-38
4.25	Chloride Concentration in the Unconfined Aquifer Under the 300 Area in January 1977	4-39
4.26	Temperatures in the Unconfined Aquifer Under the 300 Area, August 4, 1977	4-41
4.27	Temperatures in the Unconfined Aquifer at Wells 3-2, 3-3 and 8-2, and the Columbia River near Richland, Washington, during CY1977	4-42
6.1	Illustration of an Unconfined Aquifer with Boundary Conditions	6-4
6.2	The Finite Difference Grid with the Nodal Numbering System	6-6
6.3	Schematic Showing Shapes and Rotation of Available Boundary Condition Types	6-9
7.1	VTT Boundary Conditions (Calculational Types) for the Hanford Project Model Region	7-2
7.2	VTT Boundary Conditions for the 300 Area Model Region (a) Direct Interpolation from Large to Small Region, (b) Adjusted Columbia River Boundary	7-4

7.3	Hanford Site (Large Region) Initial Potential Surface.	7-6
7.4	300 Area (Small Region) Initial Potential Surface.	7-7
7.5	Hanford Unconfined Aquifer Bottom Contours	7-11
7.6	Transmissivity (gpd/ft) Distribution	7-14
7.7	300 Area May 20, 1977 Model-Predicted Potential Surface	7-16
7.8	300 Area May 27, 1977 Model-Predicted Potential Surface	7-17
7.9	300 Area June 3, 1977 Model-Predicted Potential Surface	7-18
7.10	300 Area June 10, 1977 Model-Predicted Potential Surface	7-19
7.11	300 Area Pathline Originating Near the 325 Building	7-24
9.1	SB-125 Concentration Versus Time Plot	9-7
9.2	PU-238 Concentration Versus Time Plot	9-8
9.3	PU-239 Concentration Versus Time Plot	9-9
9.4	SR-90 Concentration Versus Time Plot	9-10
9.5	AM-241 Concentration Versus Time Plot	9-11

TABLES

5.1	Comparison of Duplicate Water Quality Analyses by United States Testing Company	5-2
7.1	Recharge and Discharge Locations	7-8
7.2	CY 1977 Waste Water Discharge	7-8
7.3	CY 1977 Discharge from Ground-water in the 300 Area	7-9
7.4	Transmissivity Data as Analyzed from Drawdown and Recovery Measurements	7-10
7.5	Statistical Analysis of the Hydrograph Results	7-15
7.6	Streamline Data (for Streamlines Shown in Figure 7.8).	7-23
9.1	Transport Model Input Parameters	9-4
9.2	Summary of Transport Model Results	9-5

1.0 INTRODUCTION

Pacific Northwest Laboratory (PNL) has been conducting geohydrologic investigations on the Hanford Site since 1965 to establish and evaluate management alternatives for below-ground storage of waste material and for monitoring ground-water contamination. Major programs were developed to monitor Hanford ground water and numerically model ground-water flow and transport of ground-water contaminants.

Three subregions at the Hanford Site are of particular interest with regard to waste management: the 100, 200, and 300 Areas (Figure 1.1). The Hanford Ground-Water Monitoring Program has been focusing most of its interest on the large contaminant plumes emanating from the 200 Areas. However, routine analyses have shown that ground water beneath the 300 Area remains contaminated (Raymond and others, 1976, P. 28, 36). Therefore, a more extensive detailed hydrologic study was needed for the 300 Area.

In September 1976 PNL began an extensive ground-water monitoring, analysis and modeling program in the 300 Area. The major objective was to gain a thorough understanding of the 300 Area ground-water flow and transport system, and the location, extent, and type of of ground-water contamination. The 2-year study, sponsored by the Department of Energy (DOE), was conducted in two phases: first, an investigative phase consisting of extensive monitoring, data collection and analysis; and second, a hydrologic flow and transport modeling phase.

The investigative phase was conducted during calendar year 1977 (CY1977). The objectives of this phase were to determine the location and concentration of ground-water contaminants, to assess and evaluate the ground-water flow system, and to assist in the collection of data for the modeling phase. To accomplish these objectives, data were collected by three tasks: 1) compiling existing 300 Area data, 2) gathering information on present processes in the 300 Area which impact the ground-water system, and 3) systematic gathering of new hydrologic data from the study area through CY1977.

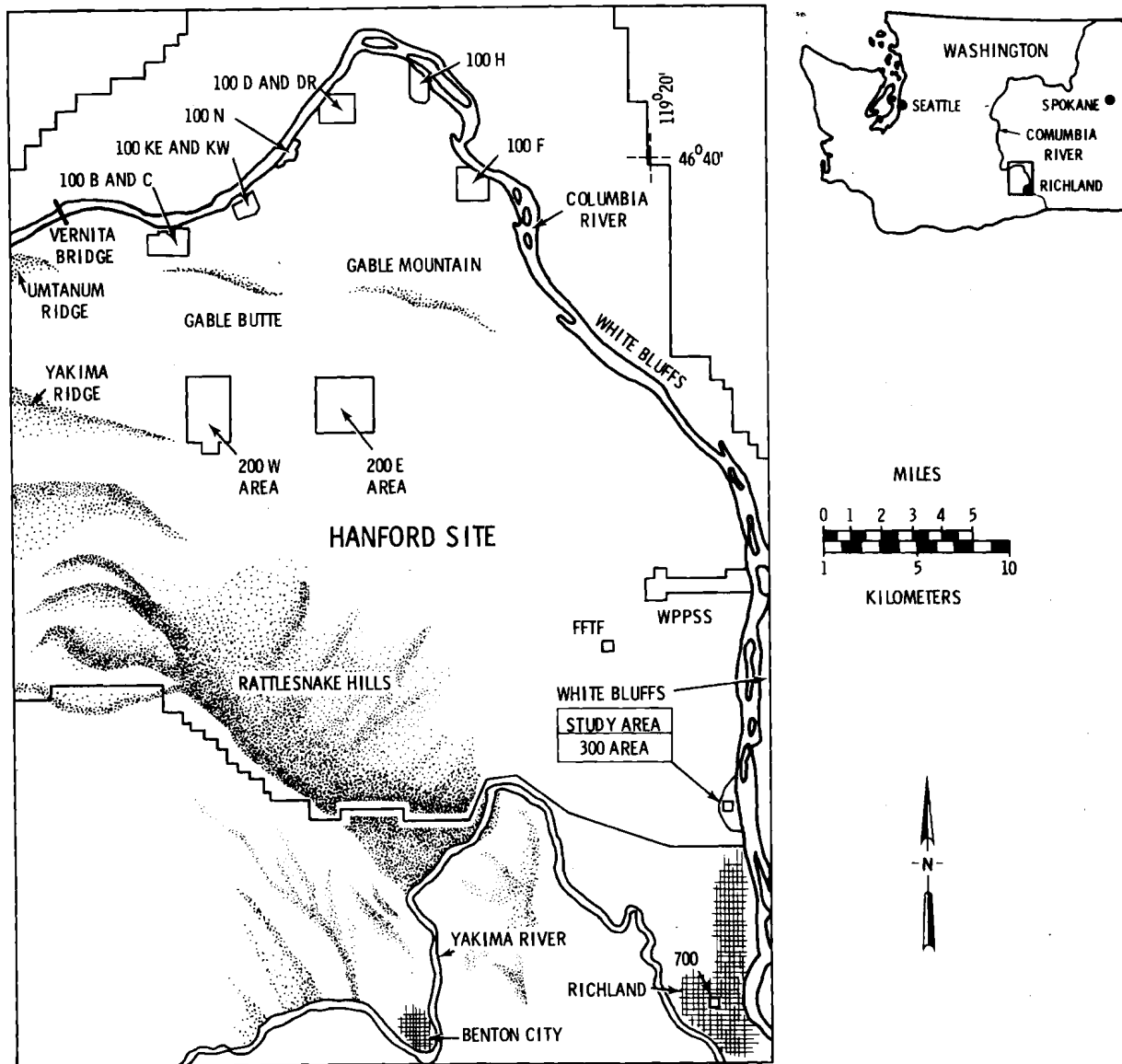


FIGURE 1.1. Hanford Site Location Map

The modeling phase was conducted during fiscal year 1978 (FY1978). The objective of this phase was to utilize the detailed data gathered in Phase I to calibrate hydrologic flow and transport models of the study area. A hydrologic flow model was developed to define ground-water flow paths and travel times (i.e., define the velocity field). The transport model utilized the output from the hydrologic flow model and contaminant source terms to describe the movement of the contaminants through the flow system. Calibrated and validated, the models may be used as a tool to assist in waste disposal management decisions.

2.0 SUMMARY AND CONCLUSIONS

Ground water enters the 300 Area from the northwest, west, and southwest. However, throughout most of the 300 Area, the flow is to the east and southeast. Ground water flows to the northeast only in the southern portion of the 300 Area.

Natural influences, as well as human-related influences, were found to affect the 300 Area ground-water system. Variations in level of the Columbia River affected the ground-water system by altering the level and shape of the 300 Area water table. When the level of McNary Pool was raised 4 ft (1.2 m) during May 1977, a reversed gradient was formed along the bank of the Columbia River. The river was elevated for a sufficient duration to give the appearance of a temporary water-table depression in the central portion of the 300 Area.

Large quantities of process waste water, when warmed during summer months by solar radiation or cooled during winter months by ambient air temperature, influenced the temperature of the ground water. During the summer months the ground water near the Process Water Trenches was warmed as much as 16°F (9°C) above the regional ground-water temperature. During the winter the ground water was cooled more than 4°F (2°C).

Leaking pipes and the intentional discharge of waste water (or withdrawal of ground water) affected the ground-water system in the 300 Area. As wastewater was discharged to the ground at the trenches, ponds, and the ground surface near the 331 Building, temporary water-table mounds or lobes were formed. Withdrawal of water from a well at the 309 Building may have caused a temporary water-table depression. Leaking pipes caused contamination of the ground water near the 340 Building. Near the 325 Building, the apparent dilution of ground-water contaminants that were in the ground already, a ground-water mound or lobe, and ground-water temperature variation, may indicate that pipes are leaking which carry Columbia River water.

Water quality tests of Hanford ground water in and adjacent to the 300 Area showed that in the area of the Process Water Trenches and

Sanitary Leaching Trenches, calcium, magnesium, sodium, bicarbonate, and sulfate ions are more dilute, and nitrate and chloride ions are more concentrated than in surrounding areas. Fluoride, uranium, and beta emitters are more concentrated in ground water along the bank of the Columbia River in the central and southern portions of the 300 Area and near the 340 Building.

Test wells in the 300 Area and the routine ground-water sampling schedule of the Ground-Water Monitoring Program are adequate to point out contamination from routine waste discharges. In addition, the well network is adequate to detect most accidental waste releases and leakage from waste discharge lines.

The Variable Thickness Transient (VTT) Model of ground-water flow in the unconfined aquifer underlying the 300 Area has been set up, calibrated, and verified. The capability of the model to accurately simulate horizontal flow with time varying boundary conditions and a heterogeneous distribution of aquifer properties has been demonstrated. The model, in its present state, may now be used to predict water flow paths and travel times beneath the 300 Area for any given period of time.

The Multicomponent Mass Transfer (MMT) Model of distribution of contaminants in the saturated regime under the 300 Area has been set up, calibrated, and tested. The simulation of point source accidental spills of contaminants is a likely subject for model demonstration. The model, in its present form, has been used to predict contaminant movement in the ground water beneath the 300 Area.

3.0 DATA COLLECTION

3.1 COMPILATION OF EXISTING DATA

A review of all pertinent 300 Area data was necessary in order to fully evaluate the ground-water data collected during this study and to relate the results to the 300 Area ground-water system. Published and unpublished reports and articles on geology, hydrology, waste burial, ground-water contamination, and well characteristics for the study area were compiled and reviewed.

3.2 300 AREA PROCESSES IMPACTING GROUND-WATER SYSTEM

The ground-water system of the 300 Area is influenced by water that is discharged to (or withdrawn from) the ground during 300 Area processes. Accordingly, Hanford contractors discharging (or withdrawing) water to the ground were contacted. Information on the location, quantity and quality of the water discharged (or withdrawn) was compiled to evaluate data collected on the water-table elevation and distribution of ground-water contamination.

3.3 COLLECTION OF NEW 300 AREA DATA THROUGH 1977 CALENDAR YEAR

Prior to this ground-water study, test wells were located to adequately test ground-water parameters throughout the entire 300 Area. Special emphasis was placed on siting test wells in locations where 300 Area activities might influence the ground-water system. Twenty-four of the 27 test wells in the 300 Area were suitable for the present study. In addition, 5 wells outside the 300 Area were tested to provide background data and information on the ground water entering the 300 Area. Figure 3.1 shows the locations of wells tested for this study.

During the last week of each month in CY1977, ground-water samples were collected from the test wells in 5-gal (19-liter) plastic containers (with the aid of the submersible electric pumps installed in each test

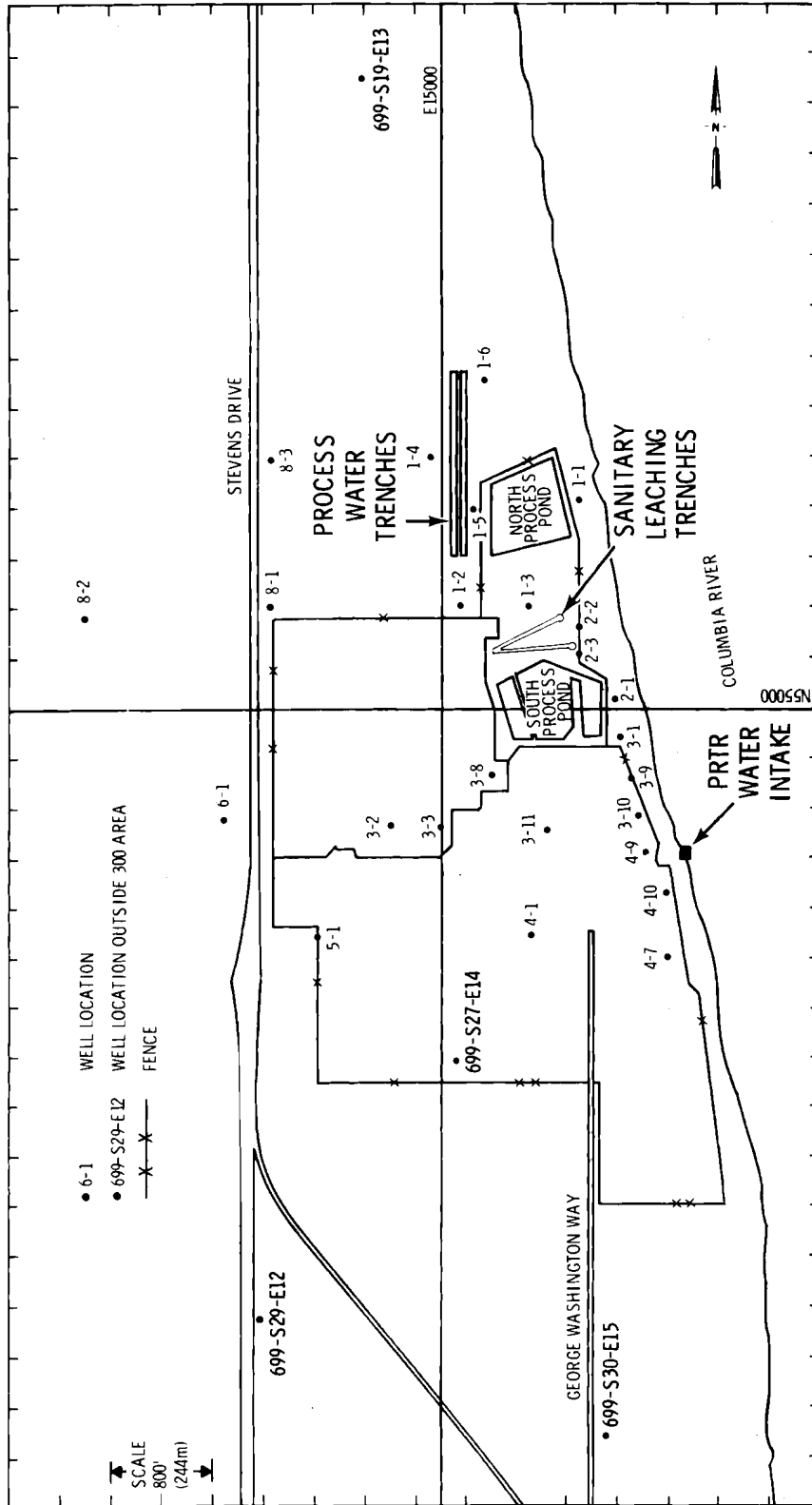


FIGURE 3.1. 300 Area Well Location Map

well) and delivered to United States Testing Company, Richland, WA for analysis. The samples were collected to inventory ground-water contaminants in the 300 Area and to follow ground-water movement in the unconfined aquifer by the use of contaminants as tracers. Ground-water samples collected during the first month of sampling (January 1977) were tested for concentrations of all suspected contaminants. Radioactive analyses included total alpha, gross beta, gamma scan, uranium, and tritium. Nonradioactive tests were for bicarbonate, carbonate, calcium, magnesium, sodium, chloride, sulfate, nitrate, chromium, copper, potassium, and fluoride. Specific conductivity and pH were also tested. The determined concentrations of each contaminant were "contoured" on well location maps so that the resulting isograms would display areal concentration.

In the months following January 1977, the sampling of ground water was modified. Samples were collected only from 300 Area wells which were not sampled routinely for the Ground-water Monitoring Program. In addition, testing for gamma radiation and for copper, chromium, and tritium was discontinued because results of the first month of analysis showed the concentrations to be near or below the detection limits. The results of water testing from this study complemented the results of the routine water analyses for the Ground-Water Monitoring Program. Together they gave a complete account of suspected contaminants in the 300 Area test wells.

Depth to water and temperature of the ground water in 300 Area test wells were measured weekly throughout CY1977. Depth to water in each well was determined by measuring the vertical distance (± 0.01 ft or 0.30 cm) from the top of the well casing to the water with a steel tape. Temperature ($\pm 0.03^\circ\text{F}$ or $\pm 0.05^\circ\text{C}$) was measured by lowering a calibrated thermistor to a level 5 ft (1.5 m) below the water surface. Ground-water temperature was measured at the shallow depth of 5 ft because most local ground-water contamination (including man-caused temperature variation) flows with the water in the upper portion of the unconfined aquifer (Eddy and others, 1978, p. 3, and Myers, 1978, p. 26).

To aid the interpretation of data on the water table and ground-water temperature, the data were "contoured" on 300 Area well location maps (Figure 3.1). The resulting contour and isothermal maps graphically show the piezometric surface of the unconfined aquifer and the distribution of ground-water temperature within the 300 Area.

The level of the Columbia River (McNary Pool) at the 300 Area Plutonium Recycle Test Reactor (PRTR) water intake structures (Figure 3.1) was also measured weekly (near well 399-4-9; the precision of the gaging station there is 0.1 ft or 3 cm). This information was collected because the unconfined aquifer discharges into the river (the base level of the unconfined aquifer). Therefore, changes in river level affect the water-table gradient. Bank storage occurs with a reversed gradient of ground water during sudden rises in the level of McNary Pool.

Transmissivity of the unconfined aquifer in the 300 Area was only partly known because relatively few 300 Area test wells were previously tested by high-discharge pumping. Additional pump tests on 300 Area wells were completed in an attempt to remedy this deficiency.

4.0 RESULTS AND INTERPRETATIONS OF DATA

4.1 GEOLOGIC SETTING

The Hanford Site is located in the Pasco Basin, one of several basins in the Columbia River Basalt Plateau. All the geologic formations present in the Pasco Basin underlie the 300 Area (Figure 4.1), with the exception of the Palouse Formation. Most of these affect the ground-water regime. The formations present beneath the 300 Area are, in ascending order:

1. Columbia River Basalt Group, including the Yakima Basalt Subgroup (Mackin, 1961), its various formations, and the interbedded sediments of the Ellensburg Formation
2. Ringold Formation (Merriam and Buwalda, 1917; Newcomb, 1958)
3. Glaciofluvial deposits [including Pasco Gravels and Touchet Silts or Touchet Beds (Flint, 1938)]
4. Eolian sediments, locally containing some water-reworked materials and volcanic ash (Atlantic Richfield Hanford Company, 1976)

Figure 4.2 shows the locations of the cross sections shown in Figure 4.1.

4.1.1 Stratigraphy

4.1.1.1 Columbia River Basalt Group

The Columbia River Basalt Group (Miocene-Pliocene) and older basalts probably extend to depths in excess of 12,000 ft (3660 m) beneath the Hanford Site (Brown, 1969). Numerous sedimentary beds within the upper part of the basalt sequence are commonly considered to be the lower portion of the Ellensburg Formation (Mason, 1953; Schmincke, 1967). The sediments were derived largely from the Cascade Range to the west. Because those beds pinch out to the east within a few miles (kilometers) of the present Columbia River, they probably represent the bottom of the Pasco Basin at that time or early courses of the Columbia River.

4.1.1.2 The Ringold Formation

The Ringold Formation includes the sediments that lie above the topmost basalt flow in the Pasco Basin (Brown and McConiga, 1960;

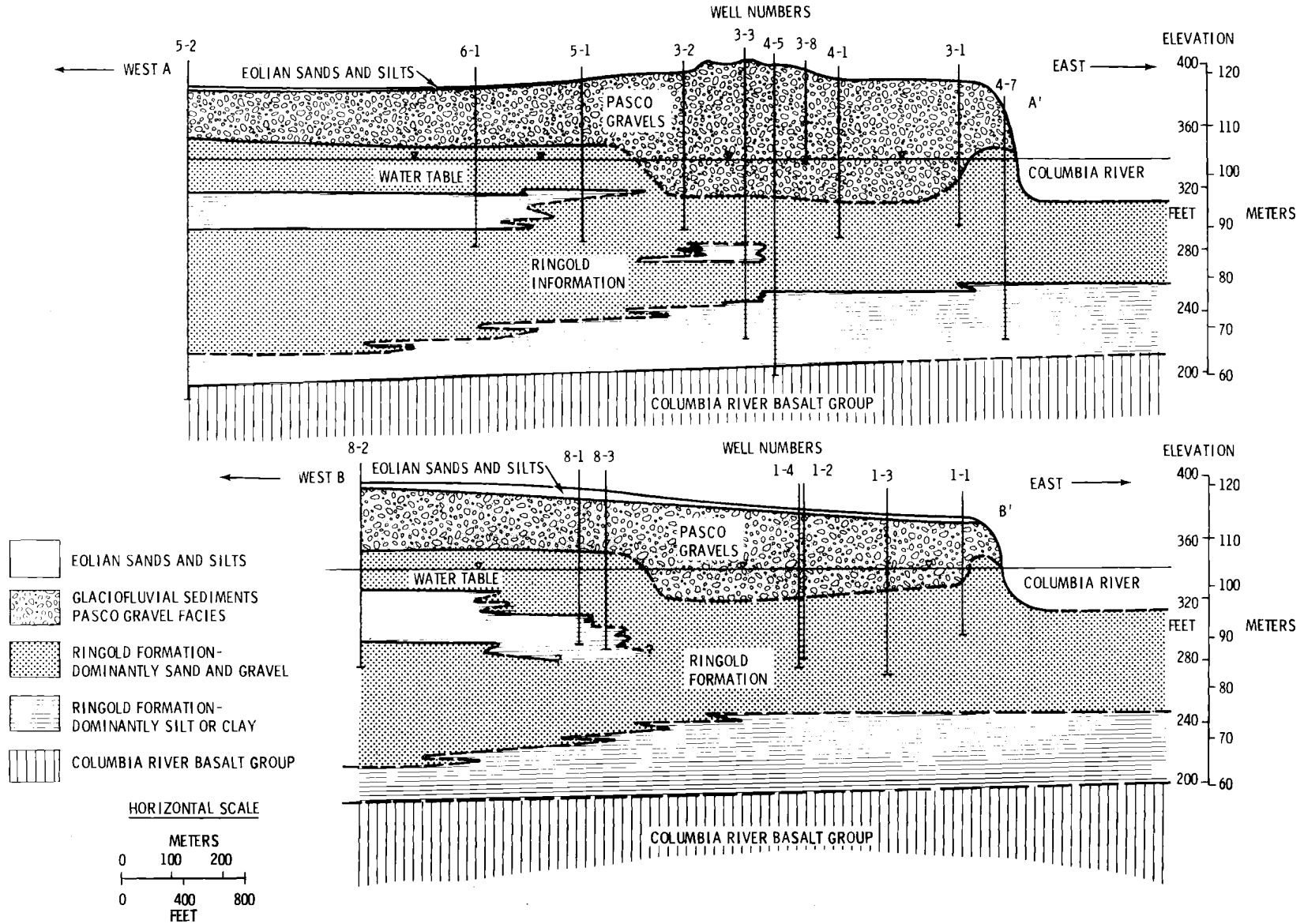


FIGURE 4.1. Geologic Cross Sections of 300 Area

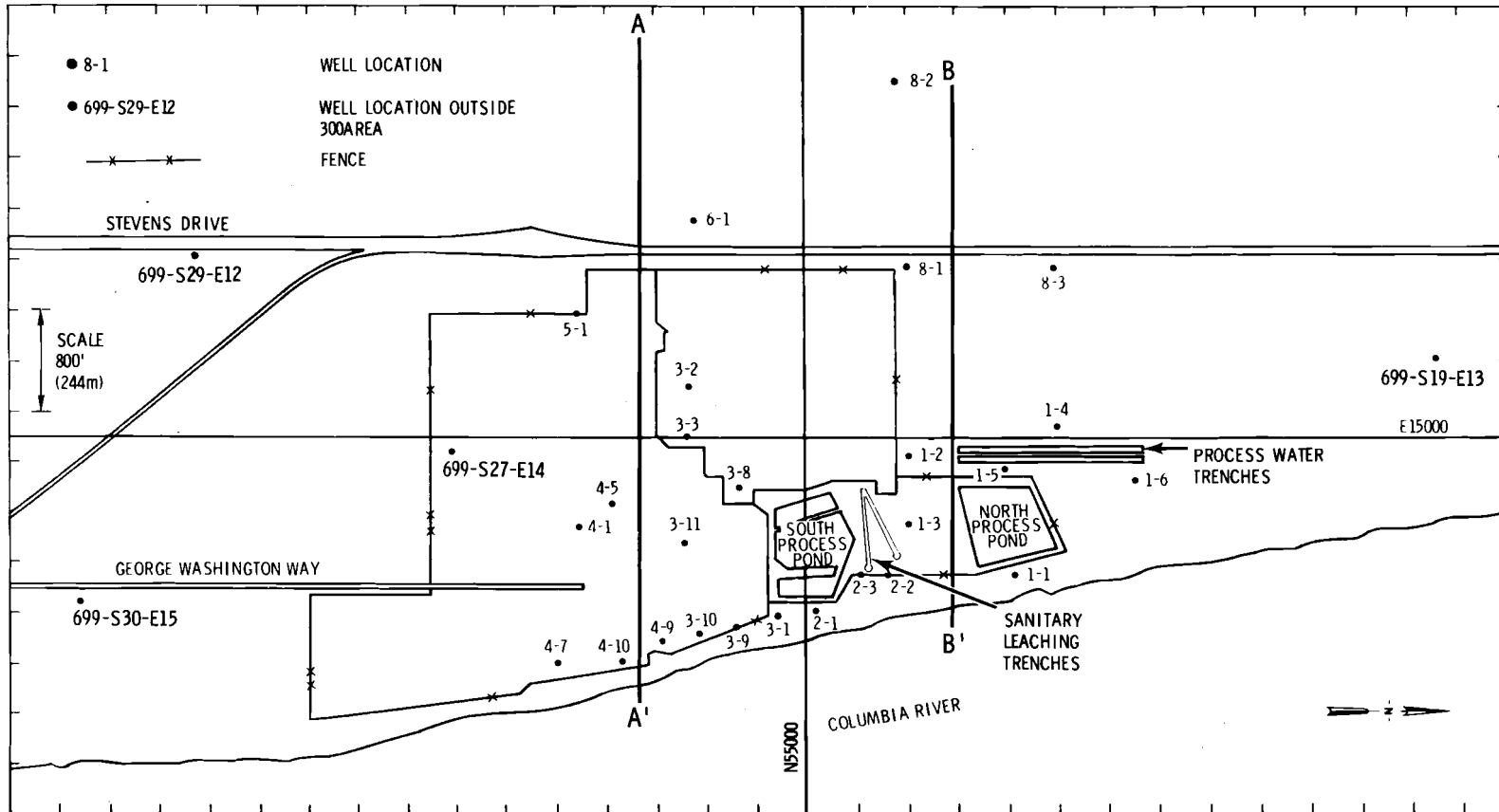


FIGURE 4.2 Location of Geologic Cross Sections Shown in Figure 4.1

Newcomb, 1958). However, because the uppermost basalt flows beneath the 300 Area pinch out northwestward (Ledgerwood and others, 1973), the interbedded sediments assigned to the Ellensburg Formation occupy the same stratigraphic position as sediments assigned to the Ringold Formation. Therefore, the distinction between the two formations is arbitrary in the Pasco Basin.

With the exception of sediments assigned to the Ellensburg Formation, the Ringold Formation is largely quartzitic gravels and quartz- and mica-rich sands derived principally from the granitic and metamorphic rocks of the North Cascades and Okanogan Highlands. Basaltic sands and gravels locally predominate, reflecting upstream erosion in basaltic portions of the Columbia River course.

Strand and Hough (1952), on the basis of paleontological evidence, determined that the age of the Ringold Formation is middle to possibly late Pleistocene. The formation was suggested to be of Pleistocene age by Mackin (1961), and as early Pleistocene or even Pliocene by Brown and Brown (1961). Later publications such as Brown (1975) consider the age of the Ringold Formation to be early Pliocene to early Pleistocene. The discovery of new fossil forms re-established the age of the Ringold Formation as Pliocene and early Pleistocene (Gustafson, 1973).

Newcomb (1958) divided the Ringold Formation into three members: the "lower blue-clay member," a "middle conglomerate member," and an "upper member" of silt and fine sand. He suggested that the lowest and uppermost members were deposited while the Columbia River was impounded by the rising Horse Heaven Hills Anticline. The "middle conglomerate member" was deposited when the Columbia River temporarily breached the Horse Heaven Hills Anticline. A final drainage of the impounded lake during rapid entrenchment of the Columbia River ended deposition of the Ringold Formation.

The section described by Newcomb (1958) is applicable only in the southern end of the White Bluffs, the type section of the Ringold Formation. Elsewhere in the Pasco Basin the sediments locally reveal a

different depositional history. The "lower blue-clay member" is most prominent beneath the Tri-Cities and parts of the Hanford Site. The "middle conglomerate member" is found beneath the Hanford Site, where the basin repeatedly contained the ancestral course of the Columbia River. The upper silts and sands are present only in the White Bluffs, because elsewhere they have been removed by erosion.

Gravels are present in all horizons in the formation at some locality up to at least 500 ft (153 m) elevation, indicating that true impoundment of the ancestral Columbia River by the Horse Heaven Hills Anticline was not necessary. A more reasonable explanation for the deposition of the complex association of interfingering sand, silt, clay, and gravel beds is that the rising Horse Heaven Hills Anticline merely raised the local base level of the ancestral Columbia River. Gravel deposits represent normal fluvial deposition. The finer grained sediments represent shallow lake or floodplain deposits in which meander scars, oxbow lakes, braided channels, backswamps, and natural levees were formed. Silts and clays could have been deposited in flood areas.

The Ringold Formation beneath the 300 Area is approximately 150 ft (46 m) thick. As shown in Figure 4.1, the lower 40 ft (12 m) are composed largely of silt and clay with occasional sand and gravel. Above the clay and silt is a complex association of gravel and sand with an occasional lens of silt or clay. Sediments deposited above the present Columbia River level (to an altitude of about 1000 ft or 305 m) were removed by erosion prior to the deposition of the Pasco Gravels.

4.1.1.3 Glaciofluvial Deposits

Coarse-grained glaciofluvial deposits overlying the Ringold Formation are called Pasco Gravels. The fine-grained, slack-water deposits known as the Touchet Silts (Flint, 1938) are largely facies variants of the Pasco Gravels (Newcomb, 1972). The Pasco Gravels and Touchet Silts were deposited in the Pasco Basin upon an irregular surface which was eroded by normal fluvial processes of the ancestral Columbia River, as well as by catastrophic floods.

Allison (1933) and Flint (1938) postulated that the glaciofluvial sediments were deposited in a lake or lakes created by ice damming in the Columbia gorge and tributaries. Newcomb (1972) considered that the deposits were largely glacial meltwater or outwash deposits. However, origin by normal glacial outwash or a local ice-dammed lake could not explain some of the unusual topographic features (Baker, 1973). Overwhelming evidence cited by Bretz (1959) and Baker (1973) indicates that the bulk of the sediments are the products of catastrophic floods which swept across the Columbia Plateau from the northeast during late Pleistocene time.

Newcomb and others (1972) summarized the major distinctions between the Pasco Gravels and the underlying Ringold Formation. The Pasco Gravels are basaltic in both the sand and gravel fractions. Quartz is the major constituent of the sand fraction in the Ringold Formation, and Ringold gravels are exotic types such as granite, volcanic porphyry, and metamorphic rocks such as quartzite. Basalt gravel in the Ringold Formation can predominate in some locales, but overall it is minor. Besides having a greater percentage of basalt, the Pasco Gravels are normally less compacted, less indurated, and more permeable than the Ringold Formation. Gravel in the glaciofluvial sediments has no appreciable alterations, whereas the gravel of the Ringold Formation has alteration rinds up to 1/8 in. (3.2 mm) thick. Another major distinction is the overall greater abundance of silt and clay in all the Ringold Formation sediments, even in gravel horizons, than in the Pasco Gravels.

At several locales within the Pasco Basin the glaciofluvial sediments are clearly graded, ranging from boulders at the base of each sequence upward through cobbles and pebbles to sand, according to R. E. Brown of PNL. Each sequence indicates deposition of coarse sediments during initial surges of floodwaters with finer sediments deposited later as each flood surge decreased. Near Ice Harbor Dam and south of the Columbia River between the cities of Richland and Kennewick, well data and outcrops show evidence for two major floods or flood surges. Similar evidence was

also reported at excavations for Washington Nuclear Project No. 4 (WNP-4, constructed for Washington Public Power Supply System) by Lindberg (1976). In those excavations two cycles of graded bedding were recognized with overlying channel fillings and lag concentrates.

Pasco Gravels underlying the 300 Area also display two cycles of graded bedding. However, the finer portion of the second, or upper cycle, is not present. The upper portion may have been removed by erosion, exposing boulders at the surface (Figure 4.1). Immediately below the boulders are finer grained sediments typical of another sequence of graded bedding. Glaciofluvial sediments were probably deposited up to 500 ft (153 m) elevation as evident at the Fast Flux Test Facility (FFTF) site. In the 300 Area the sediments deposited above the boulders were probably comparable to the coarse black sands at the FFTF and Washington Nuclear Project No. 4 sites.

In 1958, excavation for the Plutonium Recycle Test Reactor and appurtenant structures (Figure 3.1) disclosed the presence of a channel incised into the Ringold Formation beneath the 300 Area. As shown in Figure 4.1, the channel is filled with glaciofluvial sediments and separated from the present channel of the Columbia River by a natural levee of relatively impermeable Ringold sediments. Attesting to the low permeability of this levee was the small amount of water that leaked into the excavation from the Columbia River during dewatering operations. In contrast, a water flow of 15,000 gal per minute (~950 l/sec) entered the west side of the excavation through the highly permeable, glaciofluvial sediments (R. E. Brown, PNL).

Drilling logs, permeability tests, and drilling samples, along with apparent movement of uranium contaminants in the ground water, further confirm the presence of a channel beneath the 300 Area (Brown and others, 1958). Recent well drilling has further traced the channel to the north and south. The channel, which has a profile similar in cross section to the present Columbia River channel, merges with the Columbia River about 2 miles (3.2 km) to the north and about 1 mile (1.6 km) south of the 300 Area.

4.1.1.4 Eolian Sands and Silts

The surface sediments above the glaciofluvial sediments in the 300 Area are largely wind-transported and deposited sands and silts. These sediments were deposited in dunes up to 10 ft (3.05 m) in depth. The dunes are largely stabilized by vegetation. Dunes are more prominent to the southwest of the 300 Area and immediately north of the 300 Area. The northward increase of eolian sand and silt is shown by Figure 4.1.

The dunes have long dimensions oriented about N.50°E. This orientation reflects the effect of topography to the southwest (upwind). Topographic features undoubtedly affecting wind flow are the southeast end of the Rattlesnake Hills and the several lines of irregular buttes trending southeastward from the Rattlesnake Hills toward Wallula Gap.

4.1.2 Structure

The 300 Area lies above the axis of the northwest-southeast trending Pasco Syncline. This syncline plunges gently northwestward toward the structural low of the Pasco Basin about 10 miles (16 km) to the northwest of the 300 Area. The basaltic bedrock surface along the synclinal axis beneath the 300 Area dips toward the northwest at a gradient of 25 ft/mile (5 m/km or 1/4 degree). However, that dip is not entirely tectonically related. The youngest basalt flows emanated largely from the east and southeast (Brown, 1969; Schmincke, 1964; Swanson and others, 1972), and advanced northwestward into the Pasco Basin where several flows pinched out. An "offlap" relationship exists toward the south and southeast, with the older basalt flows forming the basalt surface progressively farther to the west and north. Therefore, the true dip of the individual basalt flows is slightly less than 1/4 degree including "flow" dip (the effect of thinning and pinchout) and later tectonic deformation.

Ringold Formation sediments generally have similar dips as the underlying basalt flows. However, slightly lower dips prevail upward in the section indicating deformation during deposition (Brown and

McConiga, 1960). Gently dipping Ringold Formation strata are also apparent in the southern end of the White Bluffs, and beneath the 300 Area, less than a mile away, the dips are even lower.

The 300 Area lies above what evidently was the principal course of the ancestral Columbia River during deposition of much of the Ringold Formation. This position is indicated by the abundance of gravel present in the Ringold Formation and the relatively small amount of silt or clay above the lowermost silt and clay bed. To the east and west of the 300 Area, silt and clay are much more abundant higher in the section. The Pasco Basin and the resulting common courses of the ancestral Columbia River were formed by relative subsidence of the Pasco Basin as the Rattlesnake Hills, Yakima Ridge, and Umtanum Ridge were being uplifted.

4.2 HYDROLOGIC SETTING

Ground water beneath the 300 Area occurs in confined aquifers within the basalt sequence and in the unconfined aquifer within the Ringold Formation and Pasco Gravels. The boundary between the confined and unconfined aquifers is the lowermost silt and clay member of the Ringold Formation. Water enters the confined aquifers at numerous sites around the basin, and at a few sites within the basin, but the low permeability of the lowermost silt and clay member allows little interchange of ground water between confined and unconfined aquifers (R. E. Brown, PNL).

Confined aquifers within the basalts are largely restricted to sedimentary interbeds or flow contacts where the basalt tends to be scoriaceous, brecciated, or highly jointed. These aquifers are confined because basalt flows are largely impermeable in their central parts and many of the interbedded sediments are siltstones and claystones of low permeability.

Natural recharge of the unconfined aquifer (or water-table aquifer), generally occurs at the northwest margin of the Pasco Basin where canyons enter the Hanford Site. Artificial recharge occurs at the 200 Areas. Ground water from the natural and artificial recharge areas flows down

gradient toward the basin low and eventually into the Columbia River. However, along the southeastern edge of the Hanford Site the water-table aquifer is recharged largely from the Yakima River. This is suggested by the water-table contours as shown in Figure 4.3. From the Yakima River, the ground water flows generally eastward into the Columbia River. Therefore, the 300 Area is located fairly close to the area where two unconfined ground-water sources mix: 1) ground water flowing southeasterly from the central portion of the Hanford Site, and 2) ground water recharged by the Yakima River.

Additional evidence of ground-water recharge from the Yakima River in the southeastern part of the Hanford Site is indicated by water analyses. Analyses of ground water from the Horn Rapids triangle area show slightly higher (25 versus 16 mg/l or ppm) sodium content than more northerly ground water (Newcomb and others, 1972). Other dissolved salts show similar results. These analyses are consistent with the Yakima River as a ground-water source. The ground water from this source flows through more silicic volcanic sands and gravels than ground water further north.

In 1948, concern over the possible movement of uranium-bearing ground water (and other waste products that were discharged to the process ponds) into water supply wells or into the Columbia River led to a ground-water investigation in the 300 Area (R. E. Brown, PNL). Wells were drilled around the North and South Process Ponds (Figure 3.1) and other locations where uranium contamination was potentially present.

Monitoring of water levels in the 300 Area wells disclosed that a reversed gradient was imposed on the ground water as the Columbia River level increased during spring floods (Haney, 1957). This resulted in bank storage of water that normally would have entered the river. Ground-water temperature measurements indicated that cooler river water was entering the ground-water flow system largely between the two process ponds. Well 1-3 (Figure 3.1) showed a faster response in water-level rise, an earlier drop in temperature, and a more rapid drop in uranium concentration than other wells. Subsequently, the uranium-contaminated

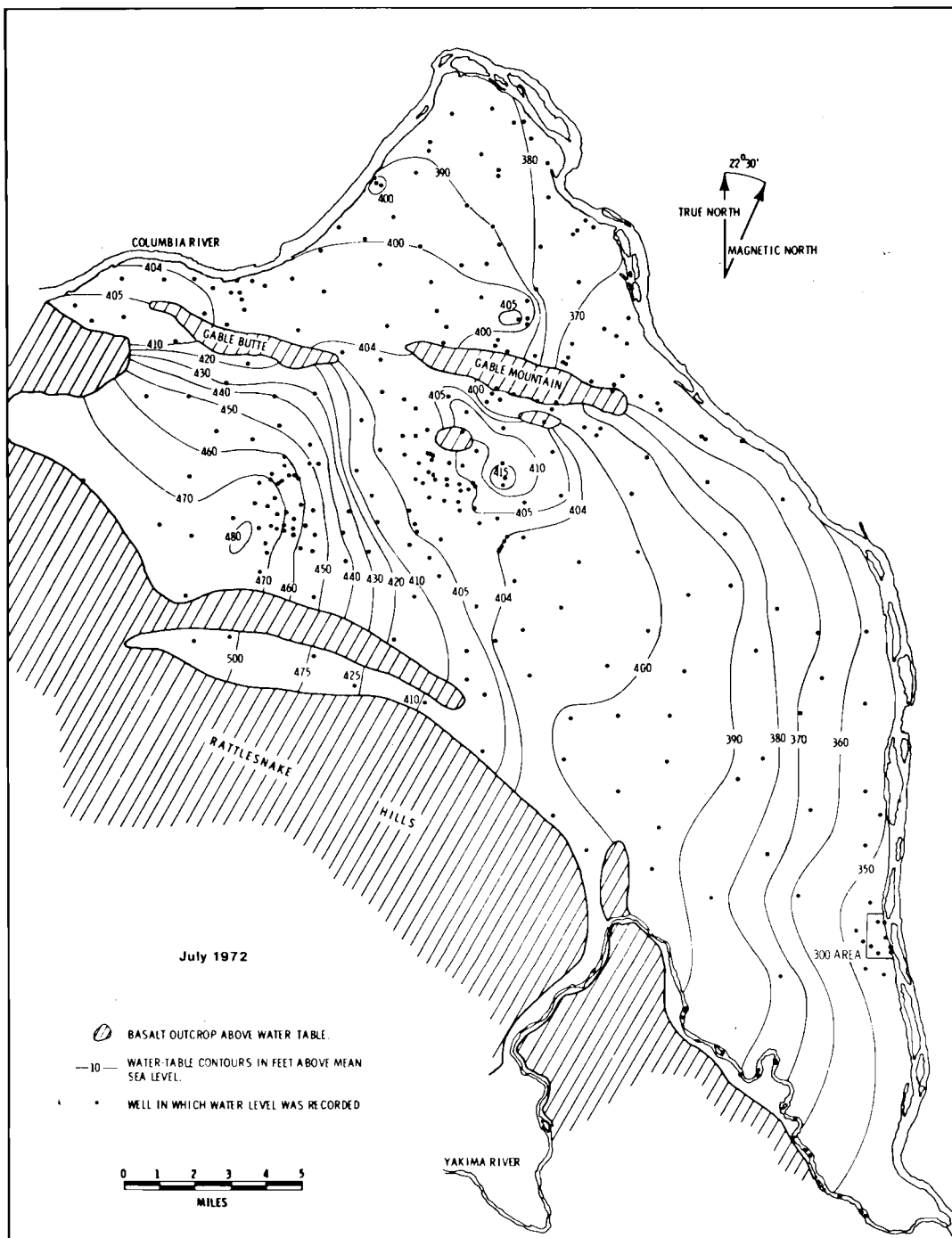


FIGURE 4.3. Hanford Site Water-Table Map, July 1972.

ground water moved inland under the influence of the reversed gradient, followed by the cooler Columbia River water. The maximum detected westward penetration of the uranium contamination caused by the reversed gradient was to Wells 8-1 and 8-3, although significant head changes occurred up to 2 to 2-1/2 miles (3.2 to 4 km) from the river.

When the river level dropped during the summer, the gradient again sloped toward the Columbia River. The peak uranium concentration flowed southward toward Wells 3-2, 3-3, and 699-S27-E14. The uranium-contaminated ground water became so dispersed and blended with uncontaminated ground water that the peak concentration was barely discernible at well 699-S27-E14.

The ancient river channel, discovered in 1958 while workers were excavating for the Plutonium Recycle Test Reactor, probably is responsible for the rapid response of the ground-water levels and contaminant movement to changes in hydraulic gradient (R. E. Brown, PNL). The Pasco Gravels within the channel are more permeable than the surrounding Ringold Formation. Westward movement of the ground water beyond the channel boundary (near 8-1 and 8-3) is inhibited by the lower permeability of the Ringold Formation. The channel was shown to extend in the north and south directions by the southward movement of the peak uranium concentration.

A breach in the natural levee separating the old channel and current Columbia River channel must be responsible for the high flow rate between the two process ponds (near Well 1-3) that rapidly admits cooler Columbia River water. The breach is of unknown width, but its presence has been confirmed by a spring along the Columbia River bank which releases warmer, uranium-contaminated water during low river stages (R. E. Brown, PNL).

4.3 PREVIOUS 300-AREA PROCESSES

Uranium-contaminated solid wastes have been buried in 300 Area Burial Grounds No. 1 through 8, and the 300 West Burial Ground (Figure 4.4) at various times from 1944 to 1968. Because the solid wastes were buried well

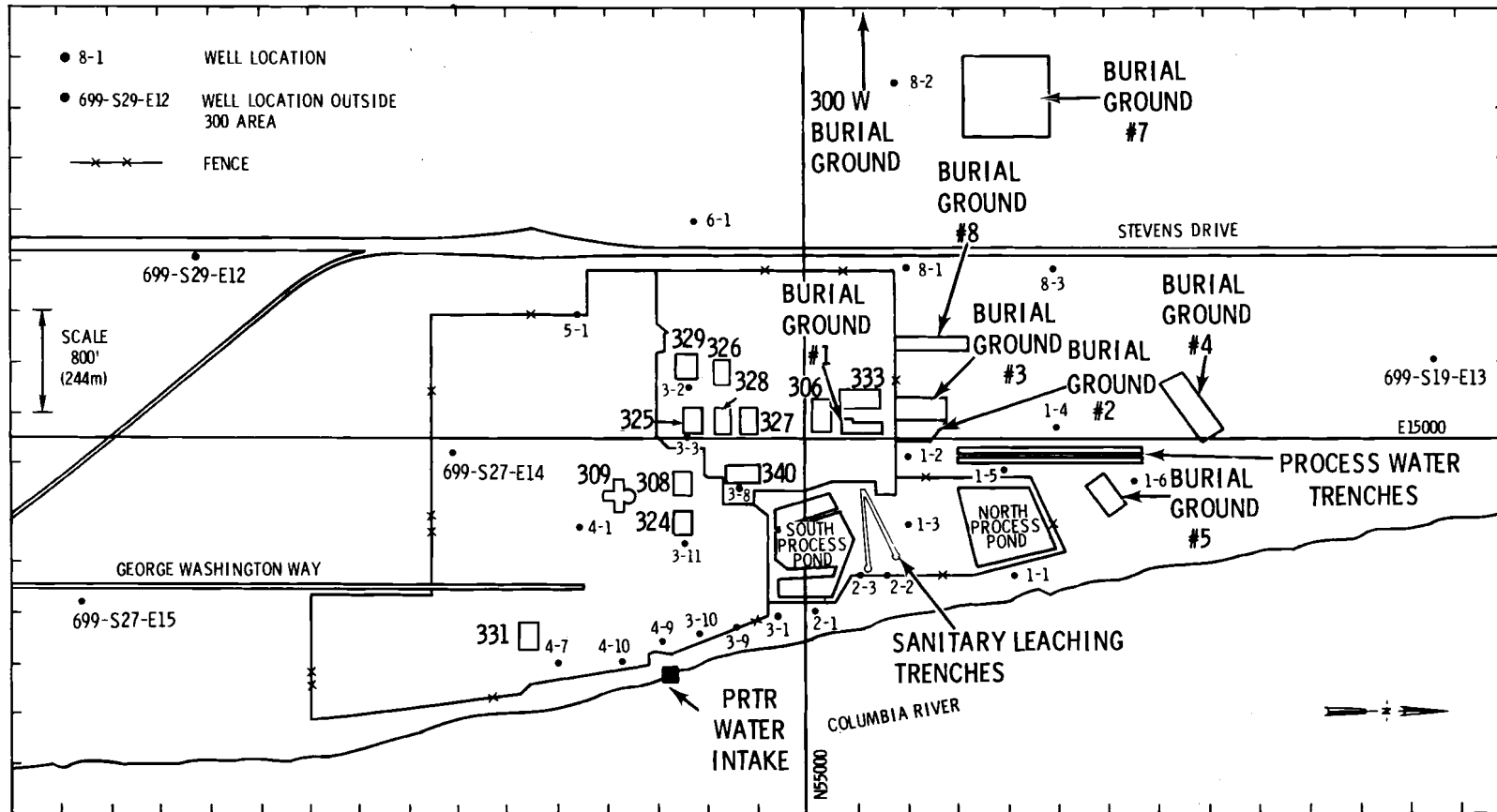


FIGURE 4.4. Location of 300 Area Wells, Burial Grounds, Buildings, Ponds and Trenches

above the water-table, ground-water contamination from those waste products was very unlikely. However, during heavy rainfall, runoff from parking lots near the 333 Building was routed to the retired Burial Ground No. 3 where solid uranium wastes are known to be buried. Although some uranium contamination could have been flushed down to the water table, water quality tests by this study did not show any increase in uranium concentration or other alpha particle emitters near that burial ground (Figures 4.5 and 4.6).

Drums of uranium-contaminated organic solvent were buried in the 300 West Burial Ground in 1955 and 1956. As with other 300 Area burial grounds, water quality tests at associated 300 Area tests wells did not show any increase in uranium concentration or other alpha particle emitters.

The discharge of uranium-contaminated waste water to the unlined process ponds and ultimately into the Columbia River via the ground water was the practice from 1944 until 1975. This practice, besides contaminating the ground-water system in the vicinity of the process ponds, also contaminated the ground-water system along the process sewer lines. The process waste lines that carried the uranium-contaminated waste water to the process ponds were constructed of vitreous clay bell and spigot sewer pipe and were known to leak at many joints. This practice of disposal is responsible for the overall increase in uranium contamination (and beta emitters from uranium daughters) beneath the 300 Area (Figures 4.5 and 4.7).

From 1967 to 1972, animal wastes contaminated with ^{90}Sr (a beta emitter) were disposed by discharge to a drainfield east of the 331 Building. Water samples tested in January 1977 indicated that the ground water near the drainfield was not contaminated with ^{90}Sr at the time of water testing (Figure 4.7). After 1972, the animal wastes contaminated with ^{90}Sr were disposed to the process ponds, and in 1973, research in the 331 Building generating ^{90}Sr -contaminated animal wastes was discontinued. Disposal of animal wastes (not contaminated with ^{90}Sr)

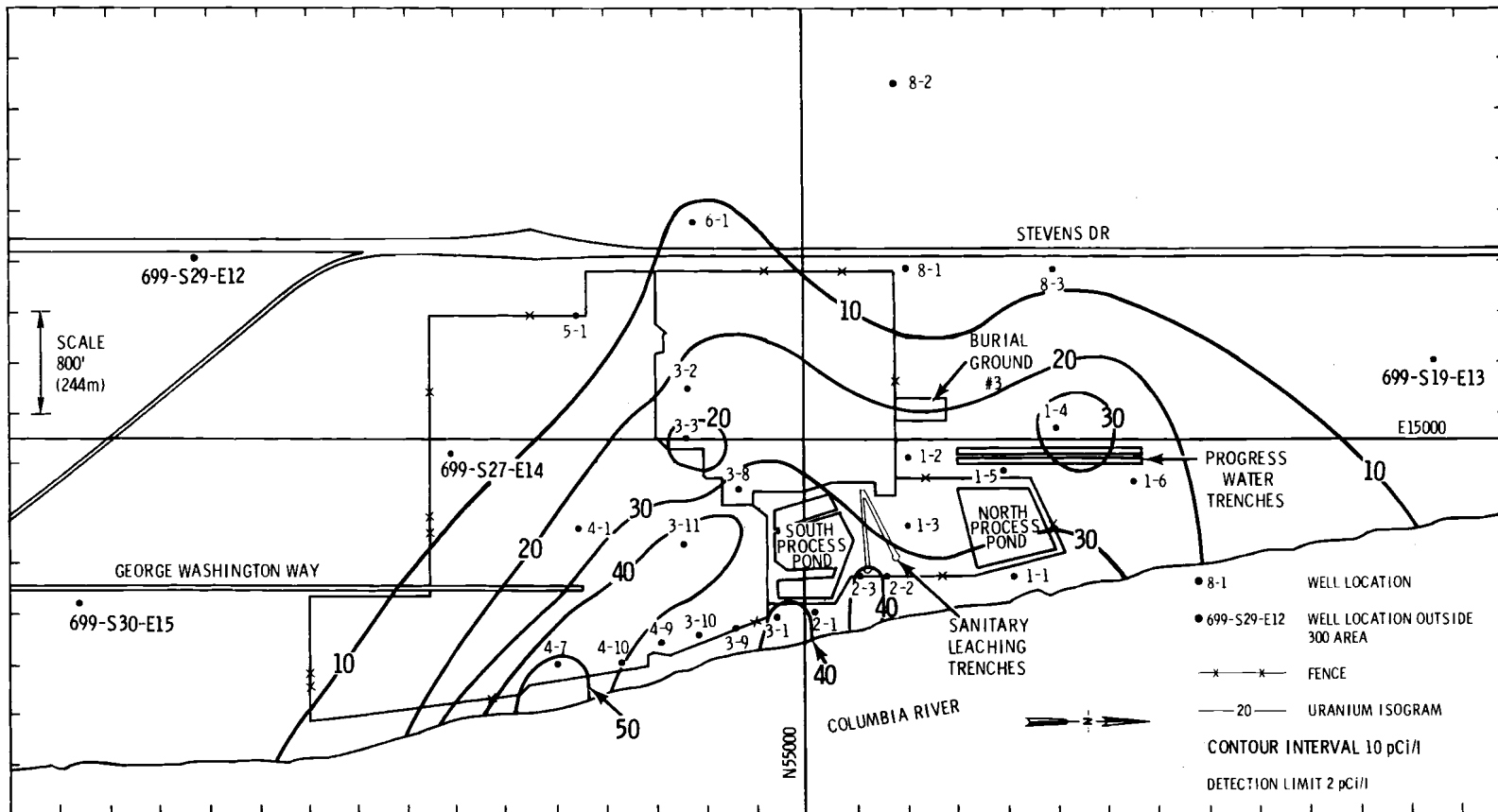


FIGURE 4.5. Concentration of Uranium in the Unconfined Aquifer Under the 300 Area in January 1977 (background concentration less than 2.0 pCi/l)

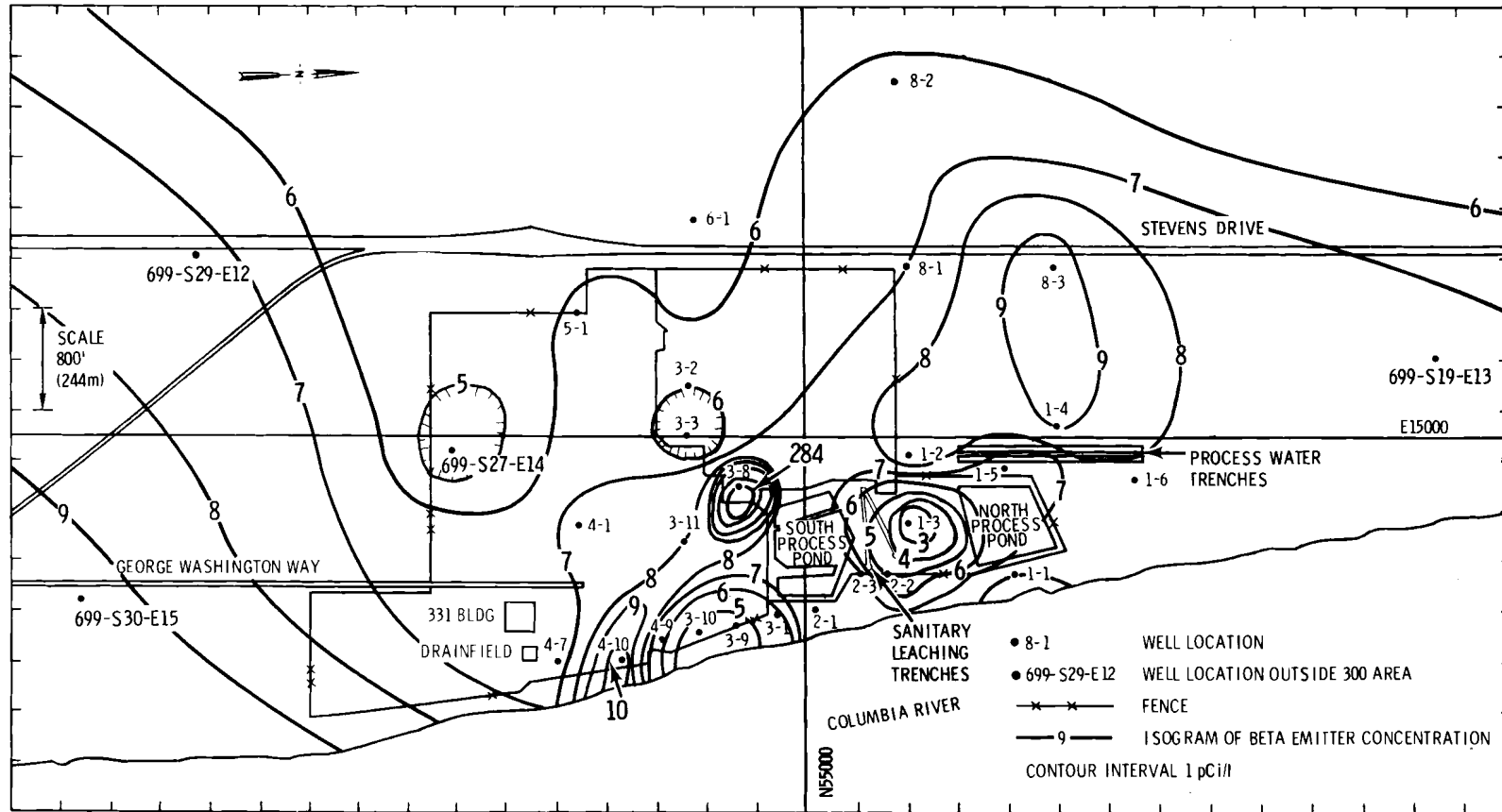


FIGURE 4.7. Concentration of Beta Emitters in the Unconfined Aquifer Under the 300 Area in January 1977 (background concentration less than 6.0 pCi/l)

to the process ponds continued until 1975 when the Process Water Trenches were put into use. In June 1977, the disposal of animal wastes was changed from the Process Water Trenches to the Sanitary Leaching Trenches.

4.4 UNPLANNED RELEASES

Small quantities of uranium wastes or wastes containing fission products have been discharged accidentally to the ground near the 321, 327, and 340 Buildings (Figure 4.4). However, most of this contamination was easily cleaned up or excavated, causing little or no impact on the ground-water system.

Steel waste lines serving the 324, 309, 325, 327, 329, and 340 Buildings (Figure 4.4) are known to be internally contaminated with fission products. Leaks in this system have occurred and one large leak was discovered in December 1969 at the position of well 3-8. Denham (1970) reported that 10 curies each of ^{90}Sr and ^{137}Cs inadvertently leaked into the soil during a period of 1 year or more. Because well 3-8 was drilled directly through this leak site to monitor the effect on ground water due to the contaminated soil which was not removed, the comparatively high concentration of gross beta emitters near that well (as shown in Figure 4-7), was expected. The gamma scan of water from well 3-8 for January 1977 showed that the only gamma emitter above detection limits was ^{137}Cs . Strontium-90, which does not emit gamma radiation, was not detected in these samples. However, it has been identified in other samples analyzed specifically for ^{90}Sr by the Ground-water Monitoring Program. Fission products have not been identified in samples from other 300 Area wells.

Another large release of radioactive waste may have occurred near the 306 Building. During the weekend of July 4, 1978, 947 gal (3585 l) of nitric acid solution containing 268 lb (121.6 kg) of depleted uranium drained from a storage tank into the 300 Area process waste-line system. However, water samples from both the waste-line system and from wells adjacent to the Process Water Trenches have failed to confirm that the

the uranium and acid ever reached the trenches (Battelle Occurrence Report, 76-BNW-14). The results of over 100 pCi/l of uranium and 100 mg/l of nitrate discovered in wells southeast of the 306 Building by the Ground-water Monitoring Program in late 1976 may indicate that the uranium waste was discharged to the ground near the 306 Building. The high results of uranium by this study in January 1977 at wells 3-11 and 4-7, as shown in Figure 4.5, further support a discharge to the ground at the 306 Building.

4.5 300 AREA GROUND-WATER SYSTEM DURING STUDY

Ground water flows beneath the 300 Area from the northwest, west, and southwest and then into the Columbia River as shown in Figures 4.3 and 4.8. Several natural influences, as well as human-related influences, affect the ground-water system of the 300 Area. Natural influences which affect the 300 Area ground-water system are changes in the level of the Columbia River and seasonal variations of air temperature. Prior to 300 Area processes, seasonal variations in air temperature probably had no discernible effect on the ground-water system of the 300 Area. However, with the introduction of surface water in the 300 Area, ground-water temperature began to be indirectly influenced by air temperature. The effects of seasonal variations in air temperature on ground-water temperature are shown in Figures 4.9 and 4.10. The temperature of surface water in the Process Water Trenches (near wells 1-4, 1-5, and 1-6) is greatly influenced by air temperature. Approximately 6.2×10^7 gallons, (2.3×10^5 kiloliters) per month of waste water percolate to the water table and alter the temperature of the ground water in the immediate vicinity. During the winter months, water standing in the Process Water Trenches becomes quite cold and cools the ground water to temperatures a few degrees (4°F or 2°C) cooler than ground water elsewhere in the 300 Area (Figure 4.9). In the summer months the process water may warm the ground water 16°F (9°C) more than unaffected ground water (Figure 4.10).

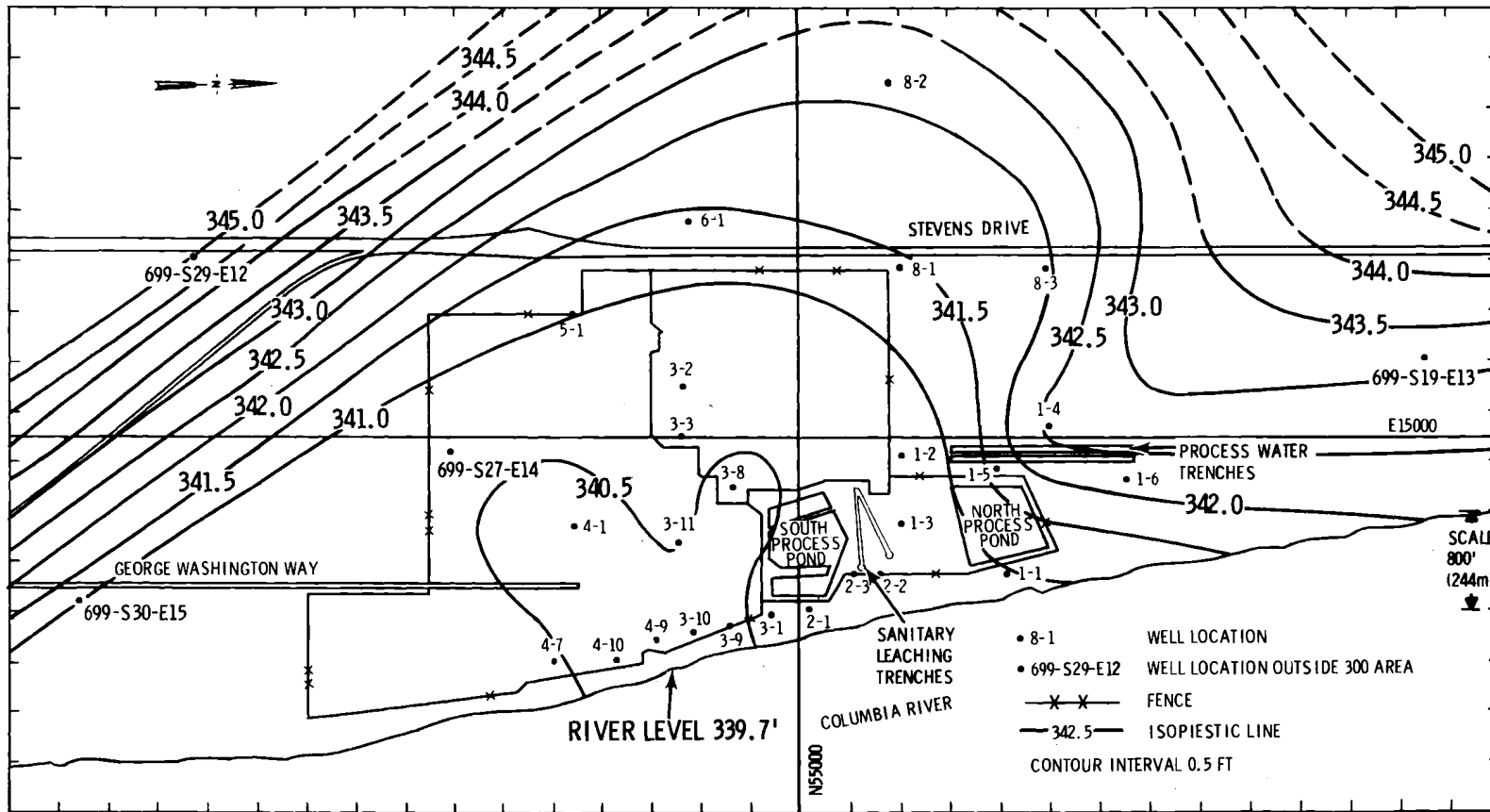


FIGURE 4.8. 300 Area Water-Table Map, July 1, 1977

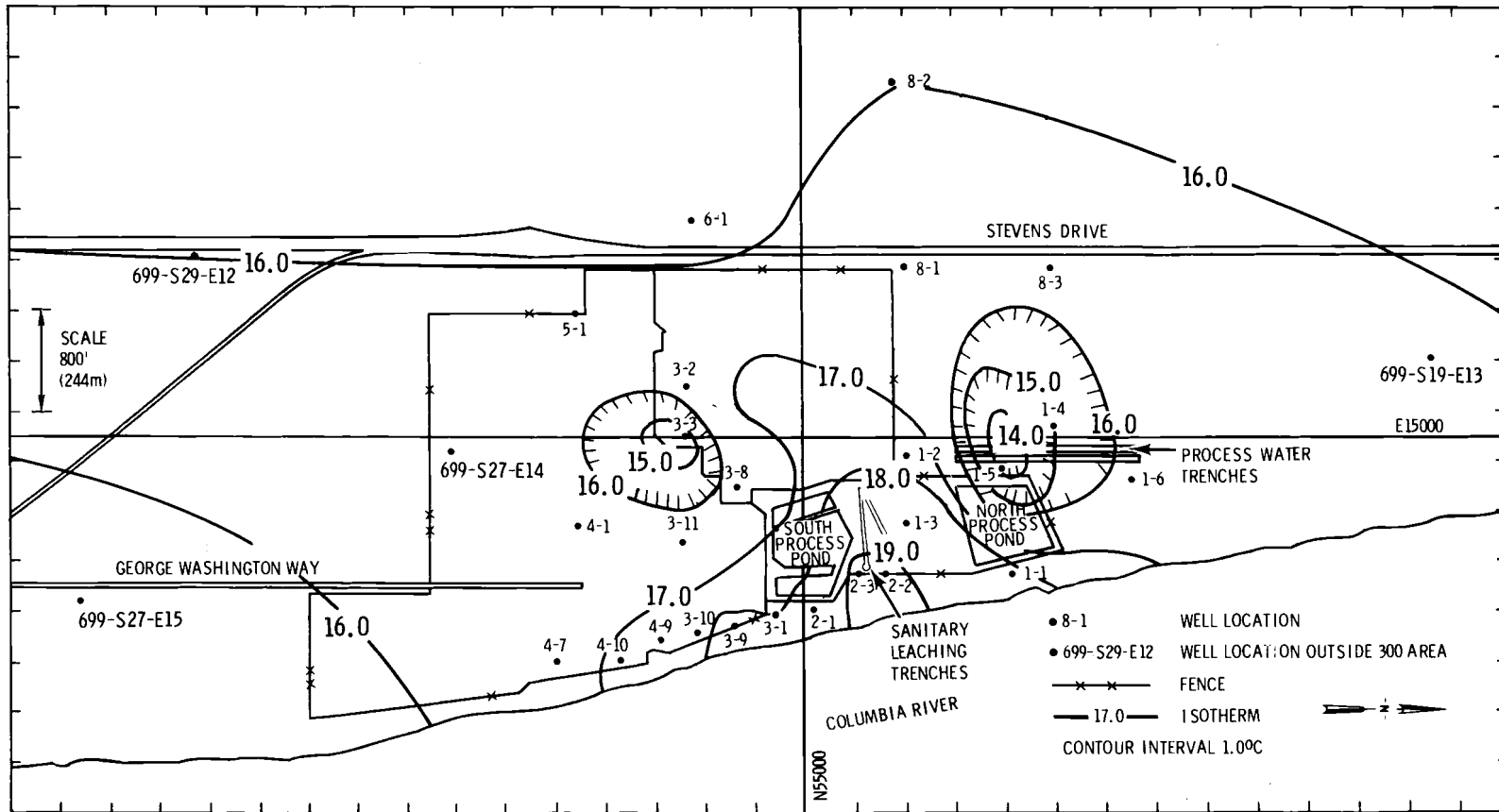


FIGURE 4.9. Temperature in the Unconfined Aquifer Under the 300 Area, February 16, 1977

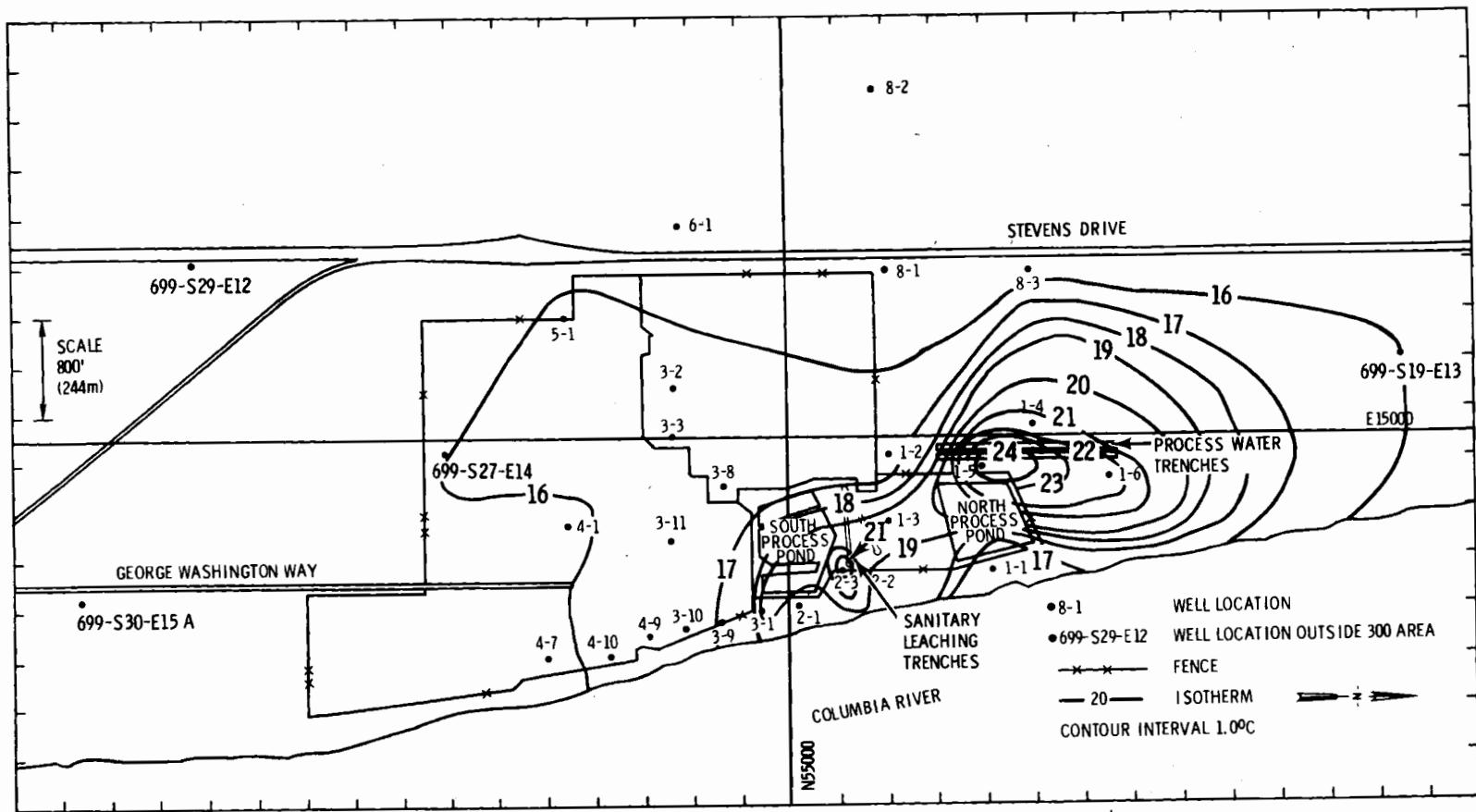


FIGURE 4.10. Temperature in the Unconfined Aquifer Under the 300 Area, September 1, 1977

Approximately 1.3×10^7 gallons or 4.9×10^4 kiloliters per month enter the ground-water system by way of the Sanitary Leaching Trenches. However, the waste water enters the ground-water system quickly and is not affected much by air temperature. As a result, ground-water temperatures near the Sanitary Leaching trenches (Wells 1-3, 2-2, and 2-3) remain relatively constant regardless of air temperature. However, the discharged water to the Sanitary Leaching Trenches is usually quite warm (50% to 75% of water discharged to these trenches is steam condensate) causing the temperature in the wells to be generally elevated above the regional ground-water temperature.

Construction of several dams on the Columbia River downstream and upstream from the 300 Area dramatically restricted fluctuations in river level normally attributed to seasonal variations. Previously, the rise in river level during the spring runoff temporarily caused a reversed gradient of ground water in the 300 Area (Haney, 1957). During 1977, the Columbia River level near the 300 Area fluctuated enough to only slightly affect the ground-water system. One occasion is shown in Figures 4.11, 4.12, 4.13, and 4.14. These figures show the water table as measured from 300 Area test wells during four consecutive weeks in late May and early June 1977. Between May 20 and May 27 the elevation of McNary Pool was raised from 340.8 to 344.4 ft (104 to 105 m). The elevated river level was of sufficient duration to cause bank storage of water and an apparent temporary water-table depression throughout much of the central portion of the 300 Area. By June 10, the river level had dropped back to 341.6 ft (104 m), and the water table was recovering to resemble the earlier configuration. Although bank storage of ground water was apparent during the period of May 27 to June 3, the quantity of water entering the ground-water system must have been small. The temperature of the Columbia River about that time was 55.4 F (13 C) and certainly would have displaced the ground water slightly in the area of bank storage had a large quantity entered the system. Figure 4.15 shows that the ground-water temperatures on June 3 near the Columbia River remained as high or higher than ground water entering the 300 Area from the west.

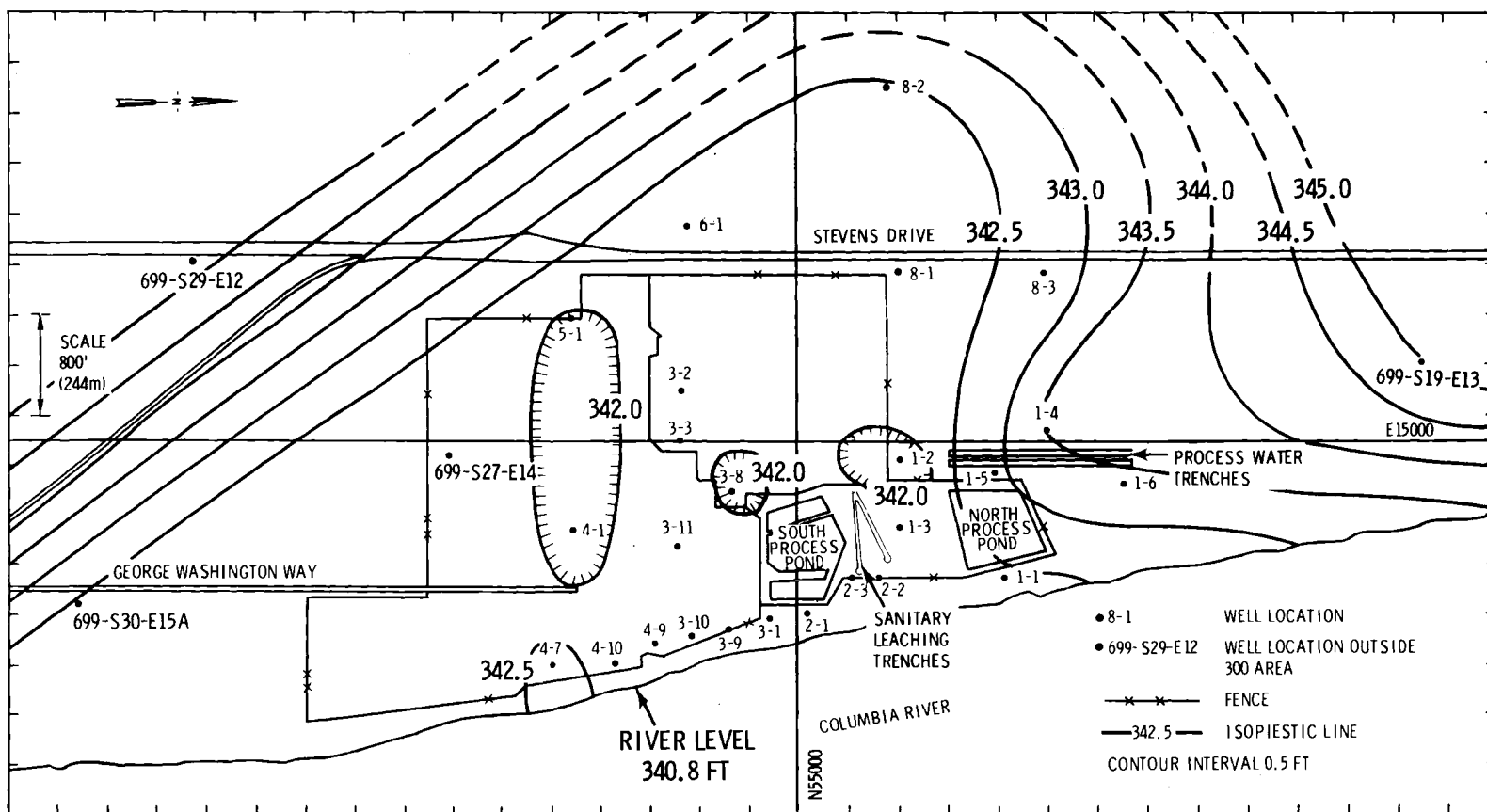


FIGURE 4.11. 300 Area Water-Table Map, May 20, 1977

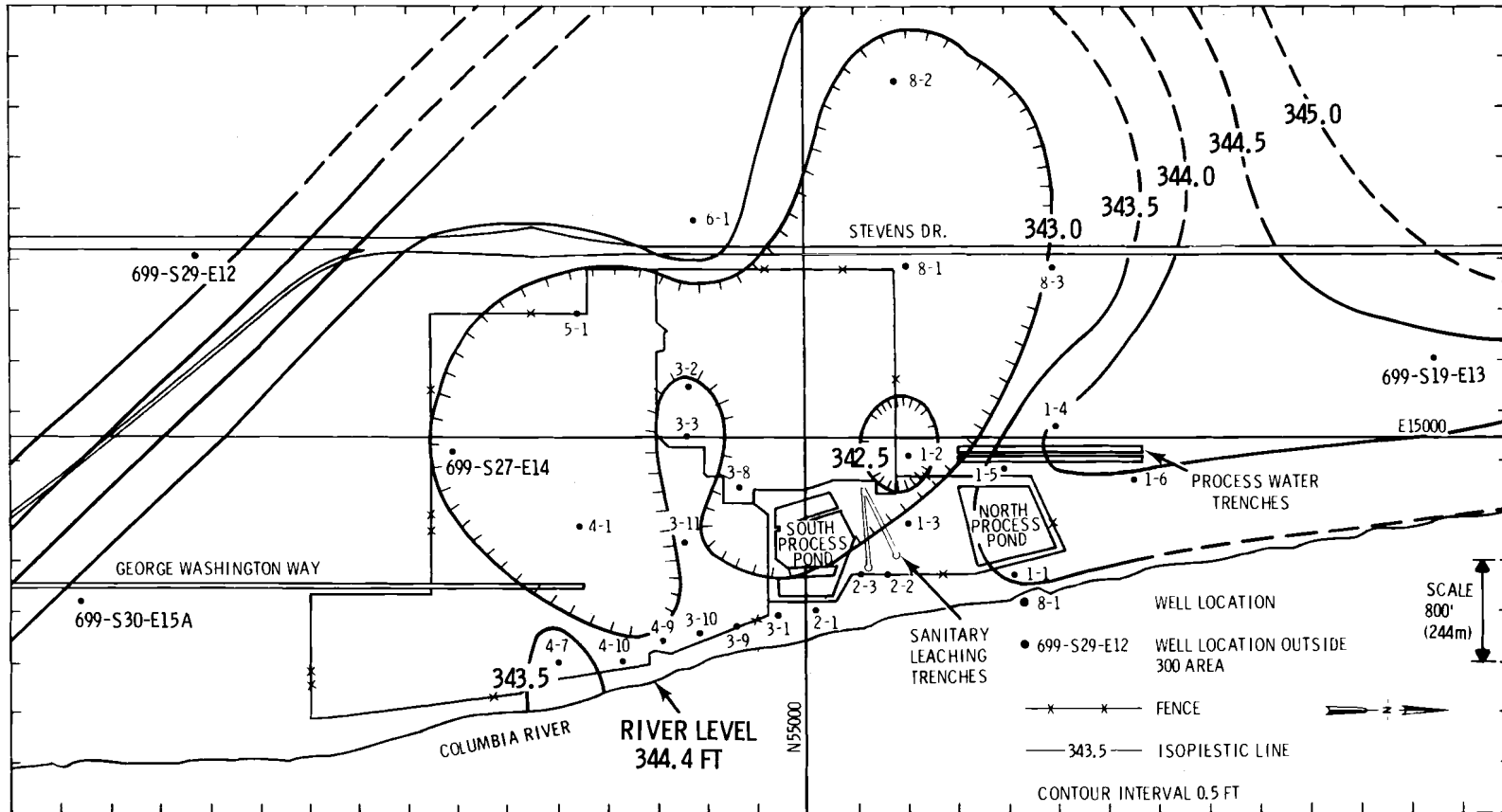


FIGURE 4.12. 300 Area Water-Table Map, May 27, 1977

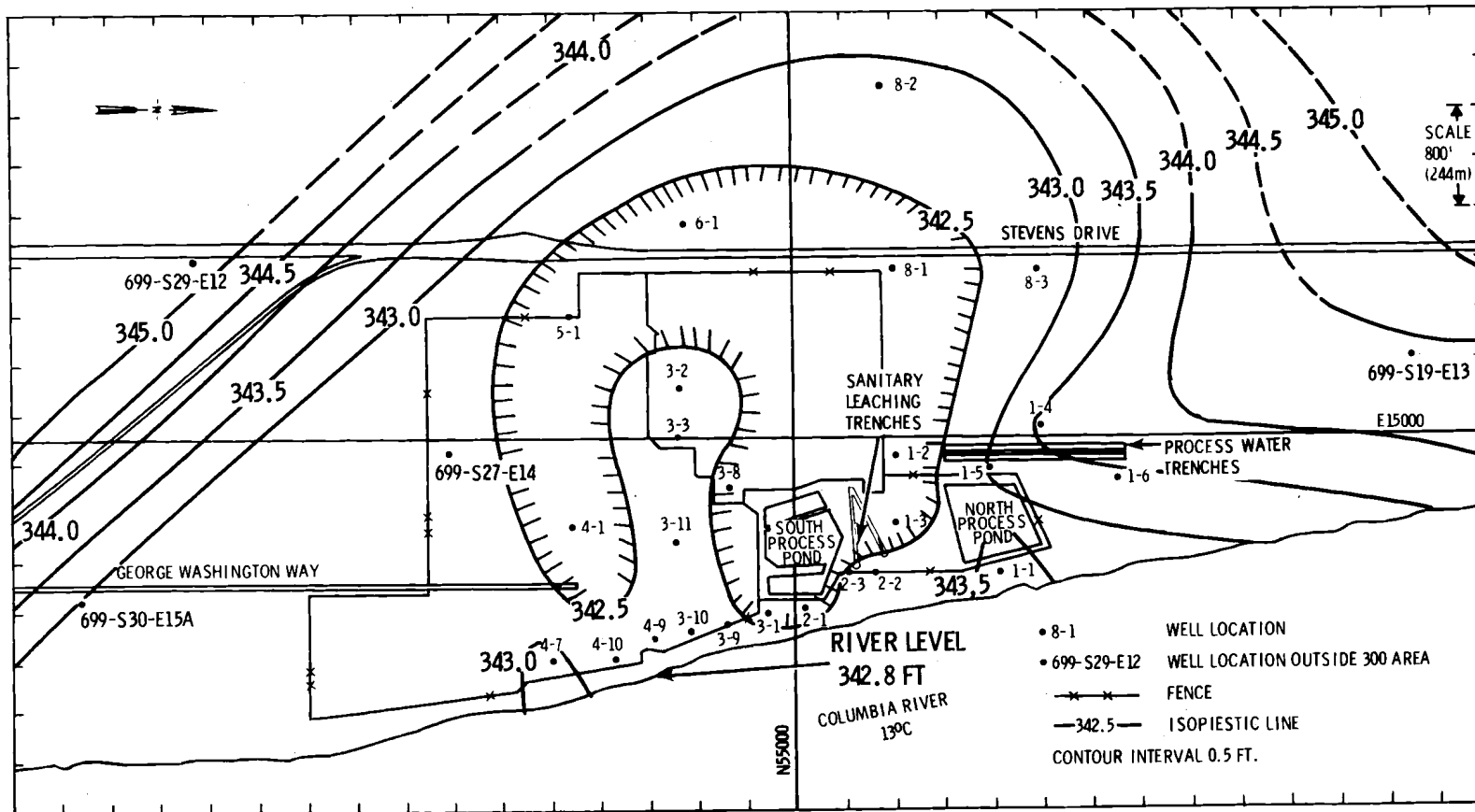


FIGURE 4.13. 300 Area Water-Table Map, June 3, 1977

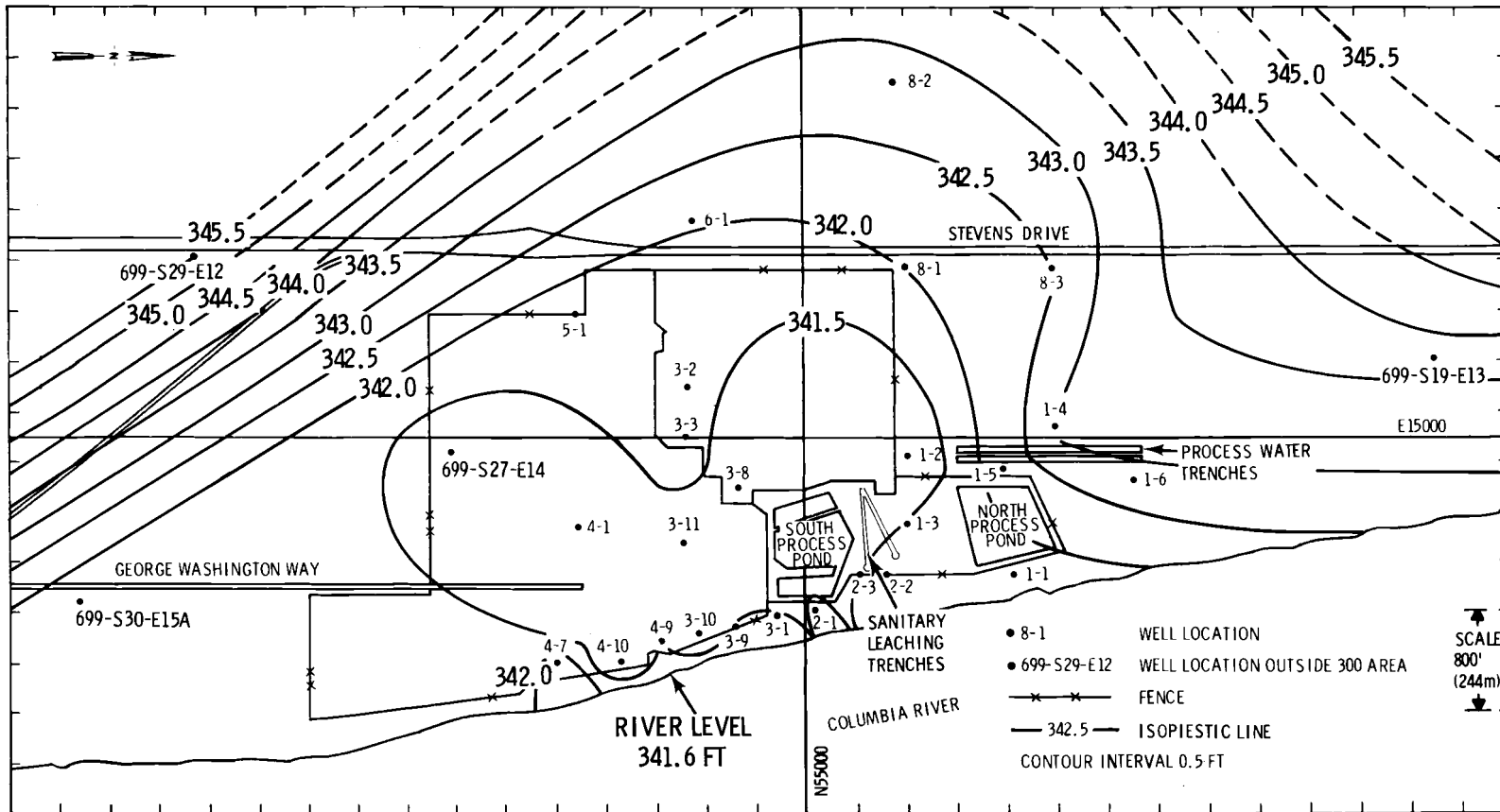


FIGURE 4.14. 300 Area Water-Table Map, June 10, 1977

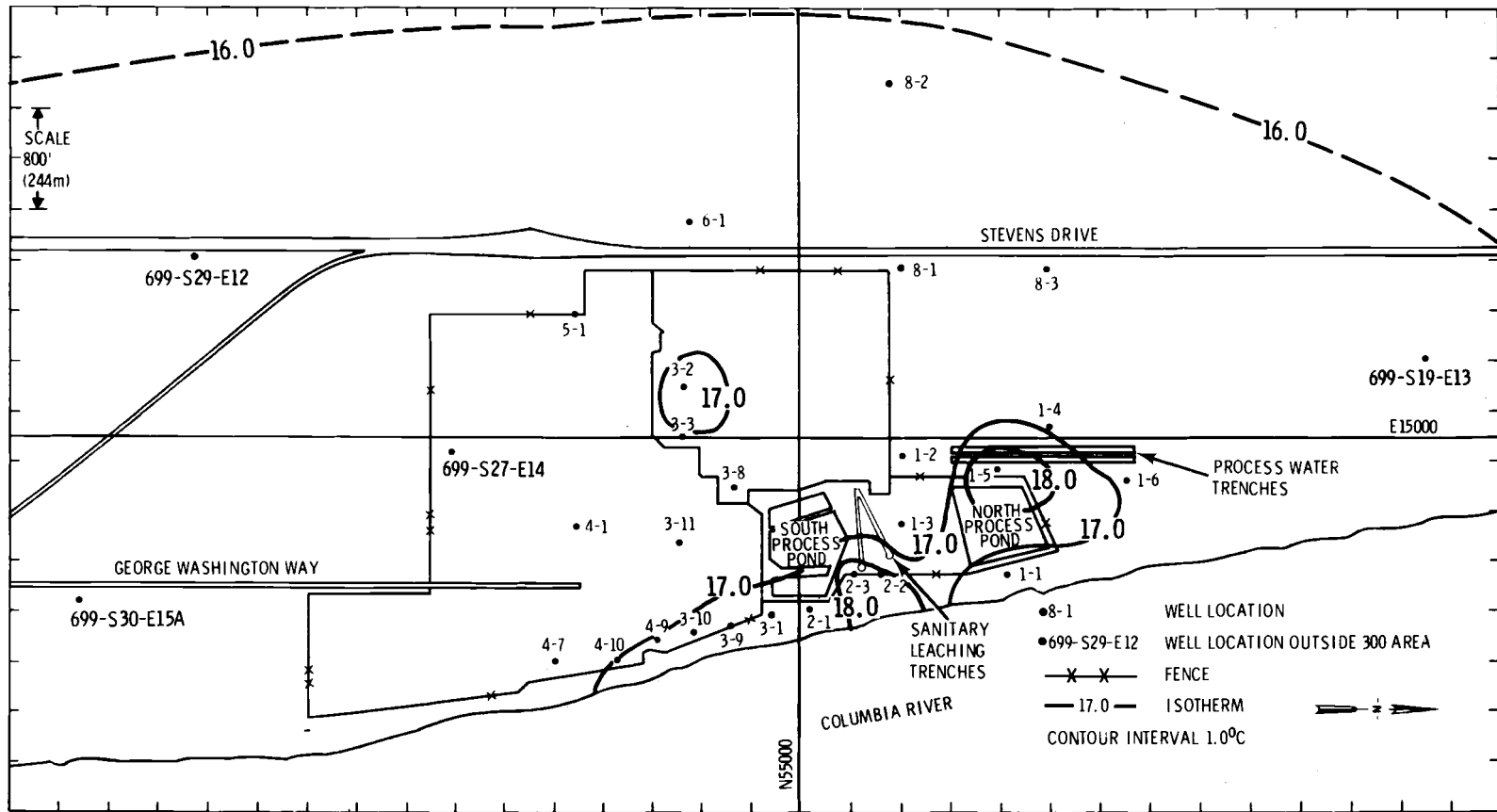


FIGURE 4.15. Temperature in the Unconfined Aquifer Under the 300 Area, June 3, 1977

300 Area processes which now influence the ground-water system are: the routine discharge of waste water to the trenches and ponds and the leaking of pipes containing contaminated waste water, steam condensate or fresh water. Figure 4.16 shows locations where substantial quantities of water are discharged to the ground. These positions are identified by ground-water "mounds" or "lobes" on the water table. The largest and most obvious lobe underlies the Process Water Trenches. Other lobes or mounds are located at the Sanitary Leaching Trenches, the South Process Pond, and near the 331 Building (well 4-7).

Water was occasionally withdrawn from the ground-water system in the 300 Area. During July 1977, 6.5×10^6 gallons (2.5×10^7 l) of water were pumped from well 4-5 in the 309 Building. This withdrawal may have been of sufficient magnitude to cause a water-table depression in the area near well 399-4-1 as shown in Figure 4.17

Water quality tests of Hanford ground water in and adjacent to the 300 Area showed that several ground-water contaminants are more concentrated and others are more dilute in the 300 Area than in surrounding areas. In the area of the Process Water Trenches and Sanitary Leaching Trenches, calcium, magnesium, sodium, bicarbonate and sulfate ions were more dilute (Figures 4.18 through 4.22). The pH near the trenches was also lower, possibly contributing to the apparent dilution of one or more of these ions.

Contaminants that are in greater concentration beneath the 300 Area are nitrate, fluoride, chloride, uranium, and beta emitters. As shown in Figure 4.23, nitrate is most concentrated near the Process Water Trenches, the Sanitary Leaching Trenches, and along the bank of the Columbia River near well 3-9. The high concentration of calcium, sulfate, magnesium, and nitrate near well 3-9 may be due to the discharge of coal ash and water in the ash waste pits a few hundred feet west of the well. Fluoride is most concentrated along the bank of the Columbia River between wells 2-1 and 4-7, or near 3-8 (Figure 4.24). Chloride, as shown in Figure 4.25, is

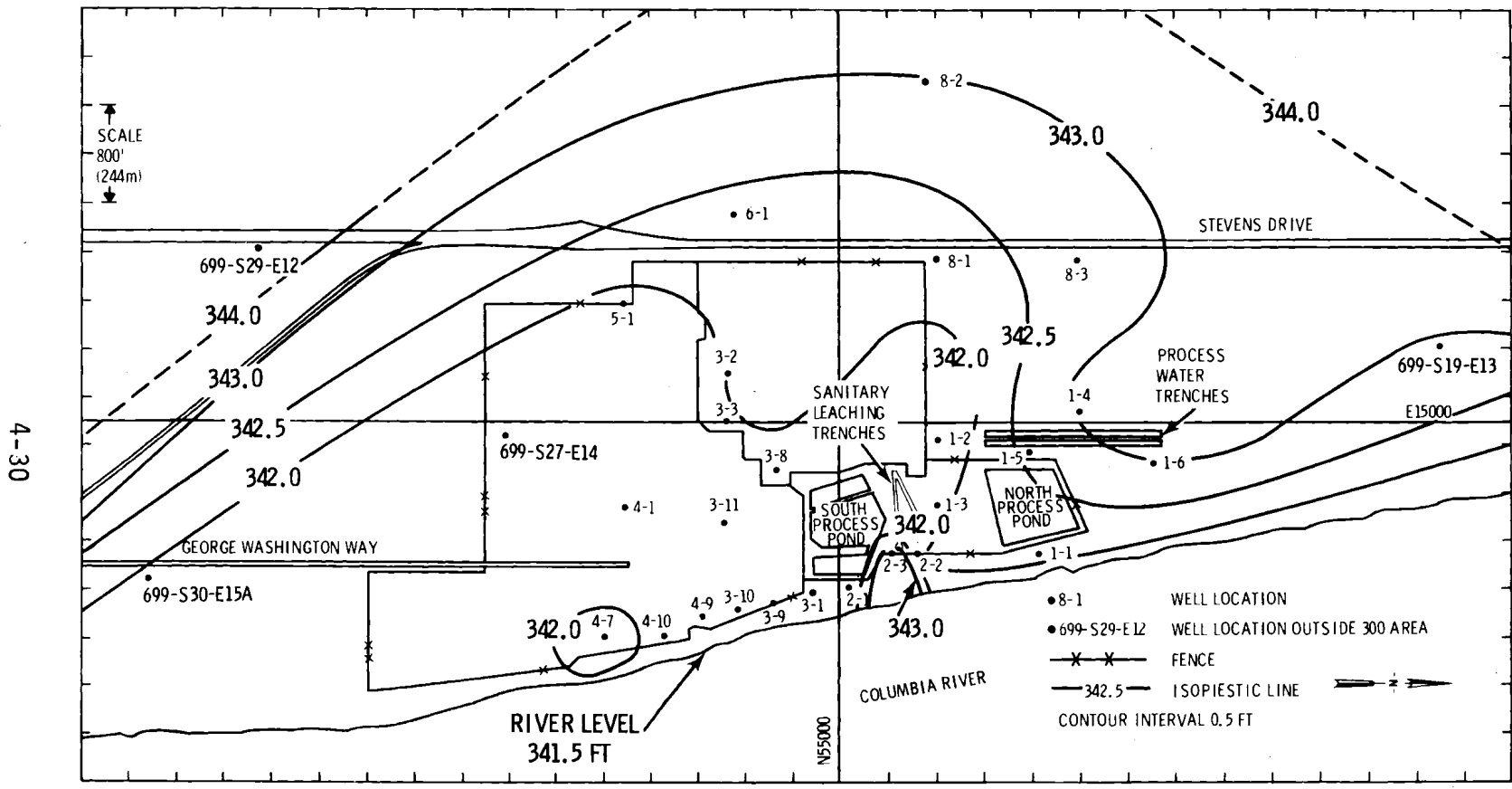


FIGURE 4.16. 300 Area Water-Table Map, February 16, 1977

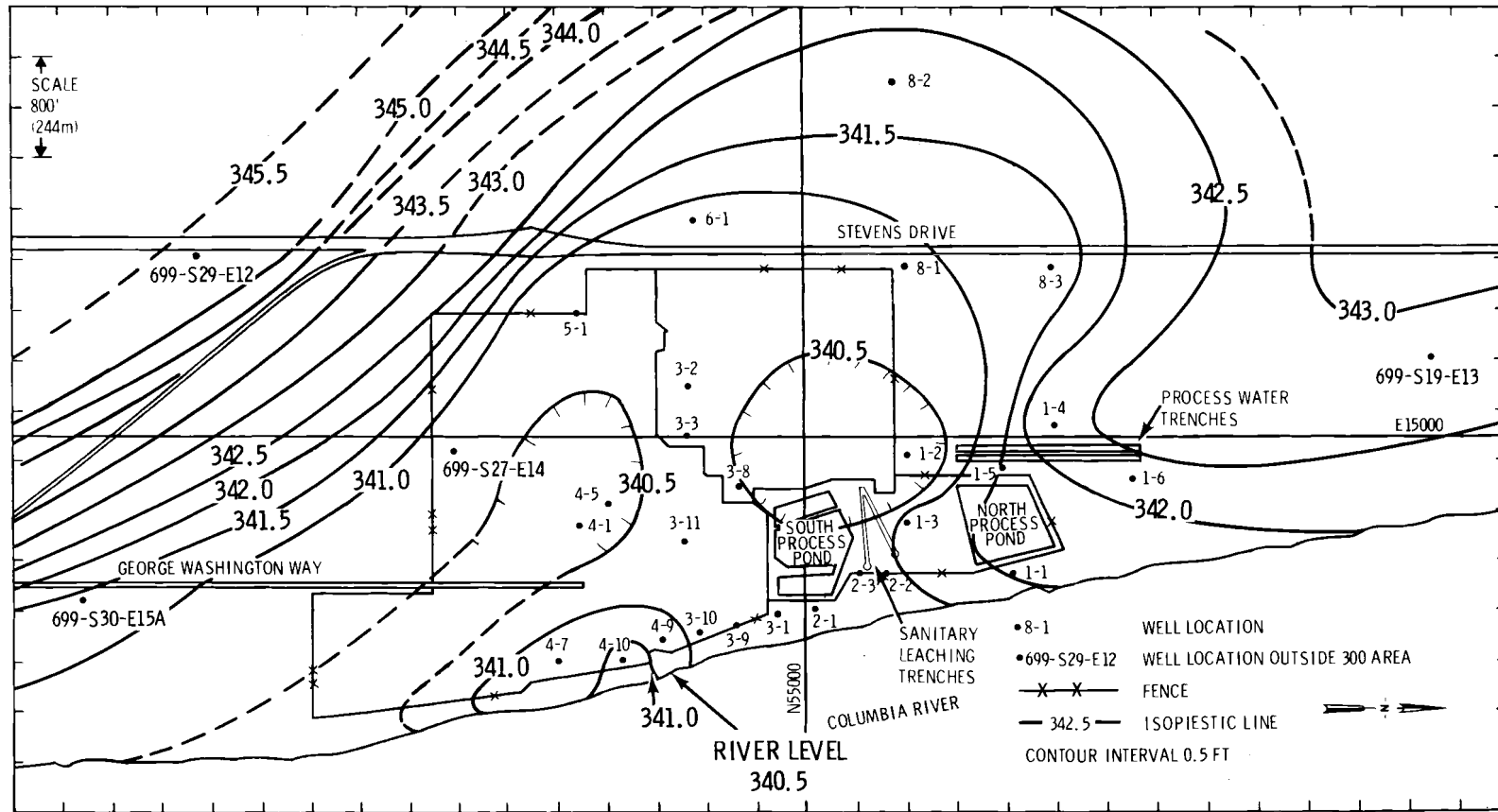


FIGURE 4.17. 300 Area Water-Table Map, July 15, 1977

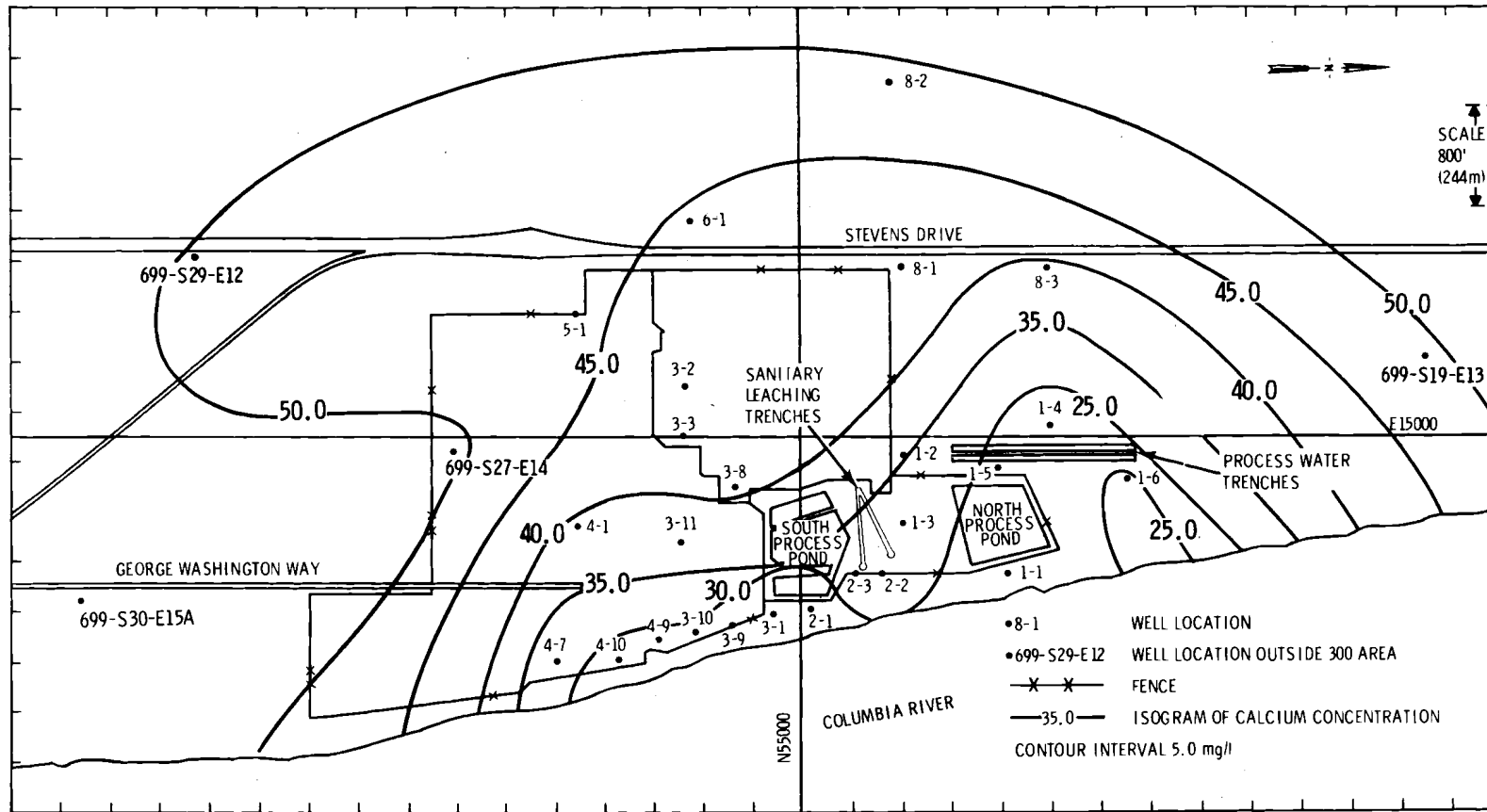


FIGURE 4.18. Calcium Concentration in the Unconfined Aquifer Under the 300 Area in May 1977 (background concentration approximately 50 mg/l)

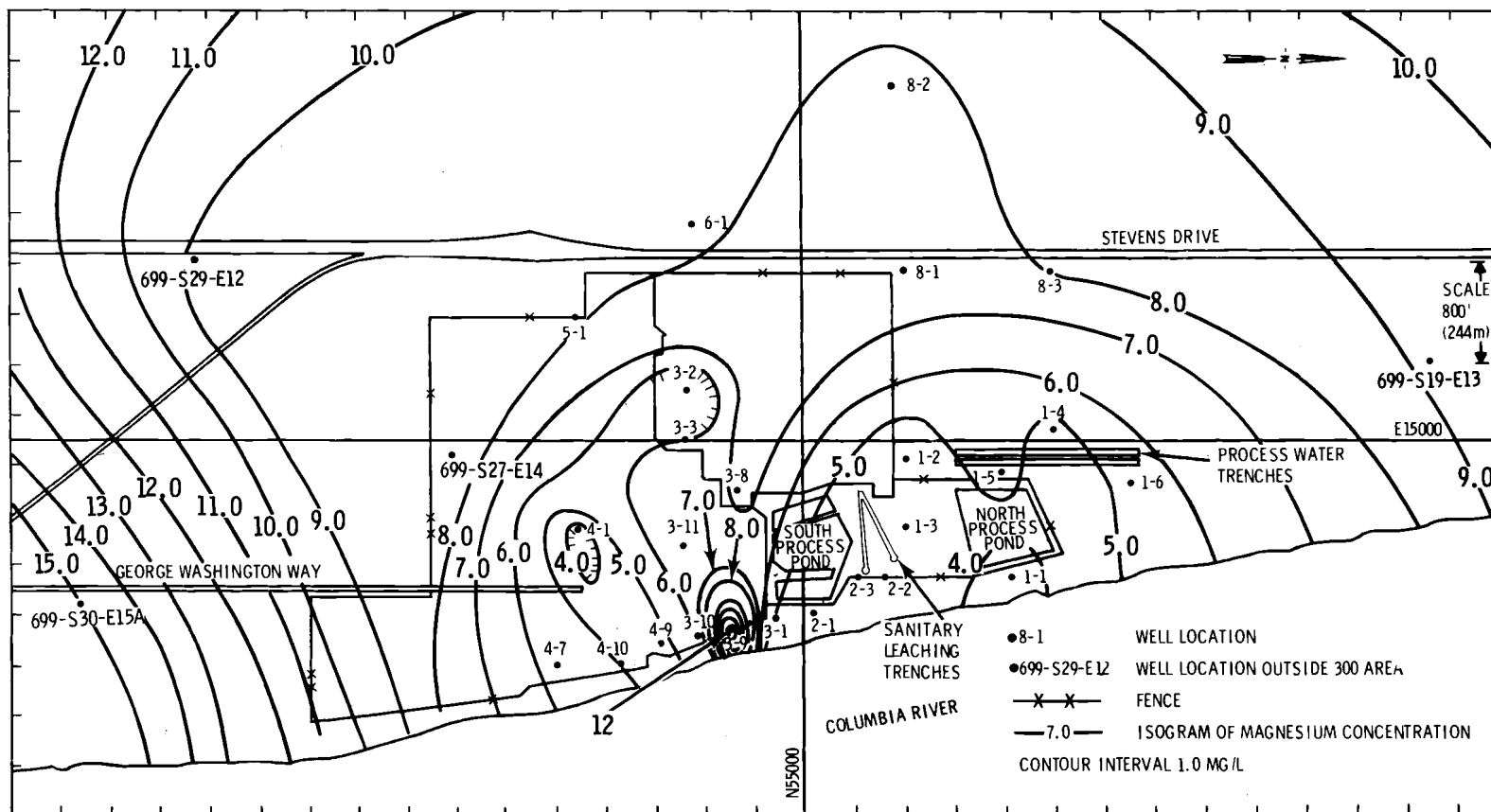


FIGURE 4.19. Magnesium Concentration in the Unconfined Aquifer Under the 300 Area in January 1977 (background concentration 8.0 to 15.0 mg/l)

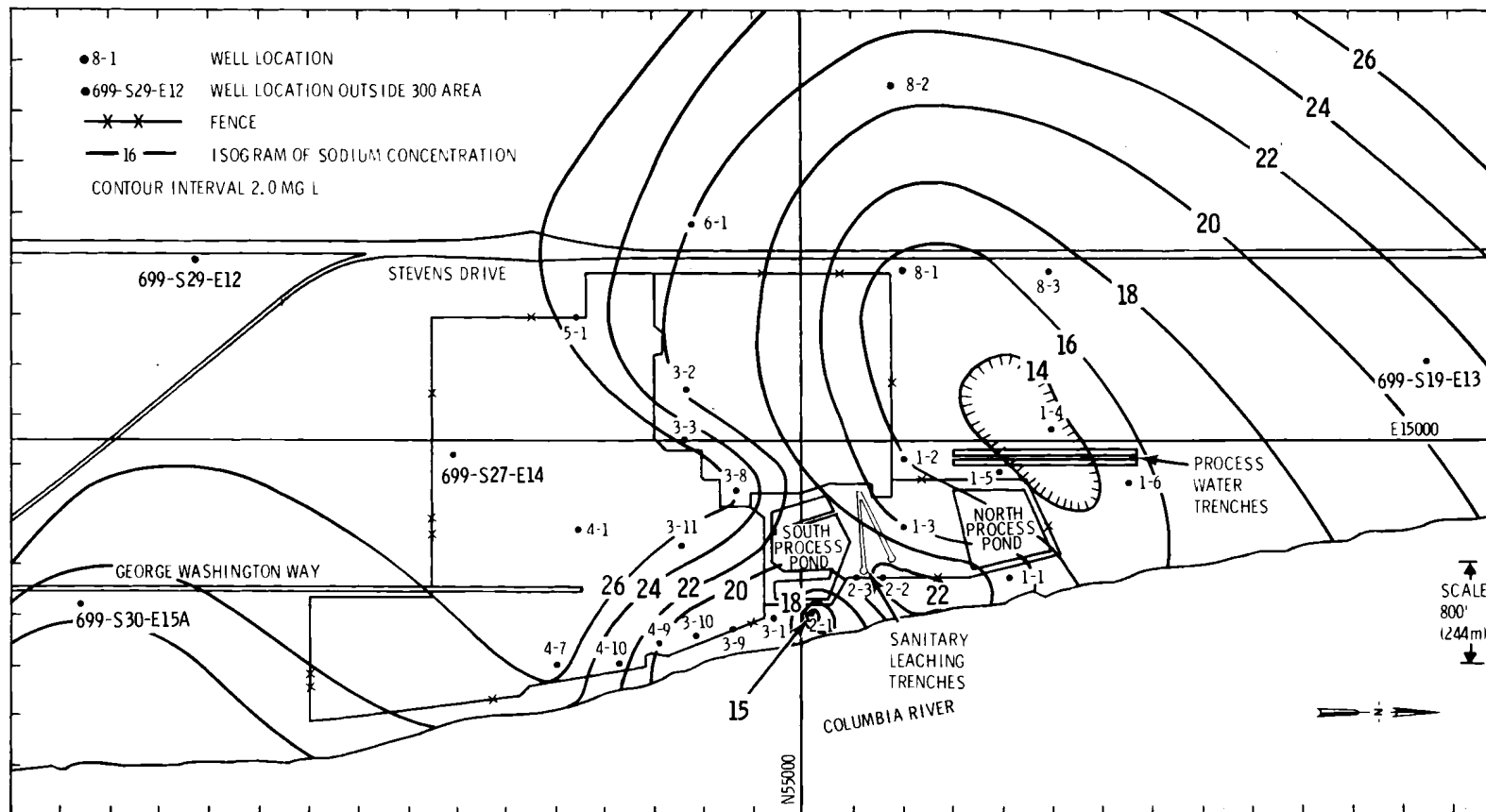


FIGURE 4.20. Sodium Concentration in the Unconfined Aquifer
 in the 300 Area in March 1977 (background concentra-
 tion approximately 26.0 mg/l)

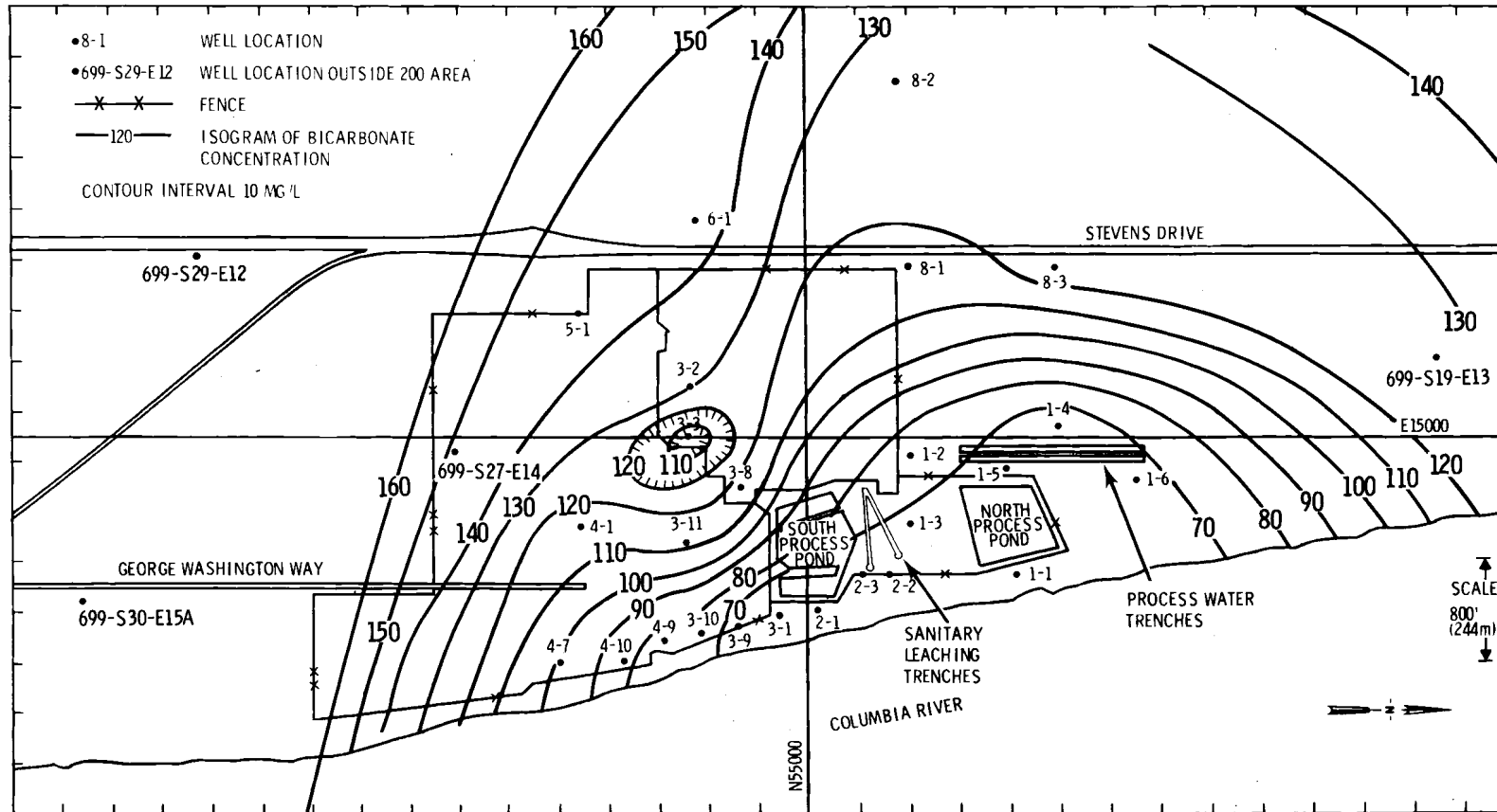


FIGURE 4.21. Bicarbonate Concentration in the Unconfined Aquifer Under the 300 Area in January 1977 (background concentration approximately 170.0 mg/l)

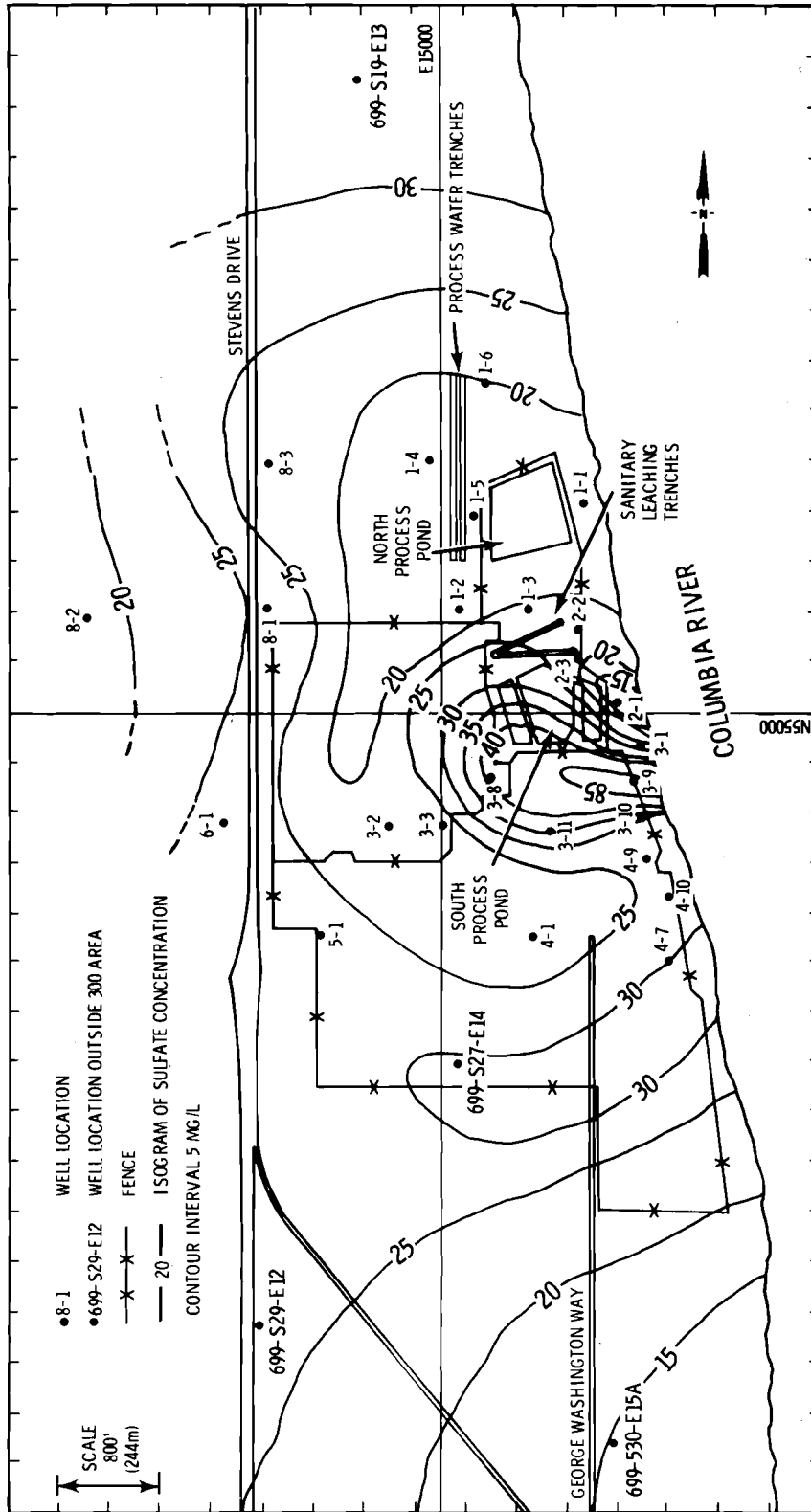


FIGURE 4.22. Sulfate Concentration in the Unconfined Aquifer Under the 300 Area in January 1977 (background concentration approximately 15.0 to 20.0 mg/l)

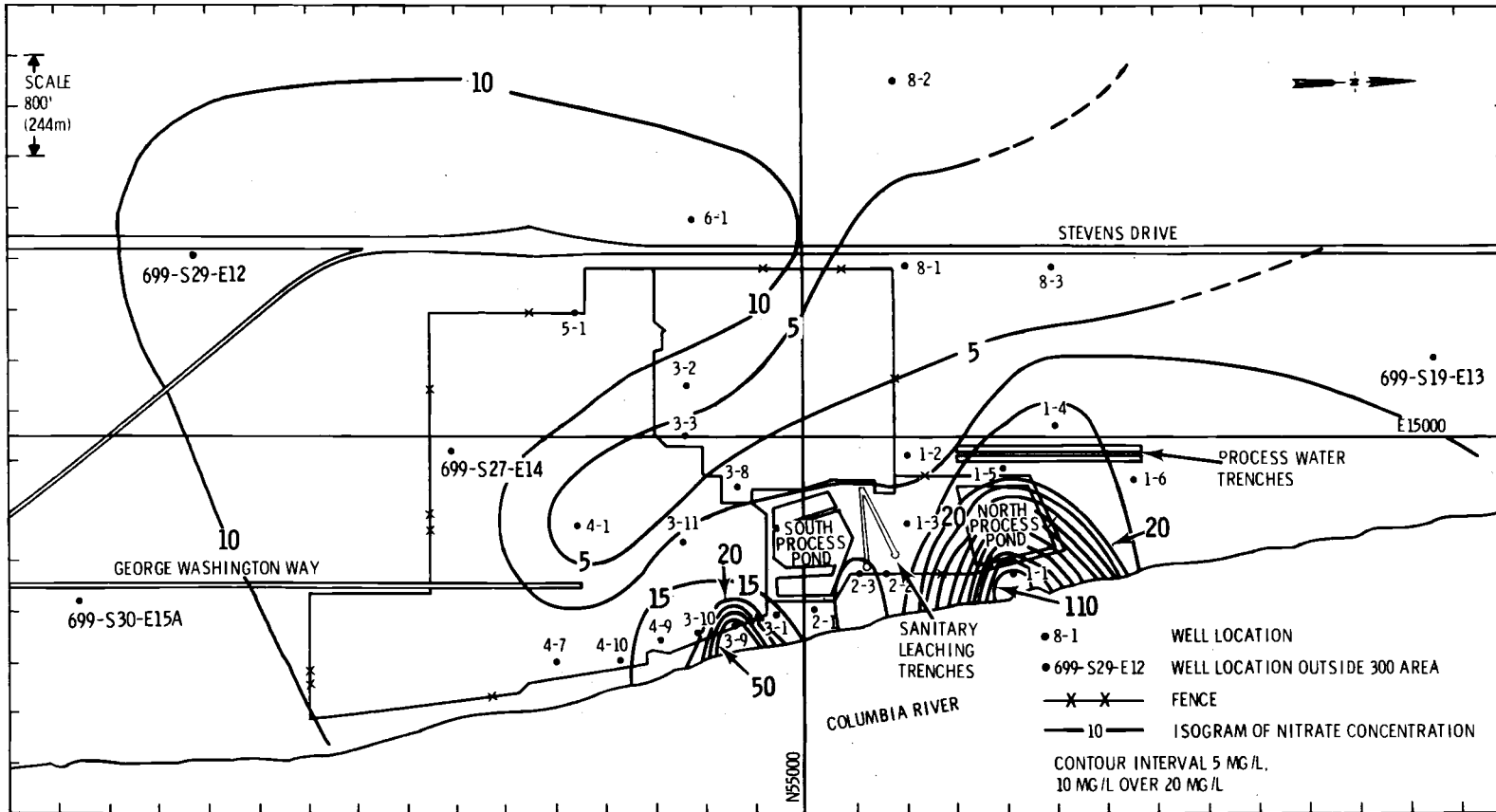


FIGURE 4.23. Nitrate Concentration in the Unconfined Aquifer Under the 300 Area in January 1977 (background concentration approximately 5.0 to 10.0 mg/l)

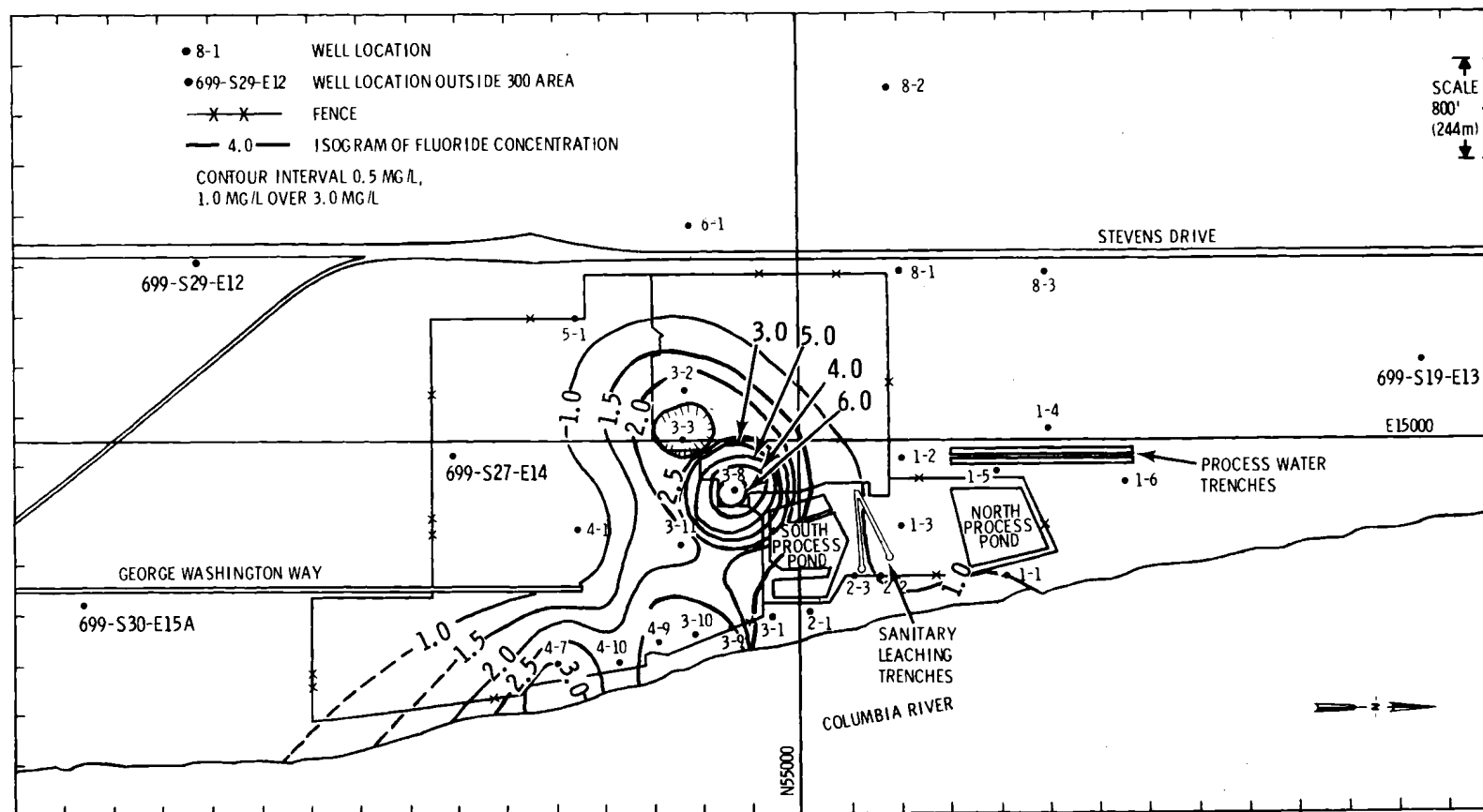


FIGURE 4.24. Fluoride Concentration in the Unconfined Aquifer Under the 300 Area in February 1977 (background concentration less than 0.1 mg/l)

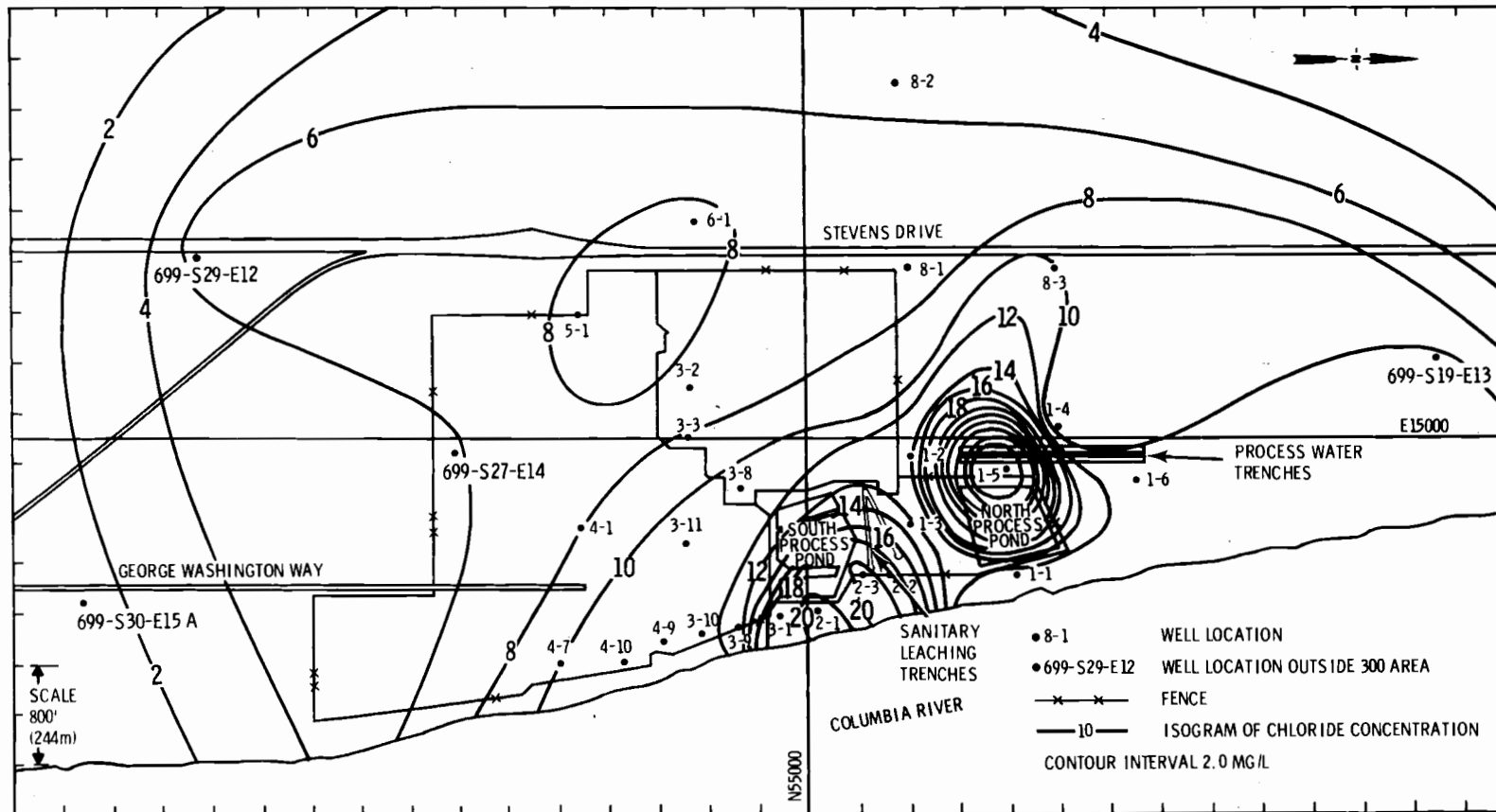


FIGURE 4.25. Chloride Concentration in the Unconfined Aquifer Under the 300 Area in January 1977 (background concentration approximately 2.0 to 4.0 mg/l)

most concentrated near the Sanitary Leaching Trenches and the Process Water Trenches. Uranium is most concentrated along the bank of the Columbia River between wells 1-1 and 4-7 (Figure 4.5). Beta emitters are most concentrated along the Columbia River from well 2-1 to 4-7 and near well 3-8, where leaks in the process sewer were discovered (Figure 4.7; Denham, 1970).

Interpretations of the 300 Area piezometric surface, ground-water temperature, and concentration of waste contaminants and natural dissolved solids indicated an anomalous input of water into the ground-water system near well 3-3. Near that well a mound or lobe (up to half a foot, approximately 15 cm) formed at the water table (Figures 4.8, 4.12-4.14, and 4.16). Well 3-3 is within the old Columbia River channel which was subsequently filled with very permeable glaciofluvial deposits (Figure 4.1). A ground-water mound no greater than a few inches (approximately 5 cm) would indicate a very significant amount of water discharged near that location.

Analyses of ground-water samples for contaminants and naturally occurring dissolved solids further supported an anomalous water discharge near well 3-3. Figures 4.5, 4.7, 4.19, and 4.21-4.24 show that the concentrations of contaminants and dissolved solids were diluted in comparison with concentrations found in surrounding wells.

Measured ground-water temperatures indicated an anomalous water discharge at well 3-3 and also suggested that the source of the water is the Columbia River. Figures 4.9 and 4.26 show temperatures of the unconfined aquifer beneath the 300 Area in winter and summer, respectively. Figure 4.27 shows temperature versus time curves for the Columbia River (measured at Richland) and for the unconfined aquifer at wells 8-2, 3-2, and 3-3. Well 8-2 is sufficiently west of the 300 Area where the unconfined aquifer is not affected by 300 Area processes. Wells 3-2 and 3-3 would be expected to have similar temperatures in the unconfined aquifer as well 8-2 if they were not influenced by leaking pipes. Because the unconfined aquifer at well 3-3 had cooler temperatures than well 8-2

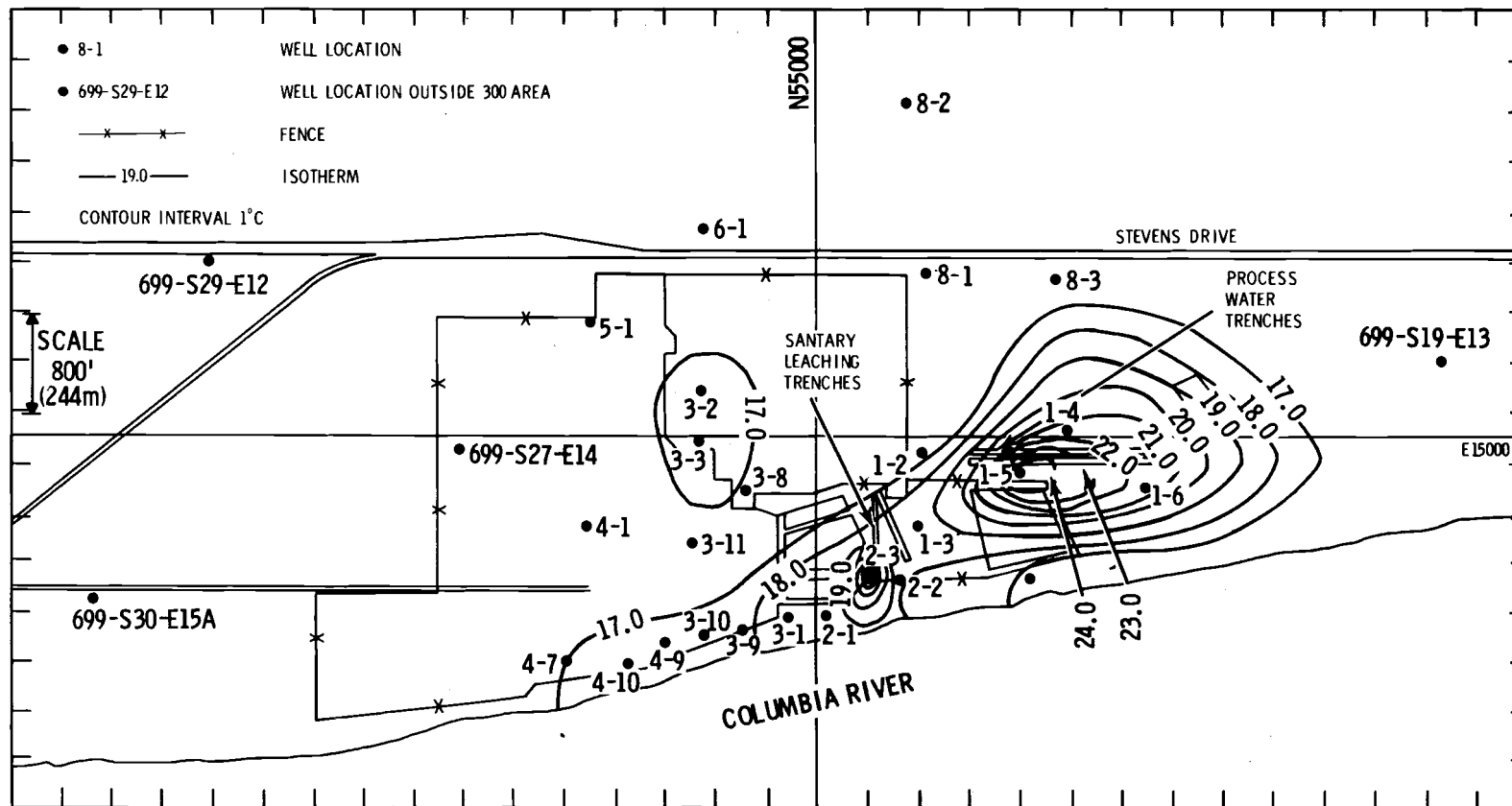


FIGURE 4.26. Temperatures in the Unconfined Aquifer Under the 300 Area, August 4, 1977

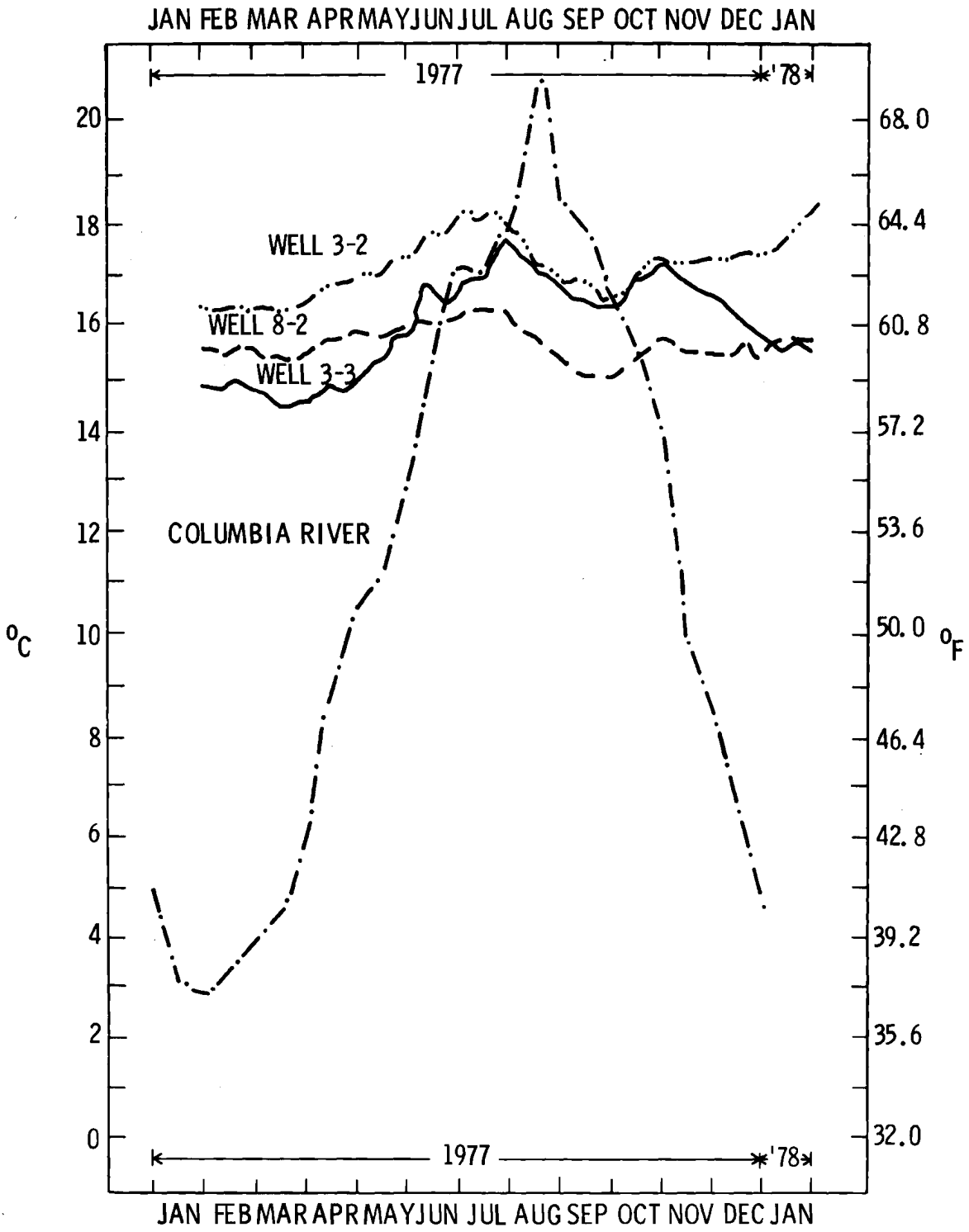


FIGURE 4.27. Temperatures in the Unconfined Aquifer at Wells 3-2, 3-3, and 8-2, and the Columbia River near Richland, Washington, during CY1977

from January to May 1977 and warmer than expected temperatures from June to December 1977, the unconfined aquifer at well 3-3 was possibly influenced by leaking pipes carrying Columbia River water. This variation correlated closely with Columbia River temperature variation (Figure 4.27).

Temperatures of the unconfined aquifer near well 3-3 were further complicated by a potential source of heat near well 3-2. Ground water in the unconfined aquifer near these wells flows from east to west (Figures 4.8, 4.11-4.14, 4.16, 4.17). A heat source near well 3-2 may be responsible for elevated temperatures in the unconfined aquifer near well 3-3 during October 1977 as well as higher than expected ground-water temperatures throughout CY1977 at well 3-2 (Figure 4.27). However, the heat source near well 3-2 (probably due to leaking pipes carrying steam condensate) is not the major source of temperature variation in the unconfined aquifer at well 3-3. The possible source of variation is leaking pipes probably carrying Columbia River water. Figure 4.27 shows that from October 1977 to January 1978 temperatures of the unconfined aquifer at well 3-2 remained warmer than expected (warmer than well 8-2) while temperatures of the unconfined aquifer at well 3-3 decreased until they were lower than temperatures recorded at well 8-2.

Many test wells are located close to trenches or ponds receiving waste water from 300 Area processes. Other test wells are located in a network throughout the 300 Area or along the Columbia River (base level of the unconfined aquifer). The Ground-Water Monitoring Program routinely samples the ground water for all suspected ground-water contaminants. Therefore, 300 Area test wells and the routine sampling schedule of the Ground-Water Monitoring Program are adequate to detect contamination from routine waste discharges or from accidental releases and leakage from waste discharge lines.

5.0 QUALITY ASSURANCE OF GROUND-WATER QUALITY ANALYSES

A system of verifying water test results was established to observe the quality of ground-water analyses by the laboratory testing ground water in the 300 Area. The quality of the ground-water analyses was checked by blind duplicate tests.

Two identical samples from one 300 Area well were delivered to the United States Testing Company (USTC), Richland, Washington, during the first month of ground-water testing for this study. One of the samples was labeled with the well number of another 300 Area well. Table 5.1 shows the results of the water analyses. Comparison of the duplicate tests shows that for the most part, the test results were within the analytical limits of accuracy.

Ground-water samples analyzed by USTC for this study were the sole source of data used to inventory and trace ground-water contaminants and naturally occurring dissolved solids. This decision was based on the following criteria:

- 1) A far greater number of ground-water samples collected for this study and analyzed by USTC were available than the routine ground-water analyses by the Ground-Water Monitoring Program.
- 2) Results of ground-water analyses of duplicate well samples (and samples collected from adjacent wells) that were analyzed by USTC for this study were in close agreement.

TABLE 5.1. Comparison of Duplicate Analyses by United States Testing Company

Analysis	Units	Results 399-8-2	Estimated Error	Results Duplicate	Estimated Error
Total alpha	pCi/l	2.50	0.73	1.69	0.63
Gross beta	pCi/l	5.39	2.9	6.79	3.2
Gamma scan					
⁵¹ Cr	pCi/l	-4.17 *	21	2.10 *	21
¹²⁵ Sb	pCi/l	-0.558	7.1	-.072*	7.1
¹⁰⁶ Ru	pCi/l	1.31 *	21	0.273*	21
¹³⁷ Cs	pCi/l	0.532*	1.5	0.009*	1.5
⁶⁰ Co	pCi/l	0.299*	1.4	0.007*	1.4
Uranium	pCi/l	2.41	2.0	2.69	2.0
Tritium	pCi/l	33.8 *	240	138 *	260
Bicarbonate	mg/l	126	5.0	129	5.0
Carbonate	mg/l	1.00 *	1.0	1.00 *	1.0
Calcium	mg/l	25.5	4.0	25.0	4.0
Magnesium	mg/l	7.30	1.5	5.30	1.5
Sodium	mg/l	19.0	2.0	19.0	2.0
Chloride	mg/l	5.50	1.0	5.75	1.0
Sulfate	mg/l	16.5	3.0	18.0	3.0
Nitrate	mg/l	7.75	1.8	8.86	1.8
Chromium	mg/l	0.01 *	0.01	0.01 *	0.01
Copper	mg/l	0.05 *	0.05	0.05 *	0.05
Potassium	mg/l	5.00	1.0	5.00	1.0
Fluoride	mg/l	0.05 *	0.1	0.05 *	0.1
Hardness	mg/l	93.7	8.0	94.1	8.0
Specific					
conductivity	mhos/cm	340	20	320	20
pH	-log H ⁺	7.60	0.2	7.60	0.2

* Result less than or equal to estimated error

6.0 VARIABLE THICKNESS TRANSIENT GROUND-WATER FLOW MODEL

A ground-water model describes mathematically the forces that determine movement and availability of water beneath the earth's surface. A model also acts as a storehouse for pertinent information gathered on the real system, and therefore, it incorporates all of the understanding of the interactions which are occurring in that system.

The model used for application to the 300 Area was the Variable Thickness Transient (VTT) Model (Kipp and others, 1972). The VTT Model was developed using the Boussinesq equation with appropriate initial and boundary conditions. This equation is derived by vertically averaging the three-dimensional equation governing incompressible, Darcian ground-water flow. Thus, the independent spatial variables are in the horizontal plane and the nonlinear, free-surface boundary condition is incorporated into the governing differential equation. All aquifer properties are represented by their average values over the vertical thickness of saturated flow. A significant capability of the mathematical model is that it can handle heterogeneous distributions of hydraulic conductivity and storage coefficient.

The model simulates the flow of an incompressible fluid that saturates a rigid, porous soil matrix. Compressibility effects of the fluid and matrix can safely be neglected under conditions of unconfined or free-surface flow. The hydraulic conductivity (K) is assumed to be isotropic but heterogeneous. Darcy's law is assumed to govern the flow:

$$\underline{q} = K\underline{\nabla}\phi \quad (6.1)$$

where

$$\phi = p/\gamma + z$$

and

\underline{q} = Darcy velocity

K = hydraulic conductivity

∇ = del operator
 ϕ = piezometric head
 p = hydrostatic pressure
 γ = specific weight
 z = elevation head

From the equation:

$$\nabla \cdot \rho(K\nabla\phi) = \rho \frac{\partial \rho}{\partial t}$$

where

ρ = density
 t = time

Mass continuity considerations for incompressible flow leads to:

$$\nabla \cdot \rho(K\nabla\phi) = 0 \quad (6.2)$$

with solutions that are potentials of the Poisson type. For heterogeneous, isotropic media with negligible soil and water compressibilities, the above equation becomes:

$$K\nabla^2\phi + \nabla K \cdot \nabla\phi = 0 \quad (6.3)$$

6.1 THE BOUSSINESQ EQUATION

The hydraulic theory of ground-water flow is suitable where streamlines are approximately parallel with little curvature as defined by the Dupuit-Forchheimer Theory. The dependent variable is the vertical distance to the free surface. The usual derivation of the partial differential equation from Equation (6.2) uses four assumptions: 1) the free surface $h(x,t)$ has only slight curvature; 2) the slope is small; 3) Darcy's law applies at any X,Y coordinate given by $v = K(\Delta h/\Delta x)$; and 4) the velocity at any cross section is essentially horizontal and constant. With these assumptions, the differential equation becomes:

$$\nabla \cdot K(h - h^0)\nabla h = \sigma \frac{\partial h}{\partial t} - q' \quad (6.4)$$

where $q' > 0$ is infiltration; the potential head $\phi(x,y,x,t)$ is replaced by the elevation of the free surface, $h(x,y,t)$; and ∇ is the two-dimensional (x,y) gradient operator.

Equation (6.4) is known as the Boussinesq (Boussinesq, 1963) equation of unsteady flow. The number of spatial dimensions has been reduced from 3 to 2 and all of the aquifer properties are represented by their averages over the total saturated thickness. The nonlinear free surface boundary condition has made the differential equation nonlinear, but the unknown surface configuration is now identical to the unknown dependent variable.

6.1.1 Boundary and Initial Conditions for the Boussinesq Equation

The partial differential equations of flow and continuity used in the VTT Model to describe saturated flow in an aquifer have an infinite number of solutions for any given set of aquifer bottom surface, hydraulic conductivity, and storage coefficient distributions. The solution is uniquely determined only when a particular set of boundary and initial conditions are established. The following boundary conditions are used in developing the mathematical model.

Water boundaries are approximated by vertical surfaces that must completely penetrate the entire saturated thickness of the aquifer. Along these boundaries the hydraulic potential (h) is:

$$h = H(x,y,t) \quad (6.5)$$

Impermeable boundaries are also approximated as vertical surfaces through which no flow occurs:

$$\frac{\partial h}{\partial n} = 0 \quad (6.6)$$

where n denotes the outward pointing normal to the boundary. Accretion caused by infiltration from above or seepage below has been imbedded into the differential equation itself as the term q' in Equation (6.4).

Infiltration across the lateral boundaries of the region is sometimes given as a specific flux across such vertical boundary surfaces. In this case, the boundary condition takes the form:

$$\underline{q} \cdot \hat{n} = -K(h - h^0) \frac{\partial h}{\partial n}$$

where n is defined above and $\underline{q} \cdot \hat{n} < 0$ means flow into the region. This condition is generally used in modeling an open aquifer region when some value of the flow from regions outside the simulated portion is assumed.

The free surface boundary condition with accretion is also incorporated into the differential equation. Surfaces of seepage had to be neglected to carry out the averaging in the vertical direction. Figure 6.1 shows a typical portion of an aquifer with the boundary conditions illustrated.

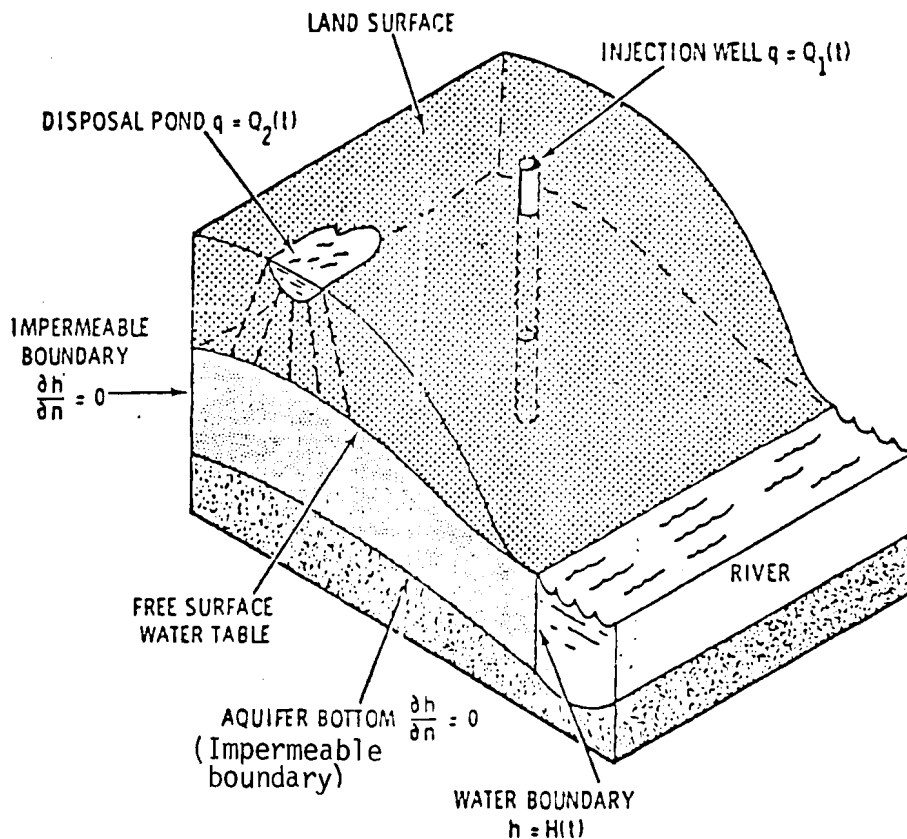


FIGURE 6.1. Illustration of an Unconfined Aquifer with Boundary Conditions

6.1.2 Boussinesq Equation Assumptions

The basic assumptions of the Boussinesq Flow Model for describing saturated unconfined flow may be summarized as follows:

- Flow is by an incompressible fluid that saturates a rigid, porous soil matrix.
- Compressibility effects of the fluid and soil matrix can be neglected under conditions of unconfined or free-surface flow; they are incorporated into the storage term for confined flow.
- Hydraulic conductivity and effective porosity can be represented by the vertical average values and are isotropic but heterogeneous throughout the region.
- The free-surface slope and the aquifer bottom slope are both assumed to be slight ($<5^\circ$).
- Vertical velocities are assumed to be small compared to horizontal velocities and can be neglected.
- Coefficient distributions and dependent variables are assumed continuous over the simulation region.
- Flow in the capillary fringe is neglected.
- Seepage surfaces cannot be handled and are therefore neglected.

6.2 NUMERICAL FORMULATION OF THE SYSTEM EQUATIONS

For numerical formulation, a horizontal x-y coordinate grid system was adopted with uniform nodal spacing of 250 ft (76.2 m). R represents the region of flow and r_{ij} the sub-area associated with node ij (Figure 6.2).

The differential equation, Equation (6.4), is then converted to finite difference form by integrating around the node area r_{ij} . Now:

$$\int_r \int_{ij} \left[\underline{\nabla} \cdot K(h - h^0) \underline{\nabla} h - \phi \frac{\partial h}{\partial t} + q' \right] dx dy = 0 \quad (6.7)$$

by Green's theorem in the first form (Kellogg, 1954):

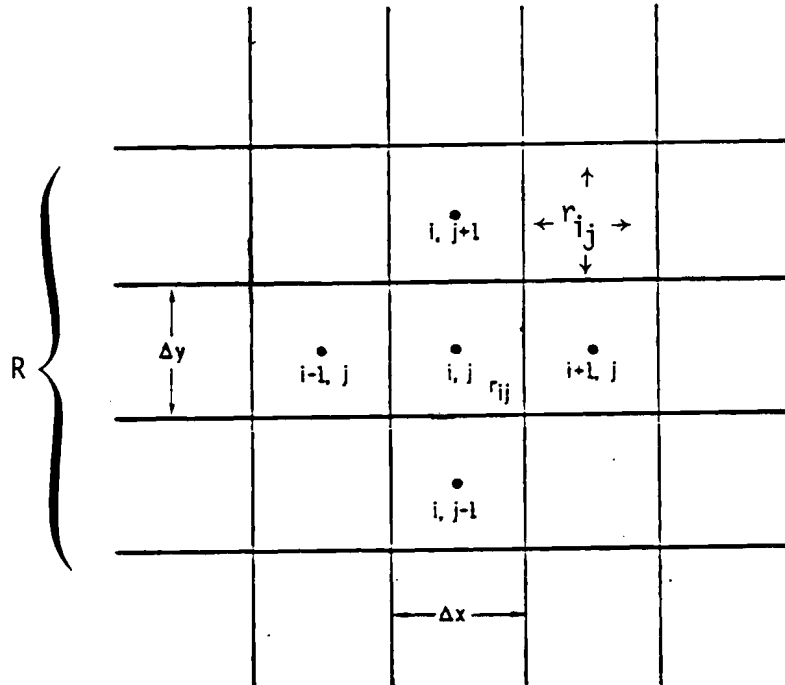


FIGURE 6.2. The Finite Difference Grid with the Nodal Numbering System

$$\int_r \int_{ij} \underline{\nabla} \cdot K(h - h^0) \underline{\nabla} h dx dy = \oint_{\Gamma_{ij}} K(h - h^0) \frac{\partial h}{\partial n} ds \quad (6.8)$$

where:

n denotes the outward pointing normal to the curve Γ which bounds the area r_{ij} . The line integral is taken in the counterclockwise direction. Using Equation (6.8), Equation (6.7) reduces to:

$$\int_{\Gamma_{ij}} K(h - h^0) \frac{\partial h}{\partial n} ds - \int_r \int_{ij} (\sigma \frac{\partial h}{\partial t} - q) dx dy = 0 \quad (6.9)$$

where s is distance and σ is the storage coefficient.

In Figure 6.2 the corner points of the node area are at $(i-1/2, j-1/2)$, $(i+1/2, j-1/2)$, $(i+1/2, j+1/2)$, and $(i-1/2, j+1/2)$. The area of r_{ij} is $\Delta x \Delta y$. The integrals of Equation (6.9) are approximated as follows with the integral along Γ_{ij} divided into the integrals along the four sides of r_{ij} :

$$\int_{i-1/2, j-1/2}^{i+1/2, j-1/2} K(h - h^0) \frac{\partial h}{\partial n} dx \approx (K\Delta h)_{i, j-1/2} \frac{h_{ij} - h_{i, j-1}}{-\Delta y} \Delta x \quad (6.10a)$$

$$\int_{i+1/2, j-1/2}^{i+1/2, j+1/2} K(h - h^0) \frac{\partial h}{\partial n} dy \approx (K\Delta h)_{i+1/2, j} \frac{h_{i+1, j} - h_{ij}}{\Delta x} \Delta y \quad (6.10b)$$

$$\int_{i+1/2, j+1/2}^{i-1/2, j+1/2} K(h - h^0) \frac{\partial h}{\partial n} dx \approx (K\Delta h)_{i, j+1/2} \frac{h_{i, j+1} - h_{ij}}{\Delta y} \Delta x \quad (6.10c)$$

$$\int_{i-1/2, j+1/2}^{i-1/2, j-1/2} K(h - h^0) \frac{\partial h}{\partial n} dy \approx (K\Delta h)_{i-1/2, j} \frac{h_{ij} - h_{i-1, j}}{-\Delta x} \Delta y \quad (6.10d)$$

$$\iint_{ij} \left(\sigma \frac{\partial h}{\partial t} - q \right) dx dy \approx \sigma_{ij} \frac{h_{ij}^n - h_{ij}^{n-1}}{\Delta t} \Delta x \Delta y - q_{ij} \Delta x \Delta y \quad (6.10e)$$

where:

Δt = time increment, and

$(K\Delta h)_{i, j-1/2} = [1/2 K_{ij} (h_{ij}^n - h_{ij}^0) + K_{i, j-1} (h_{i, j-1}^n - h_{i, j-1}^0)]$, etc.

A fully implicit representation of the time derivative has been used in Equation (6.10e). Combining the above approximations results in the finite difference approximation to the Boussinesq equation for a square grid system, $\Delta x = \Delta y$:

$$\begin{aligned} & -(K\Delta h)_{i-1/2, j} h_{i-1, j}^n + \left[(K\Delta h)_{i-1/2, j} + (K\Delta h)_{i+1/2, j} + (K\Delta h)_{i, j-1/2} \right. \\ & \left. + (K\Delta h)_{i, j+1/2} + \sigma_{ij} \frac{(\Delta x)^2}{\Delta t} \right] h_{ij}^n - (K\Delta h)_{i+1/2, j} h_{i+1, j}^n \\ & = (K\Delta h)_{i, j+1/2} h_{i, j-1}^n + (K\Delta h)_{i, j+1/2} h_{i, j+1}^n + \sigma_{ij} \frac{(\Delta x)^2}{t} h_{ij}^{n+1} \\ & \quad Q_{ij}^{n-1} (\Delta x)^2 \end{aligned} \quad (6.11)$$

For nodes on boundaries along which the hydraulic potential is specified in time and space (and therefore no calculation is needed), let:

$$h_{ij}^n = H_{ij}^n \quad (6.12)$$

where H is the water elevation at the boundary.

The impermeable boundaries of the region must be approximated in the grid system by shapes selected from Figure 6.3. This avoids right angles which cause stagnation points and singularities in the mathematical solution of the ground-water flow equation.

The boundary conditions are put into finite difference form by applying the technique described above to a node area at the boundary of the region R . The boundary types are illustrated in Figure 6.3 and the associated nodal area r_{ij} can be either inside or outside the octagon. The finite difference equations are derived by setting the appropriate portions of the integral on Γ_{ij} in Equation (6.8) to zero when the segment is impermeable, and by inputting $q'_{ij} = \underline{q}_{ij}$ when the flux across the segment is specified. In finite difference form, 24 different equations correspond to each of the different boundary point subregions illustrated in Figure 6.3. Either a specified flux or no flow can be imposed by each of the 24 equations. The accretion term, whether infiltration or withdrawal, in finite difference form becomes $Q_{ij} = q_{ij}(\Delta x)^2$ (units L^3/T) to be specified at each node. Accretion at the fractional boundary nodes must have the nodal area properly reduced from $(\Delta x)^2$.

The partial differential equation and boundary conditions subsequently become a set of N finite difference equations, one for each node of the region R being modeled. The boundary conditions have been effectively absorbed into the equations for their respective boundary nodes.

To facilitate the marking of calculational boundary types a systematic method of representing interior, exterior and boundary nodes was adapted. There are basically four nodal types, others simply arise to handle the various shapes and orientations of the impermeable boundaries.

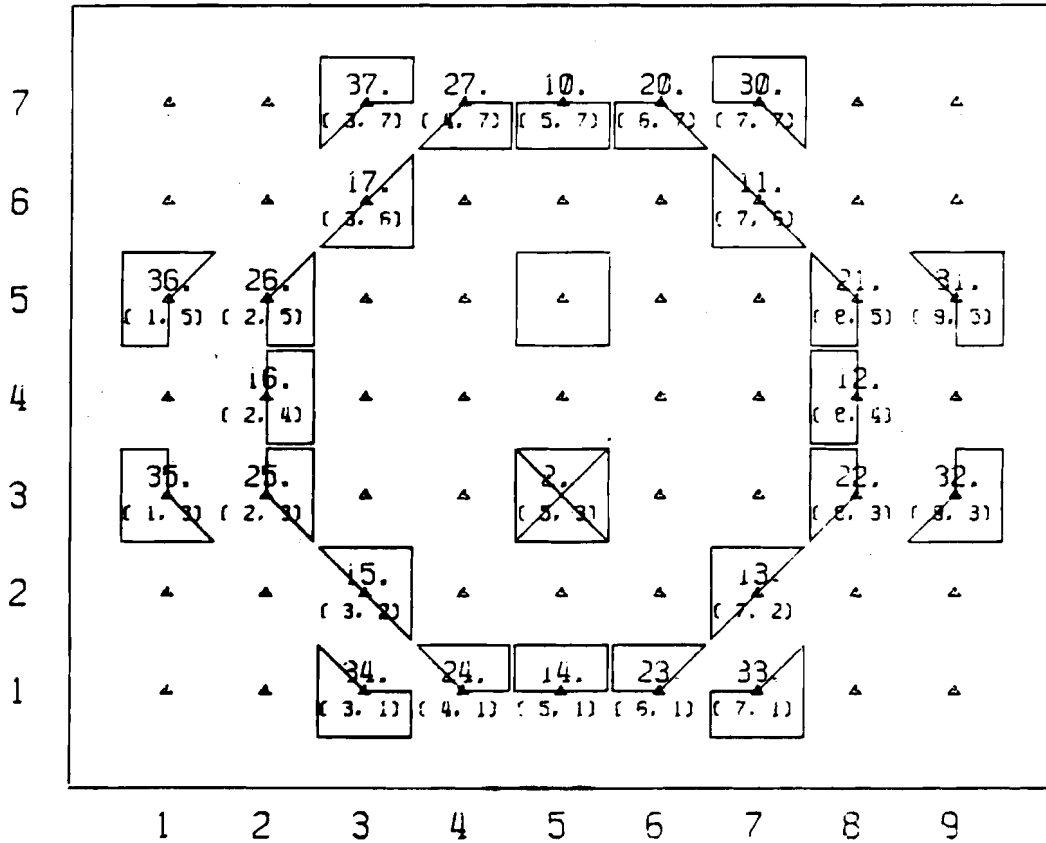



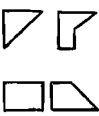


FIGURE 6.3. Schematic Showing Shapes and Rotation of Available Boundary Condition Types

-  is a water boundary, i.e., held potential boundary node [$h = H(x,y,t)$].
-  is an external node outside of the aquifer.
-  is an internal or nonboundary node which lies within the aquifer.
-  these basic shapes with all their possible rotations are used to represent the 24 kinds and shapes of impermeable boundary nodes.

It should be noted that the finite difference equations can be derived in the same form by other techniques, such as Taylor series expansions. The equations for nodes on impermeable boundaries are equivalent to those obtained by introduction of a point external to the region for purposes of forming the normal derivative.

6.3 CALCULATION PROCEDURE

Different procedures are used in solving the transient and steady-state equations. The transient form of the finite difference equation is solved by a successive line over relaxation technique. The steady-state form of the equation is solved by a Newton's method with a direct solution technique since it produces a rapidly converging sequence of iterations and is relatively easy to apply to the system of equations.

6.4 DATA REQUIREMENTS

Simulation of the system requires segmenting the physical continuum into a discrete grid. Each grid segment is then represented by a single node within the model. The VTT Model uses a finite difference algorithm with a uniform grid and requires that each node within the Cartesian coordinate system be marked with a calculation type as:

1. within the aquifer
2. external to the aquifer
3. a water or held potential boundary node [$h = H(x,y,t)$]
4. an impermeable boundary for the aquifer with $q = 0$ (aquifer boundary nodes, where the flux is known, are treated as the mathematical equivalent to an impermeable boundary node with the appropriate accretion term; i.e., $q \neq 0$).

All parameters defining the aquifer system are evaluated and assigned to each node and are considered representative of the whole cell. These model parameters are made into data files accessible to the computer. The following is a list of the parameters and their associated units.

1. altitude of the land surface (feet above mean sea level)
2. altitude of top of the regional aquifer for confined systems (feet above mean sea level)
3. altitude of the bottom of the aquifer (feet above mean sea level)
4. initial potentiometric surface of the aquifer (feet above mean sea level)

5. transmissivity of the aquifer (L^2/T) or hydraulic conductivity (ft/day)
6. storage coefficient (dimensionless)
7. recharge from precipitation (L^3/T)
8. pumping rate, (L^3/T)
9. river stage (feet above mean sea level).

Since a deterministic model attempts to provide an approximation of the real world by utilizing real world physical data, the list of parameters 1 through 7 needs to be defined for each node in the model and 8 and 9 where they apply. Realizing that a given model may contain several hundred to several thousands of nodes this may appear to be an impossible task. However, the job is simplified somewhat by geologic mapping, digitizing techniques and block data entries.

The land surface represents the upper limit to which the water in an aquifer can rise before becoming a surface water body, i.e., spring, stream or lake. These data are most easily obtained from topographic contour maps. The top of the regional confined aquifer would have to be mapped using drilled wells or geophysical techniques, i.e., seismic, etc. The aquifer bottom is generally mapped from drilled wells, and geophysical exploration and surface features such as bedrock outcrops.

Similarly, the potentiometric surface is generally mapped by contouring water level measurements taken from wells and observing physical constraints imposed by nature. For example, the surface must be smooth and continuous and the potential must intersect impermeable boundaries at right angles unless severe transients are in progress.

The transmissivity and/or hydraulic conductivity are the most difficult and expensive parameters to obtain for a model. They are generally measured by pump testing wells under controlled conditions. Although transmissivity can be inferred from specific capacity tests, the data collected are generally inadequate for accurate transmissivity calculations. Under certain conditions of potential gradients and converging streamlines, available transmissivity data can be input to a model and the

inverse problem can be solve to realize a continuously variable transmissivity for the entire system. These cases are rare and the general method used to treat this parameter is to block conductivities into model areas based on the amount of data available and the confidence placed in the data.

The transmissivity, expressed in feet squared per day (ft^2/day), is the product of the hydraulic conductivity, expressed in feet per day, and the saturated thickness, expressed in feet. Stated in other terms, the transmissivity is the rate at which water of the prevailing kinematic viscosity is transmitted through a unit width of the aquifer under a unit hydraulic gradient (Lohman, 1972).

For artesian, or confined, aquifers, the transmissivity remains constant as long as the hydraulic head is not lowered beneath the top of the aquifer. In this instance, the saturated thickness remains the same and is calculated in the program as the difference between aquifer top and aquifer bottom. In water-table, or unconfined, aquifers, the transmissivity changes in direct proportion to changes in the saturated thickness of the aquifer. The saturated thickness is calculated by the computer as the difference in altitude between the water table and the aquifer bottom. The computer program checks the changes in saturated thickness at every node for each iteration and recalculates the transmissivity. Thus, in a dynamic water-table aquifer with variable stresses imposed on it, the values of transmissivity are continuously changing. Calculation of changes in transmissivity by conventional analytical methods would be impossible.

Like transmissivity, the storage coefficient is a parameter obtained from pump testing the aquifer. Storage coefficient is defined as the volume of water an aquifer releases from or takes into storage per unit surface area of the aquifer per unit change in head (Lohman, 1972). It too is allowed to vary in the x and y directions and can be mapped or blocked into the model.

Aquifer stress is a measure of the volume of water being removed by pumping the aquifer on a node-by-node basis. Rainfall provides most of the water recharged to an aquifer either by direct infiltration or seepage from lakes and streams. Direct infiltration from rainfall is the amount of water left after evaporation from the surface, transpiration by the plants, and runoff have reduced the rainfall volume. To some degree the factors affecting the amount of rainfall infiltration depend on vegetation types, soil types, slope, temperature and land use. Another source of recharge comes from leakage across the aquifer boundaries.

An option available in the computer program permits simulation of aquifer systems which are confined in some areas and unconfined in others. If the aquifer is under water-table conditions, data sets are required for the aquifer hydraulic conductivity, the altitude of the bottom of the aquifer, and the hydraulic head in the aquifer. For the part of the aquifer system that is artesian, data sets are required for the aquifer hydraulic conductivity and the altitude of the bottom and of the top of the aquifer.

No single parameter in a model is more sensitive than the stress (recharge/discharge). In the model stress is treated by summing all fluxes, plus or minus, into one value for each node in the system.

7.0 DEVELOPMENT OF 300 AREA VTT GROUND-WATER FLOW MODEL

The procedure for developing a ground-water flow model for a particular region of interest can be outlined as follows:

1. Determine the boundary conditions, the finite difference grid and the initial conditions.
2. Interpret and refine the raw data for input to the model.
3. Calibrate and validate the model.

7.1 MODELING CONDITIONS

7.1.1 Boundary Conditions and Finite Difference Grid

The 300 Area model region (small region) exists as a subregion within the much larger Hanford Project VTT model region (large region) as shown in Figure 7.1. The large region model was used to simulate the Hanford Project ground-water system. This model is operational at PNL and was used as it currently exists. The subregion modeling capability of VTT, which runs in conjunction with the large region model, was used to develop a model for the 300 Area. The advantage of developing a subregion model, as opposed to just modeling the smaller region separately, is that the large region model can be run to provide the boundary conditions to the subregion. When working with the subregion, the finite difference node spacing can be reduced, thereby increasing the resolution and accuracy of the model results for that area.

The procedure for obtaining the small region boundary conditions is to first run the large region model and then interpolate between large region potentials, as defined at the nodes, to obtain values at the closer spaced small region nodes. The small region model is then run with the boundary nodes held constant at these interpolated potential values. For transient model runs, where the potentials change with time, the subregion boundary conditions change from time step to time step but are constant for the duration of each time step.

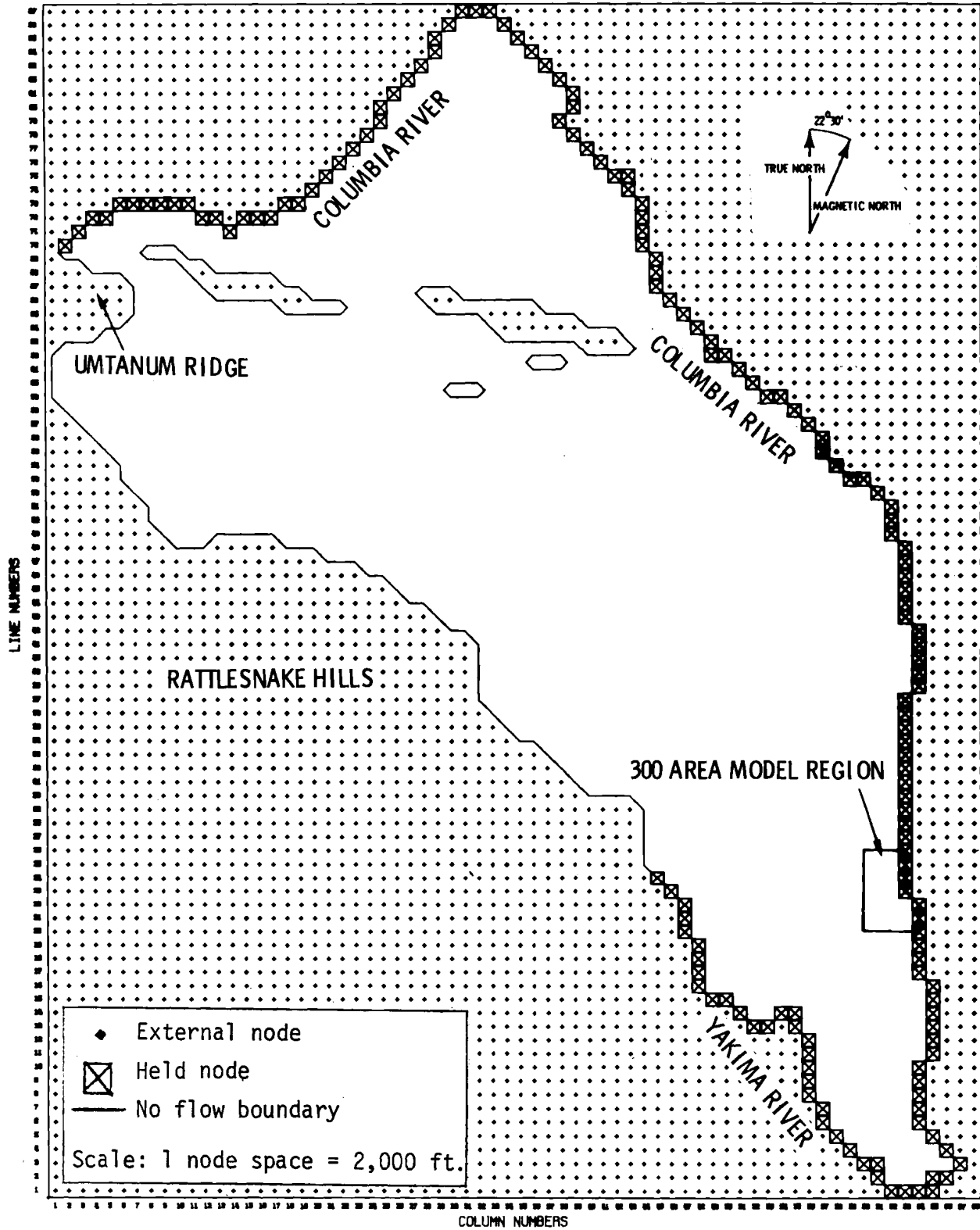


FIGURE 7.1. VTT Boundary Conditions (Calculational Types) for the Hanford Project Model Region

The Hanford Project Model boundary conditions used in this study are defined in BNWL-1703 (Kipp and others, 1972). In brief, the large region model consists of a 68 by 87 node grid with a 2000 ft node spacing. The boundaries consist of held potentials along the Columbia and Yakima Rivers and a no-flow boundary along the basalt outcrop that forms the Rattlesnake Hills and the Umtanum Ridge (Figure 7.1).

The small region was defined as the area between large region nodes 60 to 64 in the east-west direction and nodes 20 to 26 in the north-south direction (Figures 7.1 and 7.2). The small region consists of a 33 by 49 node grid with a 250-ft (76.2 m) spacing.

The subregion boundary conditions at the north, south and west boundaries are defined by the large region ground-water potentials. The east boundary is defined by the Columbia River. Direct interpolation between nodes from the large region to the small region yields a very rough interpretation of the Columbia River boundary as shown in Figure 7.2(a). As a result, the subregion boundary nodes were adjusted to better simulate the path of the Columbia River as shown in Figure 7.2(b).

The model requires that the Columbia River stage be specified at each river node. The time variation of the Columbia River elevation profile was predicted by a computer routine which used a fit curve of historical river stage versus river flow rate values. The releases from Priest Rapids Dam (just above the Hanford Site) were used to calculate a weekly average river flow rate which in turn was used to calculate the average Columbia River stage for each of the 300 Area river nodes.

7.1.2 Initial Conditions

The initial conditions consist of the initial value (time zero) of the dependent variable (i.e., potential, or elevation of the ground water above sea level) as defined at each interior node of the model region. The initial potential surface was defined from water level measurements taken on a weekly basis at 29 wells within the model region. Readings for the first week were contoured, digitized, and input to the model at the

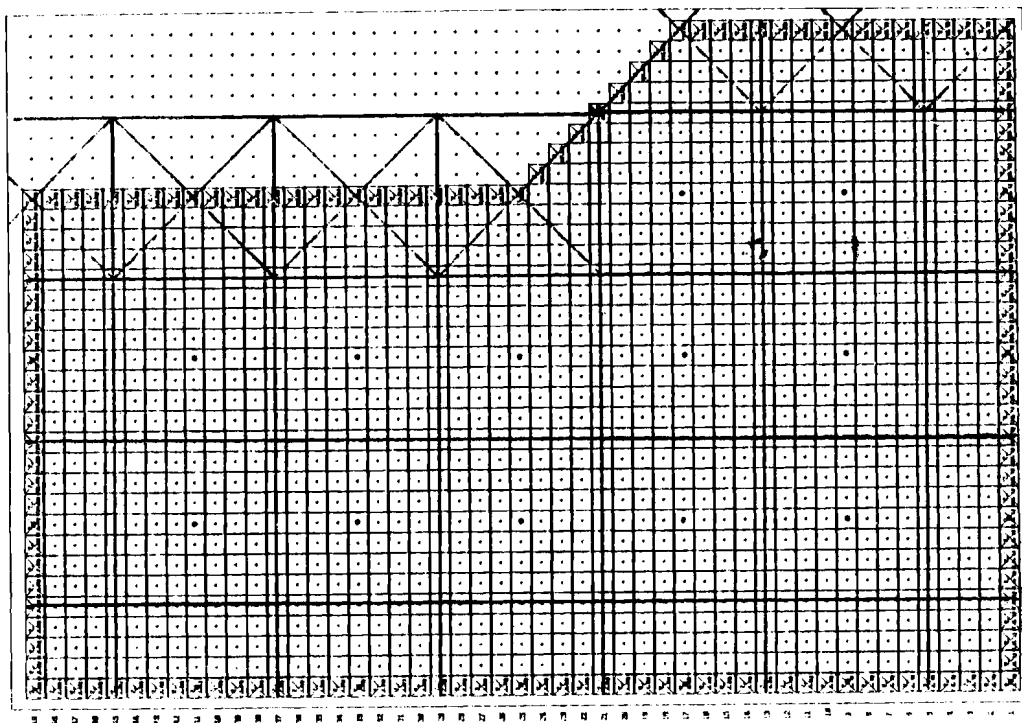
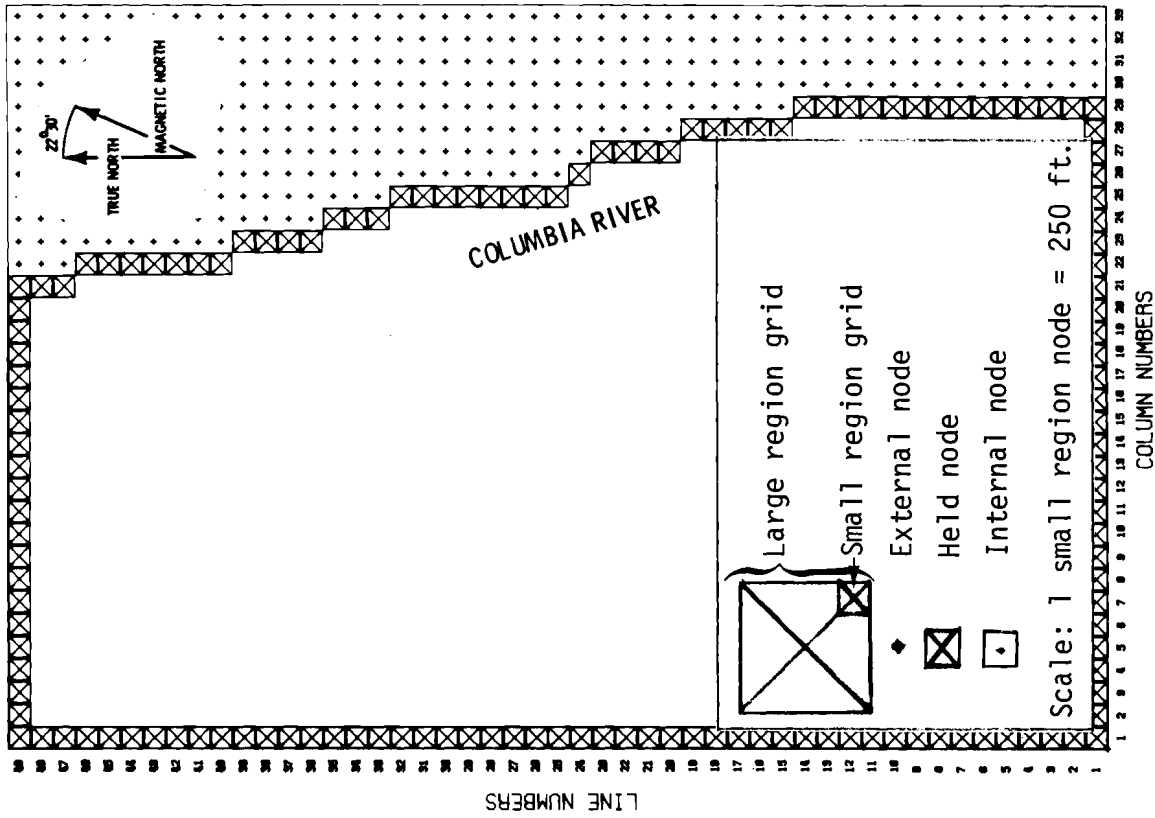


FIGURE 7.2. VTT Boundary Conditions for the 300 Area Model Region
 (a) Direct Interpolation from Large to Small Region,
 (b) Adjusted Columbia River Boundary

nodes. The model was then run in the transient mode on a weekly basis and comparison were made between measured and modeled results. Initial conditions for the Hanford Site and the 300 Area are shown in Figures 7.3 and 7.4, respectively.

7.2 DATA INPUT TO THE MODEL

7.2.1 Recharge and Discharge

The VTT model can simulate all types of recharge to or discharge from the ground-water system. Natural recharge to the 300 Area consists of rainfall, underflow (ground-water flow) from the Hanford Site to the west, and/or underflow from the Columbia River to the east (depending on river stage). Natural discharge results from evapotranspiration. It was assumed that any rainfall input is cancelled by evapotranspiration. This is a safe assumption considering that the average annual potential evapotranspiration [~ 30 - 60 in./yr (76.2 - 152.4 cm/yr)] exceeds the average annual precipitation [6.3 in./yr (16.0 cm/yr)] by a factor of at least 5 (Wallace, 1978). The underflow to the region is calculated by the large region model and incorporated into the small region model in terms of head potentials defined at the boundary nodes.

There exists a significant amount of artificial recharge to the 300 Area consisting mainly of waste water which is being released into leaching ponds or trenches at five specific sites. The only artificial discharge is a single supply well located in the 309 building. The well was only pumped for about half of one month (July) during the study. Table 7.1 contains a list of artificial recharge and discharge sites. These sites are identified on the map shown in Figure 3.1. Locations in Table 7.1 are listed in terms of X, Y coordinates (in feet from the small region lower-left-hand corner) and in terms of the small region nodes to which the recharge/discharge was applied. Table 7.2 shows the amounts of recharge, by month, for the time period modeled. Table 7.3 shows the daily withdrawal schedule for the month of July for the single pumped well.

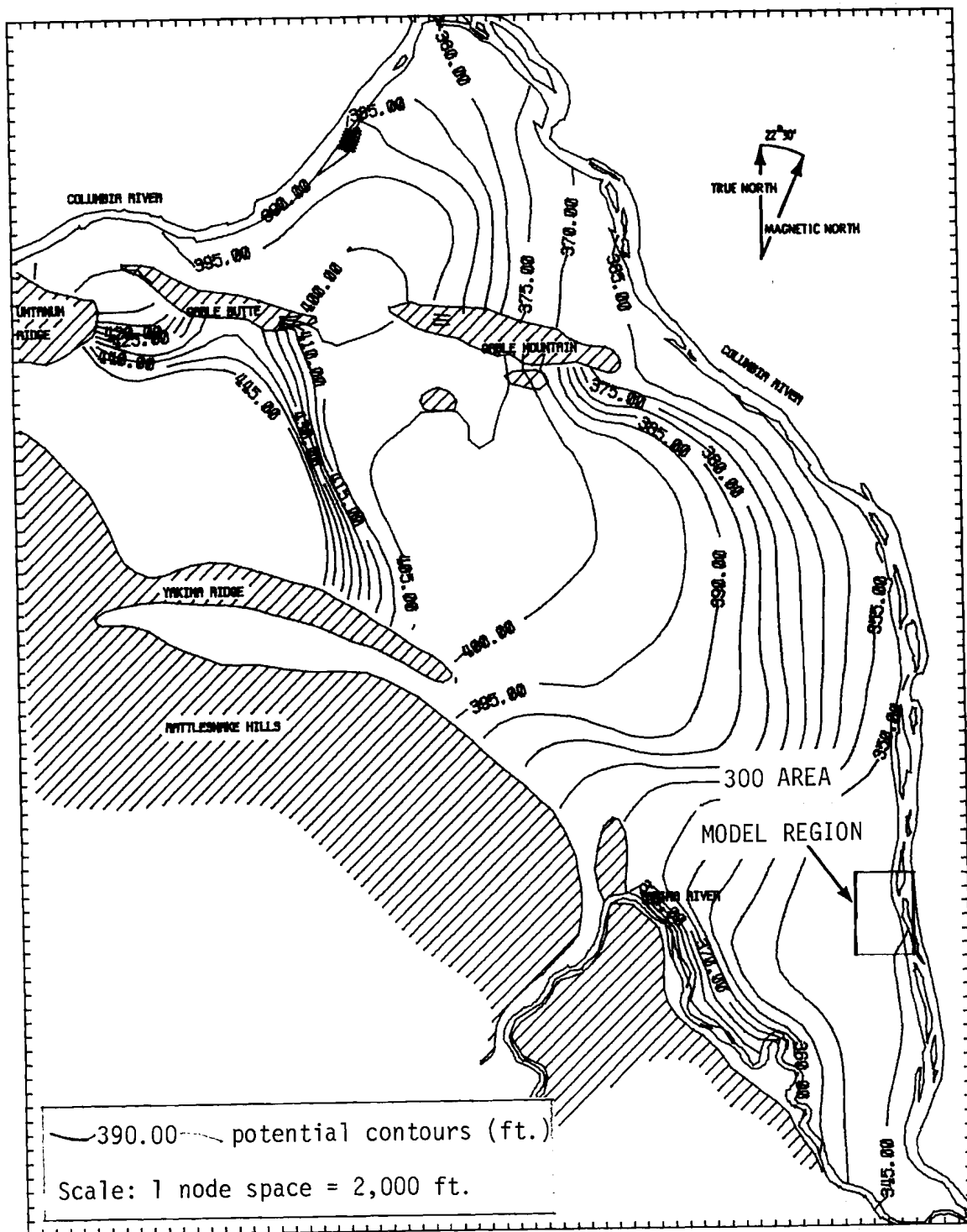


FIGURE 7.3. Hanford Site (Large Region) Initial Potential Surface (January 1, 1977)

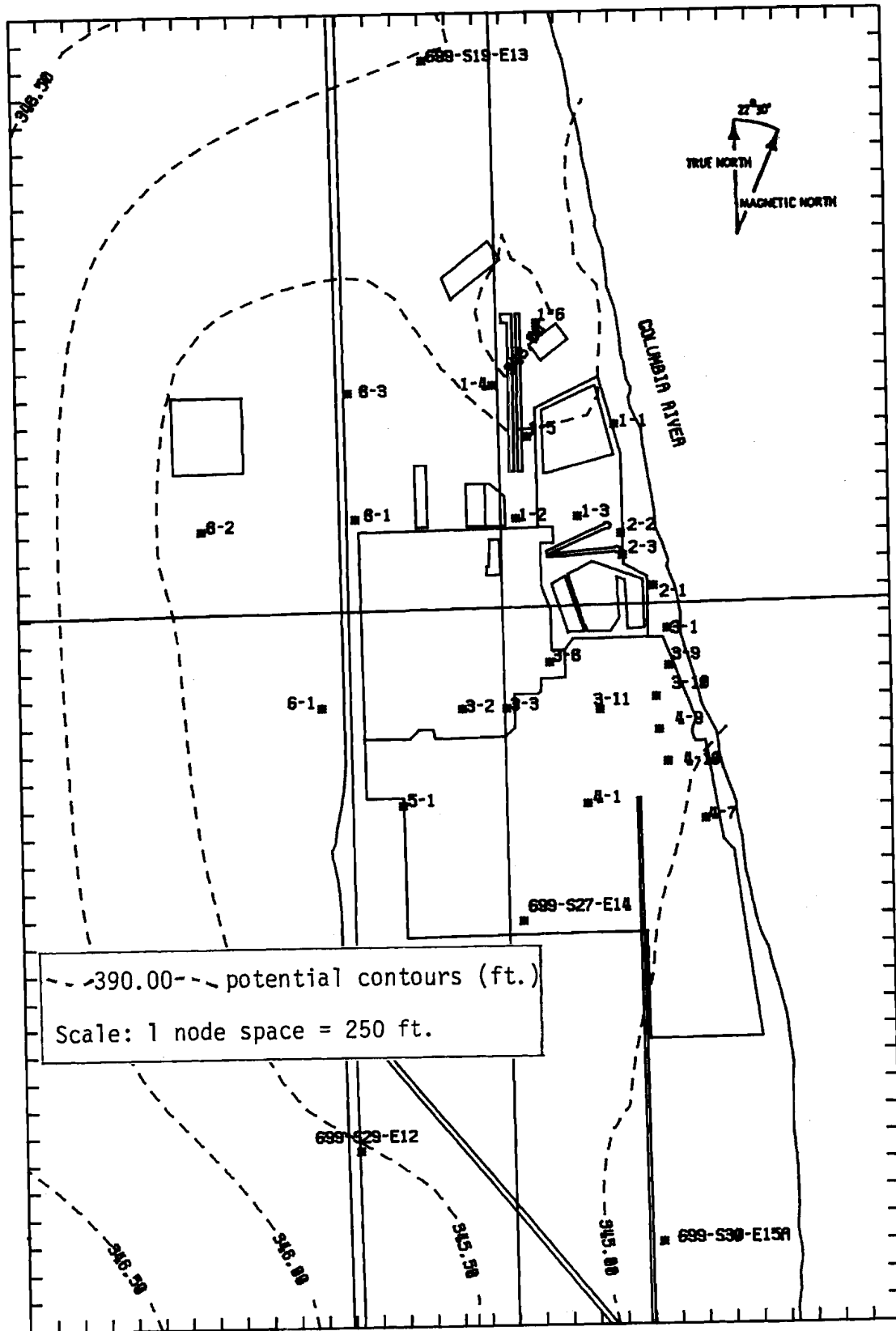


FIGURE 7.4. 300 Area (Small Region) Initial Potential Surface (January 25, 1977)

Table 7.1. Recharge and Discharge Location

<u>Waste-Water Discharge to Ground</u>	<u>Coordinates*</u>		<u>Nodes</u>
	X	Y	(Small Region)
Process Sewer Water to Trenches	4600	8500	(19,33) - (19,38)
Sanitary Sewer Water to Trenches	5100	7000	(21,29) - (22,30)
315 Building Backwash Water to South Pond	5260	6600	(22,27) - (22,28)
			(23,27) - (23,28)
Steam Condensate to Ground (Building 325)	4290	5600	(18,23)
384 Building Sluice Water to Ash Pits	5270	6230	(22,26)
<u>Water Withdrawn from Unconfined Aquifer</u>	<u>Coordinates</u>		<u>Nodes</u>
	X	Y	(Small Region)
309 Building Deep Well (July only)	4800	5080	(20,21)

*feet from the small region left-left-hand corner

TABLE 7.2. CY1977 Waste-Water Discharges in the 300 Area
(Units-million gallons per day)

<u>1977</u>	<u>Sanitary Sewage</u>	<u>315 Filter Backwash</u>	<u>Process Sewer Trenches</u>	<u>Ash Pits</u>	<u>Steam Condensate</u>
January	0.29	0.005	1.59	0.052	0.17
February	0.25	0.006	1.96	0.052	0.13
March	0.22	0.010	1.87	0.052	0.08
April	0.28	0.028	2.09	0.052	0.08
May	0.40	0.038	2.12	0.052	0.05
June	0.39	0.037	2.84	0.052	0.05
July	0.43	0.032	2.52	0.054	0.02
August	0.44	0.022	2.97	0.071	0.02
September	0.35	0.009	2.63	0.050	0.04
October	0.31	0.010	2.63	0.050	0.04
November	0.32	0.011	2.50	0.053	0.08
December	0.28	0.016	2.15	0.075	0.07
AVERAGE	0.33	0.019	2.33	0.053	0.07

Table 7.3. CY1977 Withdrawal from Ground Water in the 300 Area
309 Bldg. Well (4-5)

	<u>Date</u>	<u>Quant.</u> <u>(gal.x10³)</u>	<u>Date</u>	<u>Quant.</u> <u>(gal.x10³)</u>	<u>Date</u>	<u>Quant.</u> <u>(gal.x10³)</u>
July	1	488	12	590	23	-0-
	2	83	13	590	24	-0-
	3	-0-	14	590	25	-0-
	4	-0-	15	590	26	110
	5	38	16	584	27	-0-
	6	-0-	17	-0-	28	2
	7	476	18	-0-	29	-0-
	8	590	19	-0-	30	-0-
	9	590	20	-0-	31	-0-
	10	590	21	-0-		
	11	590	22	-0-		

7.2.2 Transmissivity

Some raw transmissivity data for the 300 Area exist from previous modeling efforts on the Hanford Site. In order to check and improve on these prior data, three pump tests were conducted at wells 1-4, 8-1, and 8-2. The results of the pump tests, for both the drawdown and recovery legs, are shown in Table 7.4.

As is typical, quite a range of transmissivities can be calculated for a single pump test depending on the interpretation of the raw data. A great deal of additional uncertainty is introduced when extrapolating measured transmissivity data over the entire model region. Due to this uncertainty, transmissivity is usually the principal variable adjusted when calibrating the model. In this study, rather than change the model to agree with the measured transmissivities, the range of pump test results was used as a guideline in the calibration process.

7.2.3 Aquifer Top

When dealing with an unconfined aquifer, as exists in the 300 Area, aquifer top refers to the elevation of the land surface. This information was obtained by digitizing topographic maps and input to the model on a nodal basis.

TABLE 7.4. Transmissivity Data as Analyzed From Drawdown and Recovery Measurements

<u>Well Number</u>	<u>Transmissivity (ft²/day)*</u>	
	<u>Drawdown</u>	<u>Recovery</u>
1-4	180,000	70,000
8-1	625,000	350,000
8-2	15,000	40,000

* Results were obtained by using a Jacob semilog analysis with straight line fitting

7.2.4 Aquifer Bottom

The aquifer bottom surface was established from information provided by driller's logs, geologic cross sections developed from these logs, and clay content analysis of certain soil samples. The information was contoured, digitized, and input to the model on a nodal basis. The aquifer bottom was assumed to be impermeable for the purposes of this study. A contour map of the Hanford Site unconfined aquifer bottom surface is shown in Figure 7.5.

7.2.5 Storage Coefficient

Due to the lack of more accurate data, the same storage coefficient (0.1) used in the large region model was held constant over the small region.

7.3 MODEL CALIBRATION AND VERIFICATION

Once the required data have been input, the model will produce model predicted ground-water potential (elevation) surfaces. Because the water-table elevation field data were measured weekly, the model was run in the transient mode on a weekly basis. Thus, the model output consisted of a 300 Area ground-water potential surface for each week of calendar year 1977.

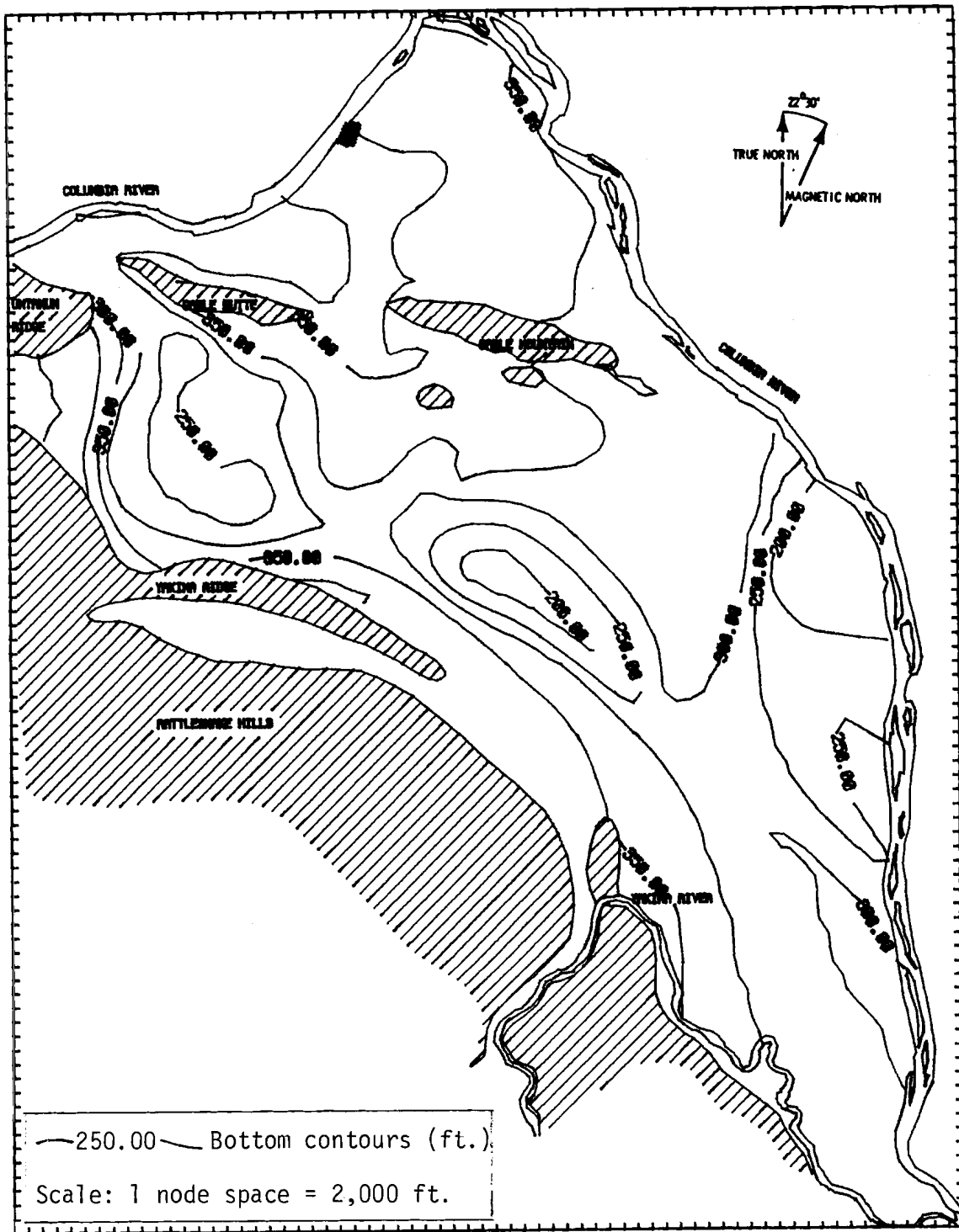


FIGURE 7.5. Hanford Unconfined Aquifer Bottom Contours

Degrees of uncertainty surround even the most carefully measured or mapped physical data. Point data are interpolated to produce maps (potential, transmissivity, storage coefficient, etc.) and test maps from a conceptual model of the system. Filtering of data occurs during this step as well as during the process of moving from the conceptual model to the working model. The degree of reliability of the model is dependent on the agreement of the predicted ground water potentials from the model with the measured ground-water system behavior. The final model reliability is directly dependent upon the adequacy of the field data available and on the conceptualization of these data for use in model calibration. The calibration involves a series of computer runs where the model inputs are modified within accuracy limits to make the model better represent the observed behavior of the system.

The changes in the model input parameters made during the calibration procedure and the justification for these changes on a realistic physical basis are the essential aspects of the model calibration and verification process. The most commonly adjusted parameters are transmissivity and storage coefficient because they are often the parameters of greatest uncertainty and for which we have the least amount of data. Changes in the recharge/discharge, to include river stage, usually have the greatest influence on the model output and when well known, enable rather satisfactory verification of the transmissivity data. Changes are rarely made in the initial and boundary conditions and/or the aquifer top and bottom surfaces, though occasional changes can be made if additional detailed data are obtained.

The initial estimates of the 300 Area ground-water potential, storage coefficient, and transmissivity distributions were obtained from the Hanford Site model as discussed earlier. The aquifer stress and recharge data were gathered in the field portion of this study. After each simulation run, model-predicted potentials were compared with field-measured potentials. Based on these comparisons, the model used to predict Columbia River stage and the transmissivities were adjusted until

the agreement between the computed and observed potentials was acceptable. Figure 7.6 shows the final transmissivity distribution as modified to provide the best potential fit.

After calibration, it is desirable to run the model on an independent set of data to verify that the model does simulate the ground-water system. In order to obtain two sets of data, the model was calibrated to the first 26 weeks of 1977 physical data and then validated with the data for the second 26 weeks.

7.4 VTT MODEL RESULTS

The model output was evaluated by two methods: 1) comparing model-predicted hydrographs to field-measured hydrographs for each of the 29 test wells (i.e., point comparisons), and 2) comparing model-predicted with hand-interpreted water-level contours. The appendix contains the hydrograph plots for each of the 29 observation wells. The hydrographs make weekly comparisons of the field-measured versus model-predicted ground-water elevations (above mean sea level) for CY1977. The first half of the time scale on each plot shows the calibration period results, while the verification results are shown in the second half of the time scale. A statistical analysis of the hydrograph results appears in Table 7.5. Model-predicted contour maps can be drawn for any given week during 1977 and compared with the hand-interpreted contours. Such a comparison was made for a 4-week period starting with the week of May 20, 1977 (Figures 7.7 through 7.10). The model-predicted contours in Figures 7.7 through 7.10 can be compared with the hand-interpreted contours shown in Figures 4.11 through 4.14.

The comparison is excellent where good field data exist (i.e., where the majority of the observation wells are located) and generally poorer in less well-known areas. From the hydrographs, maps, and statistics, the following evaluations of the quality of this simulation can be made:

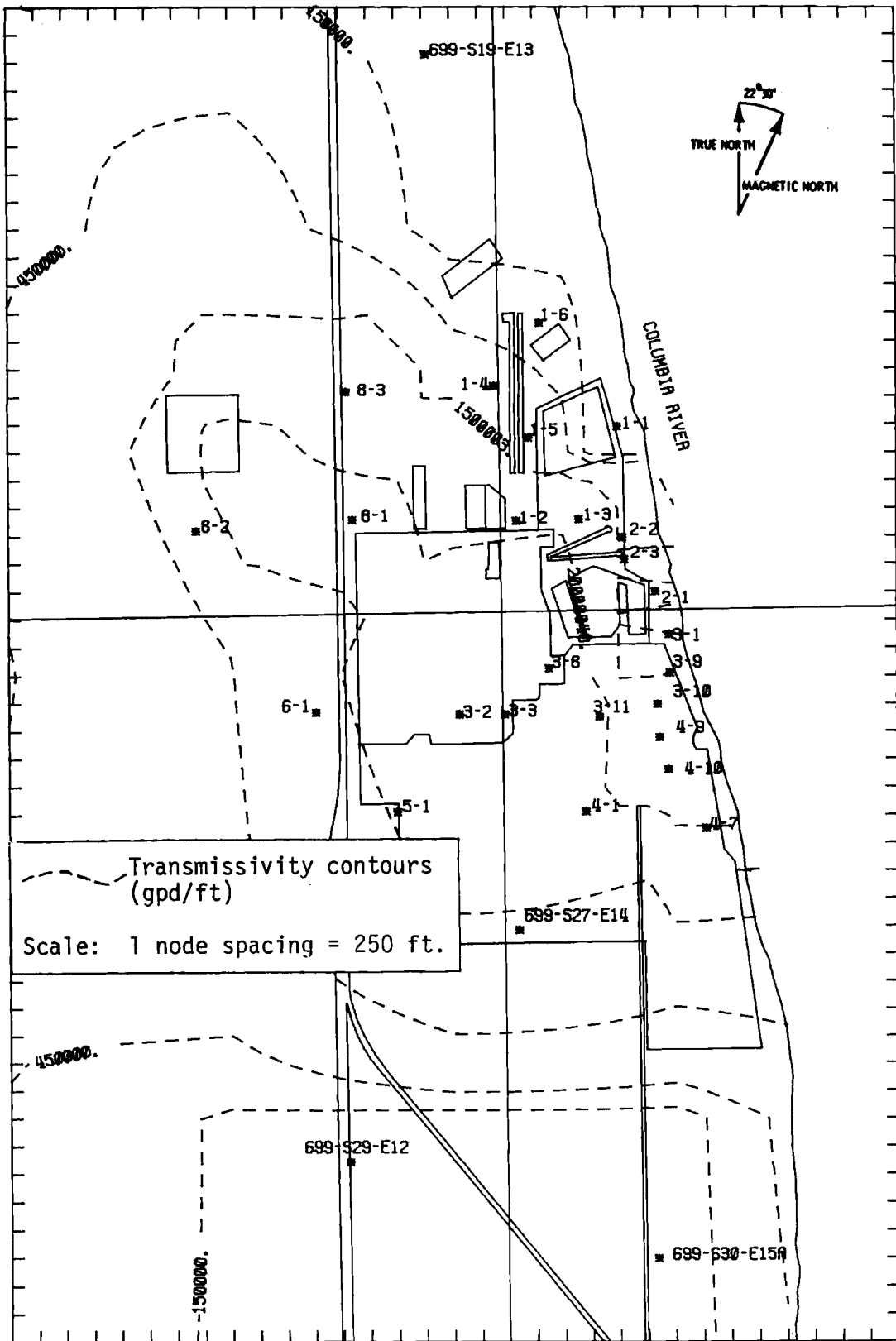


FIGURE 7.6. Transmissivity (gpd/ft) Distribution

TABLE 7.5. Statistical Analysis of the Hydrograph Results
(Comparison of Field-Measured to Model-Predicted
Water Level in Each of the 29 Wells)

<u>Well Identification</u>	<u>Average Difference (ft)</u>	<u>Root-Mean-Squared Difference (ft)</u>
399-1-1	0.29	0.57
399-1-2	-0.73	0.88
399-1-3	-0.16	0.54
399-1-4	0.39	0.54
399-1-5	0.61	0.74
399-1-6	-0.61	0.74
399-2-1	-0.71	1.07
399-2-2	-0.06	0.49
399-2-3	0.01	0.43
399-3-1	0.24	0.43
399-3-2	-0.04	0.47
399-3-3	-0.08	0.50
399-3-8	-0.59	0.86
399-3-9	0.18	0.49
399-3-10	0.07	0.44
399-3-11	0.47	0.57
399-4-1	0.00	0.53
399-4-7	-0.12	0.39
399-4-9	0.59	0.74
399-4-10	0.15	0.45
399-5-1	-0.41	0.83
399-6-1	-0.40	0.60
399-8-1	-0.17	0.51
399-8-2	-0.29	0.55
399-8-3	0.22	0.46
699-S30-E15A	0.15	0.62
699-S29-E12	2.48	2.71
699-S27-E14	-0.21	0.54
699-S19-E13	0.50	0.78

1. The agreement is excellent in the central portion of the 300 Area and along the river. The average and root mean square difference for the 25 wells in this region are 0.29 ft (8.84 cm) and 0.58 ft (17.68 cm), respectively (see Table 7.5).
2. The two areas of greatest discrepancy are the northern and southern extremities of the model region away from the river. In both areas there is only a single observation well; therefore, it is difficult to put much confidence in the contour map comparisons. With regard

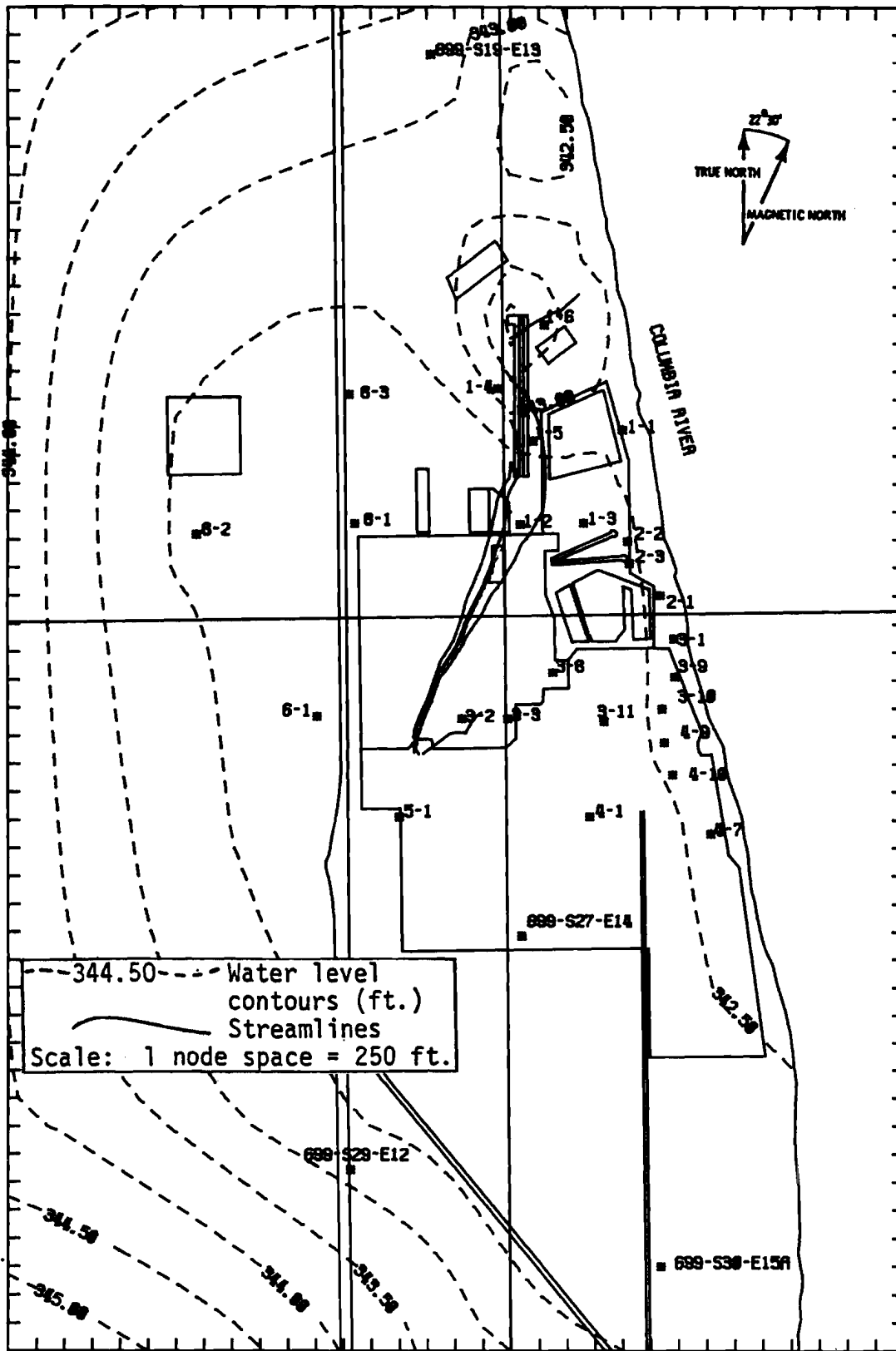


FIGURE 7.7. 300 Area May 20, 1977, Model-Predicted Potential Surface

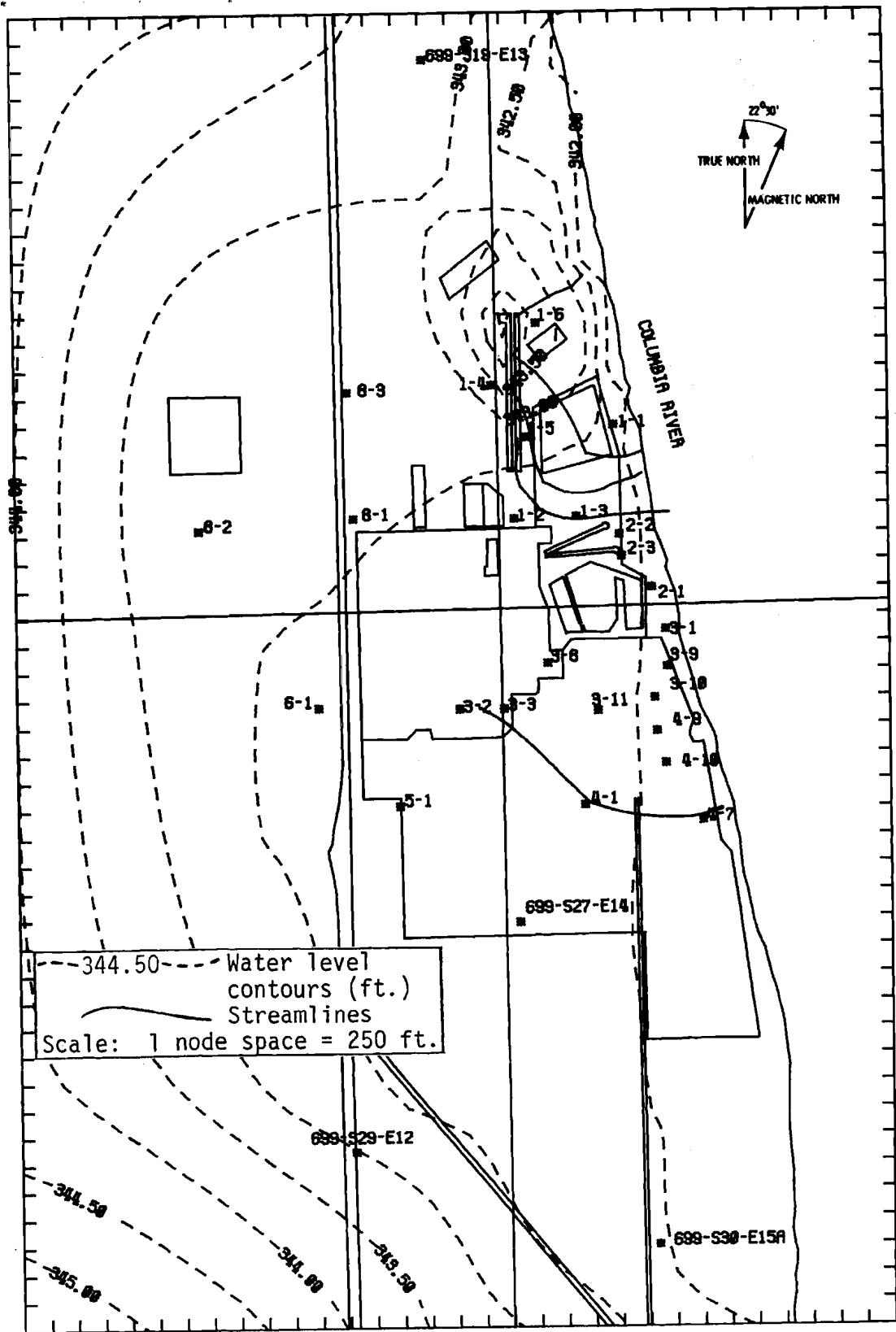


FIGURE 7.8. 300 Area May 27, 1977, Model-Predicted Potential Surface

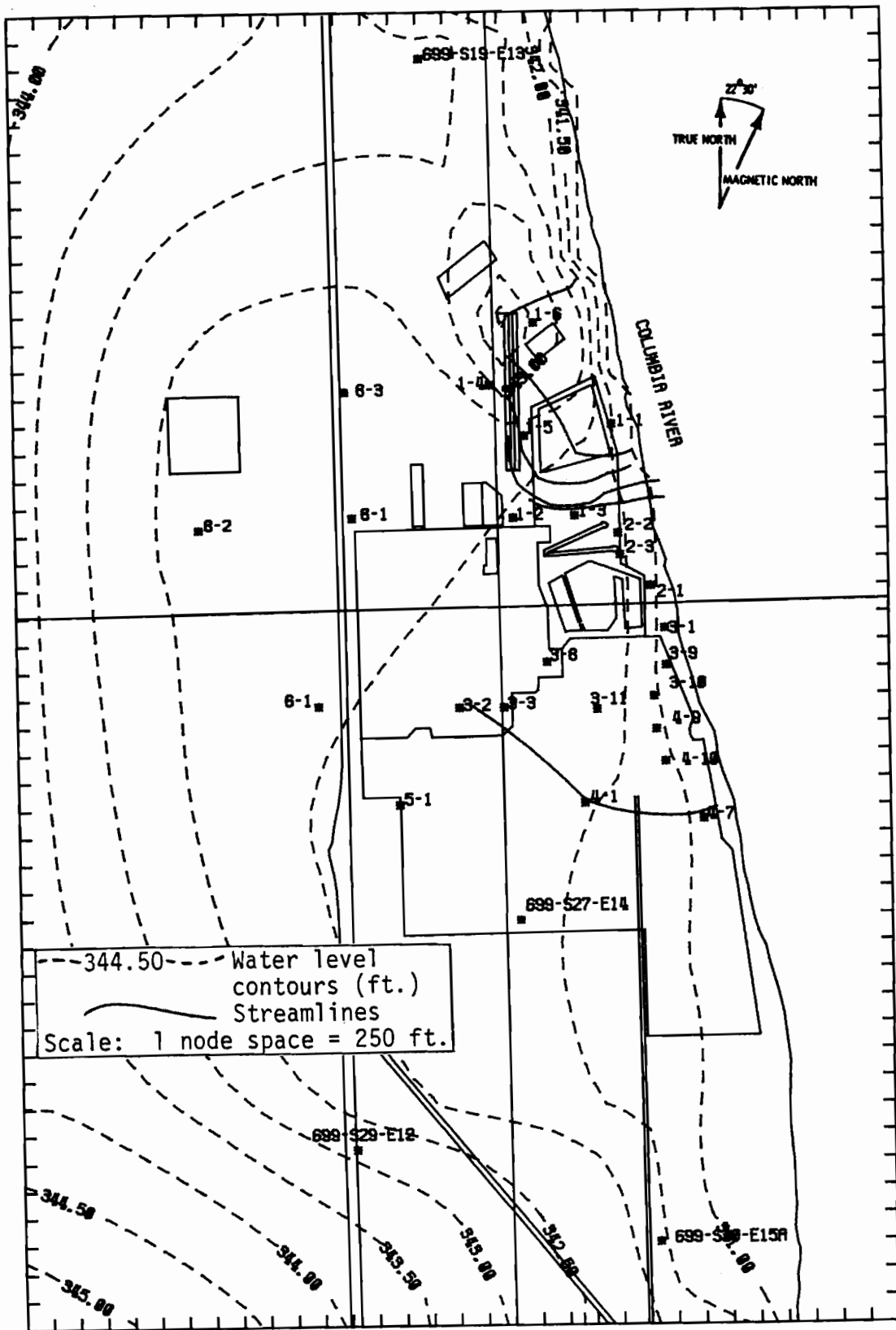


FIGURE 7.9. 300 Area June 3, 1977, Model-Predicted Potential Surface

to the point comparisons at these two wells, the average difference is 2.48 ft (75.59 cm) and 0.50 ft (15.24 cm) for the southern and northern wells, respectively.

3. In general, the comparison between the model-predicted and field-measured water level weekly trends, as shown in the hydrograph plots (appendix), is excellent.

After several calibration attempts, the transmissivity surface as shown in Figure 7.6 was used. Additional adjustments could be made in an attempt to even better calibrate the model; however, there is little justification for further changes without first obtaining additional field measurements.

The transmissivities are very high in the central portion of the 300 Area model region and decrease considerably to the north and south. A dike of low transmissivities was placed along the river over the central portion of the 300 Area, extending to just north of the process water trenches. This transmissivity distribution seems to be justified in that an ancient river channel, composed largely of gravel, has been postulated (R. E. Brown, PNL) through the central portion of the 300 Area and a strip of material with lower permeability appears to exist between the ancient river channel and the present river channel (see Section 4.2, and Figures 4.1 and 4.2).

7.5 MODEL APPLICATION

Once the flow model has been verified it can be used as a management tool to predict future (or past) ground-water conditions and travel times of the water beneath the 300 Area. Two examples are presented to show how the model may be applied.

A possible use of the model would be to estimate the rate of recharge required to create the ground-water anomaly that exists near well 3-3 (see Section 4.3.3). The field data indicate that the water level at well 3-3 is consistently 0.25 ft (7.62 cm) higher than the water level of other wells in the immediate vicinity. A mound of this size may seem

insignificant, but in this region of very high transmissivity, the recharge required to maintain such a mound would be quite large. In order to maintain such a mound the model calculated that about 1100 gpm (5959 m³/day) would be needed. Since there is no obvious source of recharge in the area, this rate of input is difficult to explain. With the support of additional evidence from the field data, it has been postulated that a pipeline is leaking in this area. It is difficult to believe that a leak of 1100 gpm (5959 m³/day) has gone undetected, suggesting this number may be high. A feasible explanation may be a local area of lower transmissivity combined with a lower leakage rate; however, the mound likely could not be present without some leakage. This evidence indicates that some recharge is involved causing the mound in this local area.

Another example of using the model as a management tool would be to predict travel times of the water within the 300 Area. Contaminants in the ground water can only move as fast as the water. Therefore, the travel time of the water can be considered the "worse case" arrival time of a contaminant.

The streamlines shown in Figures 7.7 through 7.10 depict the movement of water beneath the 300 Area under steady-state conditions. The multiple streamlines originating along the process water trenches depict the southward movement of ground water from the trenches. Depending on the Columbia River stage, these streamlines either move southwest toward the center of the 300 Area (high river stage - Figure 7.7), or southeast toward the river (low river stage - Figure 7.8). The model predicted that the average travel time for the water to reach the river (an average distance of 1550 ft) under May 27, 1977, steady-state conditions (Figure 7.8) is about 0.23 years (2.8 months).

Figures 7.7 through 7.10 also show a single streamline originating at a point between wells 3-2 and 3-3 (i.e., 325 Building). If contaminants were released into the water at this well, their earliest possible arrival time at the river, a distance of about 2625 ft (800 m), would be about

0.05 years (18.5 days) under the May 27, 1977, steady-state conditions (Figure 7.8). Table 7.6 is an example listing of the travel times and distances traveled for all streamlines shown in Figure 7.8.

It is important to note that the streamlines discussed above were studied under steady-state conditions and therefore are not valid travel time estimations for times greater than 1 week. Under transient conditions the potential gradients, the rate of flow, and the direction of flow change in the model on a weekly basis (model time step interval is 1 week). These changes are based on fluctuations in the river stage and the amount of recharge or discharge to the 300 Area. When predicting travel times greater than 1 week, the model parameters and the potentiometric surfaces should be updated weekly in order to accurately represent the direction and rate of flow. An example of the transient movement of the water (pathlines) for the same time period (beginning May 20, 1977) and starting at the same location (325 Building) as discussed above is shown in Figure 7.11. Under the transient conditions it took the water 6 weeks to reach the river, a distance of 3000 ft (914 m), whereas under the May 27, 1977, steady-state conditions the water traveled 2600 ft (792 m) directly to the river in 2.5 weeks.

TABLE 7.6. Streamline Data (for Streamlines shown in Figure 7.8)

I. Process Water Trenches Multiple Streamlines

AQUIFER 1

POROSITY = 0.1000
 ENDPOINTS OF STARTING BOUNDARY
 IN NODE COORDINATES

X1 = 19.5000 Y1 = 32.0000
 X2 = 19.5000 Y2 = 38.0000

NO.	X-END (NODE)	Y-END (NODE)	TIME (YEARS)	DISTANCE (FEET)
1	25.1120	30.7243	0.12	1575.0
2	25.1124	30.7338	0.15	1950.0
3	24.1336	32.1842	0.22	1800.0
4	24.1355	32.9737	0.43	1650.0
5	22.0413	39.5252	0.25	750.0

AVERAGE TIME (YEARS) = 0.24
 AVERAGE DISTANCE (FEET) = 1545.
 AVERAGE VELOCITY (FEET/YEAR) = 6553.8848

II. Single Streamline Originating Between Wells 3-2 and 3-3

POROSITY = 0.1000
 ENDPOINTS OF STARTING BOUNDARY
 IN NODE COORDINATES

X1 = 18.0000 Y1 = 23.5000

NO.	X-END (NODE)	Y-END (NODE)	TIME (YEARS)	DISTANCE (FEET)
1	27.0282	19.7154	0.05	2625.0

AVERAGE TIME (YEARS) = 0.05
 AVERAGE DISTANCE (FEET) = 2625.
 AVERAGE VELOCITY (FEET/YEAR) = 56275.5000

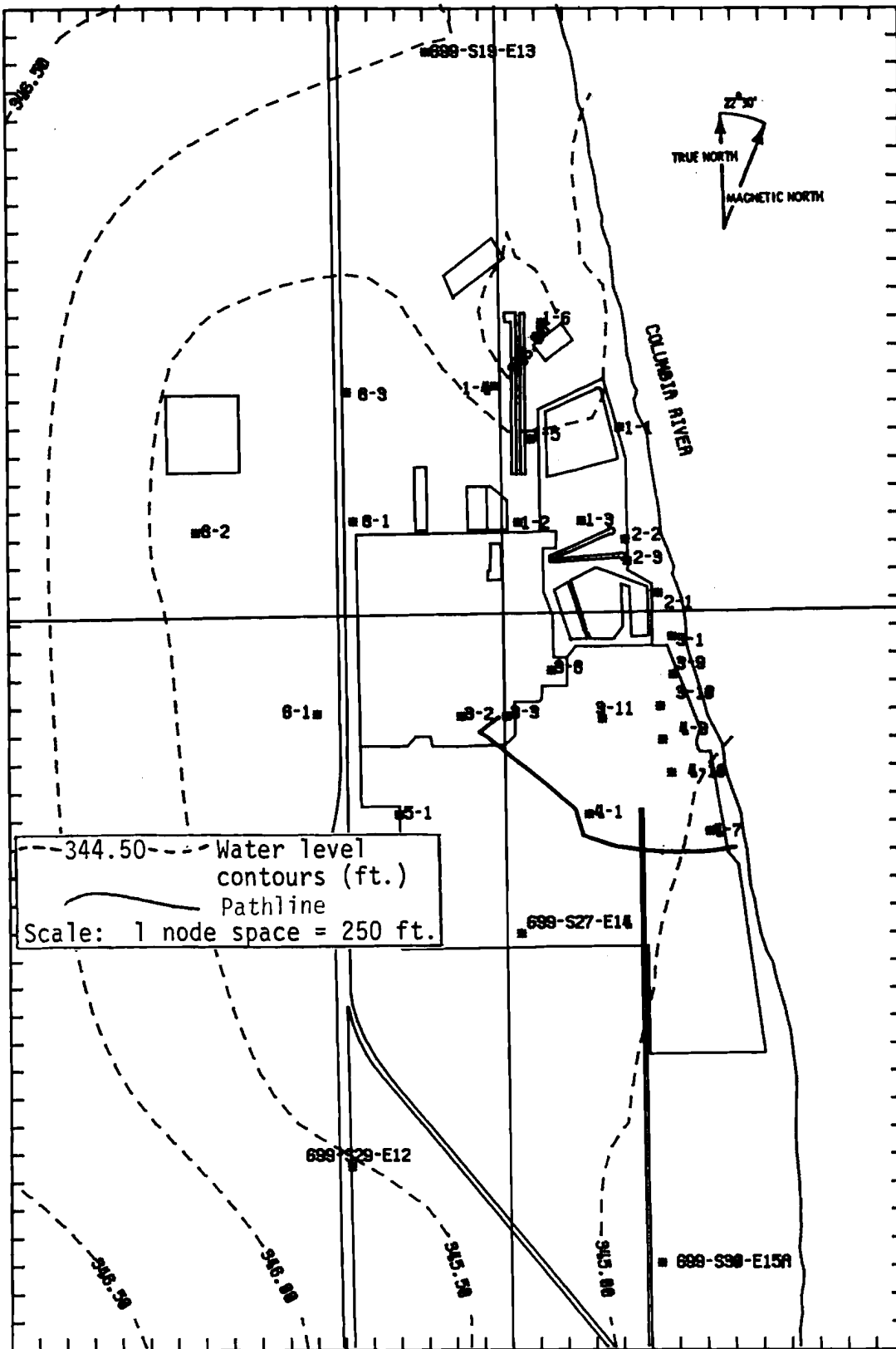


FIGURE 7.11. 300 Area Pathline Originating at the 325 Building (Beginning with the May 20, 1977, Potential Surface)

8.0 THE MULTICOMPONENT MASS TRANSFER MODEL

A transport model describes mathematically the forces that determine the movement of contaminants within a ground-water flow system. The model used to simulate the movement of contaminants within the 300 Area was the Multicomponent Mass Transfer (MMT) Model. MMT is designed to combine the ground-water movement data generated by the VTT flow model with dispersion and pertinent soil-waste reactions to predict the spatiotemporal distribution of contaminants in the saturated regime. MMT is a two-dimensional, Discrete-Parcel-Random-Walk (DPRW) solution to the general transport equation which can consider:

- transient convection
- variable dispersion
- sorption
- variable sorption for Sr and Cs
- radioactive decay
- N-membered decay chains
- multiple layers connected with dispersion
- destructive and reflective boundary conditions
- circular, three, and four-sided discharge shapes
- complex chemical interaction for major ground-water constituents.

8.1 THEORETICAL DEVELOPMENT OF THE MODEL - THE DIRECT SIMULATION APPROACH

The development of a mathematical model of a given physical-chemical system or process may be approached using two different methods. One approach attempts to describe the system with a representative mathematical equation and then solves this equation with appropriate boundary conditions. The other approach attempts to simulate reality more directly. It defines numerical structures that represent specific constituents and allows these numerical representations to react and interact as determined by the physical driving forces or constraints that are active in the real system.

The first approach is termed the "model-equation" method and usually leads to complex partial-differential equations which must be solved numerically, most often by using finite-difference or finite-element techniques. The second, or "direct-simulation" method, normally requires only that an efficient bookkeeping structure be established to control the response of the numerical representations so that all physical constraints are satisfied. Each approach, if properly implemented, can yield an adequate simulation of reality.

The direct-simulation version of MMT was selected for use in this study. Its primary advantages are:

- always mass-conservative
- no cumulative numerical dispersion
- inherent numerical stability
- facilitates handling of multicomponent systems.

The conceptual development of the MMT model using the direct-simulation approach is discussed below. Each important assumption will be indicated by italics. Although the current computerized version of MMT is a two-dimensional vertically average formulation, the conceptual model development is presented in three dimensions in anticipation of future model updates. Assumptions specific to the vertically averaged version are discussed when necessary.

8.1.1 Numerical Implementation Algorithm

The vertically averaged MMT model equation that describes transport in saturated uniform porosity systems is:

$$\frac{\partial \rho^k}{\partial t} + \left(\bar{v} - \frac{\bar{D}}{H} \nabla H \right) \cdot \nabla \rho^k = \nabla \cdot \bar{D} \nabla \rho^k + r^k \quad (8.1)$$

where

ρ^k = the mass concentration of species $[M/L^3]$

t = time

∇ = the Del operator

\bar{v} = the mass average pore velocity of the fluid $[L/T]$

\bar{D} = second order tensor

H = aquifer thickness

r^k = the net rate of production of species k within the control volume $[M/L^3T]$.

A state-of-the-art numerical technique referred to as a Discrete Parcel Random Walk (DRPW) algorithm is used to compute a solution to Equation (8.1). When constructing a mathematical analog for simulating mass transport, the physiochemical system can be viewed as a large, but finite, ensemble of small discrete quantities of mass.

This method, which is similar in some ways to Monte-Carlo transport analysis, is based on the movement of a hypothetical entity referred to as discrete parcel. Each parcel has associated with it a set of spatial coordinates as well as a set of discrete quantities of mass, and its movement in space is assumed to be independent of any other parcel. A Lagrangian approach is used for simulating the parcel advection and a homogeneous Markov random walk process is used to model the dispersive component. If thousands of such parcels are released in a passive flow field and their discrete paths are followed and recorded as a function of time, then the density of the ensemble may be interpreted as the concentration of a particular constituent or contaminant.

8.1.2 Particles of Mass

An important first step in creating a direct analog of a mass transport system is to define a numerical construct with which to represent the chemical species. Engineering-oriented approaches to mass transfer processes traditionally have tended to view chemical solutions as continuums that are defined with respect to a fixed or "Eulerian" frame of reference. It can also be useful to view material systems as being

comprised of a large number of discrete particles of matter. Carried to the molecular or atomic level, this concept has been established as a reliable description of the nature of matter.

It is not feasible at present to consider molecular-scale subdivisions when attempting to model large environmental systems, but the same concept can be used to create a workable analog. *The direct approach assumes that the material that is dissolved or suspended in subsurface water can be represented as an ensemble of a finite number of discrete particles of matter.* Computational restrictions usually limit the number of particles that can efficiently be used to something on the order of 10^4 or 10^5 . *The water mass that is carrying the material is assumed to be a continuum subject only to laminar flow. All particles are assumed to move with the continuum and at its velocity.*

Each particle has a defined location and a finite mass quantity associated with it. *The particles are assumed to be independent of one another, or in other words any one particle is not affected by the proximity or behavior of others.* This assumption is strictly valid only for dilute solutions, but is approximately true for all except very highly concentrated systems. The particles occupy zero volume by definition. *Because of their relatively large mass, the motion of the particles is assumed to be governed by Newtonian rather than relativistic mechanics.*

8.1.3 Advective Transport

The advective motion of the particles is controlled by the host medium in which they are immersed. *It is assumed that the flow properties of the host medium (water) are not significantly affected by the number or type of particles present.* This simplification is analogous with the assumption that the momentum and mass balance equations are decoupled in the equation-based approach. This also implies that the advective motion of each particle is only a function of the physical properties of the carrier and the geometry of the system.

The flow properties of the host water body usually are represented as a matrix of velocity components. This matrix must represent a mass conservative flow field if a proper transport simulation is to take place. Of course, this requirement is also necessary when the model is developed from an equation-based approach. Several methods are available for constructing the required flow fields, but most commonly they are the result of a flow model simulation. Each particle is allowed to move for a time interval, Δt , as determined by its location in the flow field. For best results the time-step size should be restricted so that the maximum distance moved by a particle is not larger than the matrix spacing of the flow field.

8.1.4 Dispersive Transport

The next transport process that must be accounted for is the readily observable property usually referred to as diffusion or dispersion, which results in a net flux relative to the ambient velocity. Dispersive transport consists of both mechanical dispersion and molecular diffusion. In porous media systems, mechanical dispersion is small-scale advective motion. Molecular diffusion takes place in the absence of fluid motion when mechanical dispersion ceases. Both have the same net result of causing foreign material to spread throughout the medium as the result of apparently random movements.

The particles of mass used to simulate dissolved or suspended material are subject to *the various dispersive mechanisms which are assumed to cause statistically random displacements*. View a single particle from a Lagrangian frame of reference at position x at $t = 0$ which has moved with the fluid to x' at a later time, t . Its displacement $x' - x$ is then a random function of time which can be described in terms of a spatial probability distribution function, $P(x' - x, t)$. As more steps are taken, the particle trajectory can be described as having the properties of a process known in statistics as a random walk. The probability distribution of a particle executing random steps is a standard problem of

probability theory (Feller, 1957 and Chandrasekhar, 1943). The following discussion is based on a summary of random walk theory given by Bear (1972) and Csanady (1973).

The main features of the problem can be understood most simply by the analysis of a random walk in one dimension with each step having a unit length and the probability of a step in either direction being exactly one half. Thus, assuming a particle is released at the origin of an arbitrary coordinate system, it could be at any of the points:

$$-N, -N+1, -N+2, \dots, N-2, N-1, N$$

after N steps.

The problem then is determining with what probability a particle reaches a given point m when $-N \leq m \leq N$. That probability, denoted by $P(m,N)$, can be calculated by enumerating all of the possible outcomes of a random walk consisting of N steps and determining which ones of those will result in the particle finishing up at point m .

The probability of any one sequence of N backward and forward steps is given by $(1/2)^N$. The required probability is therefore this value times the number of distinct sequences which will lead to the point m after N steps. If the number of forward steps taken is f and the number of backward steps b , then in order for the particle to arrive at m after N steps, the following relationships must be true:

$$f + b = N \tag{8.2a}$$

$$f - b = m \tag{8.2b}$$

which yields

$$f = (N + m)/2$$

$$b = (N - m)/2$$

The number of different sequences consisting of exactly f forward and b backward steps is:

$$\frac{N!}{(f!b!)} \tag{8.3}$$

therefore:

$$P(m,N) = \frac{N!}{[1/2(N+m)]! [1/2(N-m)]!} (1/2)^N \quad (8.4)$$

which is known as a Bernoulli distribution (Chung, 1974).

For modeling large-scale ground-water flow the case of most interest occurs for very large N. For this case the result for P(m,N) can be simplified by making use of Stirling's formula (Chung, 1974):

$$\ln(N!) = (N+1/2)\ln(N) - N + \ln(2\pi) \quad (8.5)$$

After some algebraic manipulation (Chung, 1974), Equation (8.4) reduces to:

$$P(m,N) = \sqrt{\frac{2}{\pi N}} e^{-(m^2/2N)} \quad (8.6)$$

which is a Gaussian or normal distribution with standard deviation \sqrt{N} . The convergence of the Bernoulli to the Gaussian distribution is quite rapid as N increases. For example, the differences are within a few percent for N=10 except at the extremes of the distributions.

The "discrete" distribution expressed by Equation (8.6) can be made continuous by *assuming that the individual steps are small compared to the length Δx over which we may want to define particle concentrations. If the step length is ℓ , which is assumed to be characteristic of a particular medium, then:*

$$m = x/\ell \quad (8.7)$$

where x is the displacement from the origin. The total probability of finding a particle over a range Δx , centered at x, is then approximately:

$$P(m,N) (\Delta x/2\ell) \quad (8.8)$$

The factor 2 is in the denominator because the discrete neighboring probability points are always separated by two step lengths. In a diffusing cloud of independent particles, having total mass Q, the fraction of the material contained within the range Δx is then given by:

$$\text{total mass} \int_{x-1/2\Delta x}^{x+1/2\Delta x} = \Delta m = Q \cdot P(m,N) \frac{\Delta x}{2\ell} \quad (8.9)$$

which can be expressed in terms of concentration as:

$$\rho = \frac{\Delta m}{\Delta x} = \frac{Q}{2\ell} \sqrt{\frac{2}{\pi N}} e^{-\left(\frac{x^2}{2N\ell^2}\right)} \quad [M/L] \quad (8.10)$$

The total number of steps, N , may be related to a diffusion time, t , if the particle is assumed to undergo n displacements per unit time:

$$t = N/n \quad (8.11)$$

and a "diffusion velocity," u , can be defined as:

$$u = \frac{1}{2}n\ell \quad [L/T] \quad (8.12)$$

Defining a dispersion coefficient, D , as:

$$D = \frac{1}{2}n\ell^2 = u\ell \quad [L^2/T] \quad (8.13)$$

yields:

$$\rho(x,t) = \frac{Q}{2\sqrt{\pi Dt}} e^{-\left(\frac{x^2}{4Dt}\right)} \quad (8.14)$$

This equation is recognizable as a Gaussian distribution with standard deviation, $2Dt$, and also as a solution to the classical one-dimensional diffusion equation (Carslaw, 1959, and Crank, 1956). The above arguments have been extended to three dimensions for a homogeneous isotropic system by Scheidegger (1954), yielding:

$$\rho(x,y,z,t) = \frac{Q}{(2\sqrt{\pi Dt})^3} e^{-\left(\frac{x^2}{4Dt} + \frac{y^2}{4Dt} + \frac{z^2}{4Dt}\right)} \quad (8.15)$$

which is a solution to the three-dimensional diffusion equation.

Chandrasekhar (1943) has shown for a general, three-dimensional Markovian random walk that this probabilistic approach can be connected directly to the diffusion equation without having to enumerate all possible sequences of displacements. A brief summary of Chandrasekhar's arguments is presented by Csanady (1973) showing that the asymptotic ($N \rightarrow \infty$) temporal transition probability of the random walk problem has a form identical to the classical diffusion equation.

In Scheidegger's (1954) formulation *the motion of a particle through a specific medium was assumed to be made up of a sequence of straight elementary displacements of equal duration in which the direction and length of each displacement take on random values.* However, his model does not take into account the observed difference in rate of dispersion with respect to the directions longitudinal and transverse to flow. De Jong (1958) shows that for a homogeneous system the longitudinal dispersion can generally be expected to be five to seven times larger in the pores oriented in the direction of flow. However, when irregularities are present in the system this ratio is not readily predictable or quantifiable.

The most important point to be gained from this very brief discussion of the statistical description of dispersion is that the rms (root-mean-square) distance an ensemble of parcels undergoing a random walk will move during a time step, Δt , can be expressed (for the one-dimensional case) as:

$$\Delta X_{\text{rms}} = \sqrt{2D\Delta t} \quad (8.16)$$

based upon the result shown in Equation (8.14). Similar displacements will also occur in the other spatial directions. The numerical analog adopted for the dispersion portion of the direct simulation model approach is based on Equation (8.16) and is similar to Scheidegger's approach with the extension that the rates of dispersion are allowed to differ with respect to the longitudinal and transverse flow directions.

8.1.5 Total Particle Movement

To summarize particle movement, a particle of mass is defined that is assumed to be subject to displacements resulting from both advective and dispersive mechanisms during a given time step. If a large number of particles are released at a concentrated location after several time steps, an ellipsoidal cloud will result with a center point moving with the average flow velocity and the major semi-axis coincident with the direction of flow.

Another significant point to note is that based upon the assumptions presented above, the motion of a particle is dependent only on the nature of the flow system and not on the type of species being transported. This suggests that each particle can be tagged with more than one mass quantity, each representing a different species. By computing the movement of one set of particles, the transport of several species can be simulated simultaneously with considerable savings in computer time.

8.1.6 Concentration Distribution

At the end of any desired time step, the solution can be halted and the amount of mass residing within any defined volume can be tabulated yielding an average concentration value for the volume. The solution can then continue transporting each particle from where it was halted, stopping again to compute another concentration distribution when desired. This procedure is completely mass conservative as opposed to some earlier Lagrangian solution techniques such as the PIC method (Pinder and Cooper, 1970) which tagged each particle with a concentration rather than a mass. Averaging a set of concentrations to calculate an overall cell concentration can often lead to serious mass conservation problems.

8.1.7 Source/Sink Terms

The simple injection or withdrawal of contaminants from the system is easily simulated by adding or removing particles at appropriate locations. Other types of source/sink mechanisms such as radioactive decay or chemical reaction require that the mass quantities associated with each particle be adjusted or redistributed.

Prior to the computation of one of the more complex types of non-conservative mechanisms it is usually most convenient to convert the particle location distributions into a set of concentration distributions. New concentrations for each subdivision are calculated from a reaction rate or equilibrium type of reactive submodel. The concentration change within each summation interval (Δx , Δy , Δz) for each species is accounted for by appropriately adjusting the mass quantities associated with each parcel within the interval.

8.1.8 Boundary Conditions

The boundary conditions for the direct approach model can be specified quite easily. Two distinct types can be identified:

1. Free flow boundary - any particle transported out of the system across this type of boundary is assumed to have exited from the system. New particles with appropriate mass are created at inflow boundaries.
2. Reflecting or no flow boundary - any particle encountering this type of boundary is reflected back into the system.

8.1.9 Assumptions for the Vertically Averaged Version

The preceding discussion describes the assumptions in the current vertically averaged version of MMT-DPRW with one exception. Local reductions in aquifer thickness should hinder horizontal spreading and increases in thickness should increase the spreading rate. In a fully three-dimensional model this is taken care of by specifying the aquifer top and bottom as reflecting boundaries. However, in the 2-D vertically averaged version the particles do not have vertical coordinates associated with them that could make use of this boundary condition.

Fortunately, it is still relatively easy to account for this phenomenon in the 2-D model. In Equation (8.1) this spreading rate adjustment is computed by the $\frac{D}{H} \nabla H \cdot \nabla \rho^k$ term. Careful examination of Equation (8.1) indicates that the net result of this term is to increase or decrease the pore velocity, \bar{v} . Consequently, *the vertically averaged model formulation approximates these spreading rate perturbations by adding a $\frac{\bar{D}}{H} (\nabla H)$ component to each velocity vector of the flow field.*

8.2 MMT DATA REQUIREMENTS

The data requirements of the MMT-DPRW model can be listed as follows:

- ground-water velocity field
- retardation coefficient
- dispersion

- leach rate
- initial inventory
- half-lives for all nuclides
- mapping of parent-daughter relationships.

The MMT model requires a velocity field describing the flow patterns of the transporting media (water) as input data. The velocity distributions are usually derived from a hydrodynamic numerical model, a physical model, and/or an extensive field measurement program prior to running the contaminant transport simulation. The most common practice is to use the VTT model output as a direct input to the MMT model.

Dispersion is simulated by using random numbers between 1 and -1, multiplied by a length factor characteristic of the dispersion constant and the time step. The retardation coefficient, K , is calculated from the distribution coefficient, K_D (V/m), and the soil-to-solution ratio, B (m/V), by Equation (8.17):

$$1 + B K_D = K \quad (8.17)$$

The initial inventory is a measure of the initial quantities of contaminants either entering the system from a source or which exist from the system. The factor controlling the rate of entry of contaminants into the system from a source is the leach rate.

The approach to developing a ground-water mass transport model for a region is to:

- obtain flow and boundary information from the VTT ground-water simulation
- determine important contaminants
- determine initial concentrations and inputs of the contaminants within the region
- obtain contaminant-related data (retardation coefficient, dispersion coefficient, reaction rates, other soil-contaminant interactions)
- calibrate and validate the model with a known result at a time later than that associated with the initial concentrations.

9.0 DEVELOPMENT OF MMT MODEL FOR THE 300 AREA

9.1 MMT DATA REQUIREMENTS

9.1.1 Boundary and Flow Data

The boundary conditions obtained from VTT are used to create the boundary conditions for MMT. An impervious boundary is one that reflects the parcels back into the flow field. A boundary that allows flow to leave the flow system destroys parcels. The basalt outcrops throughout the Hanford Site act as impervious or reflecting boundaries, while the Columbia River is a destructive boundary. The held nodes surrounding the 300 Area modeled region constitute a destructive boundary.

The flow data received from VTT is in the form of potentials, permeabilities, and storage coefficients. The x,y velocity field used by MMT is then calculated using Darcy's law in two dimensions from the data in the VTT finite difference grid.

9.1.2 Important Contaminants

The important constituents to be modeled are chosen by two methods. The first test is based on the toxicity of the constituent to the environment. The second test is based on a non-toxic contaminant which has a significant effect upon the movement of a toxic contaminant. For the purposes of the simulations reported, only the first test was used because the concentrations of the important toxic contaminants are low enough to neglect interactions between constituents.

9.1.3 Initial Concentrations and Sources

For many transport simulations it is necessary to know the initial concentration of a particular contaminant in the ground water and the location and rate of input of that contaminant to the system. The initial conditions are normally obtained by sampling observation wells within the model region, contouring the data, and inputting the digitized contour surface to the model. Contaminant sources are identified by sampling the recharge to the ground water and inputting contaminant concentration data at the proper locations in the model.

9.1.4 Contaminant Related Data

The contaminant-related data used for the 300 Area model included distribution coefficient (K_d) and dispersion coefficient. These values are normally obtained experimentally from laboratory tests.

9.2 CALIBRATION AND VALIDATION

The transport model can be calibrated against observed contaminant movements by altering:

- velocity field
- retardation coefficients
- dispersion coefficients.

The best way to alter the velocity field is to recalibrate the VTT model. Therefore, assuming VTT is calibrated the velocity field need not be altered. Altering retardation coefficients retards or hastens movement. Changing the dispersion coefficients either increases or decreases spread of the component of interest. Therefore, if the component has moved too far in a given time period, then increasing the retardation coefficient would slow it down, while if the contaminant affected too large an area with respect to a known result, then decreasing the dispersion coefficients will decrease the areal spread of contaminant.

9.3 MMT TEST CASE

The primary application of the MMT Model in the 300 Area will likely be the simulation of point source accidental spills of contaminants. A radioactive waste was accidentally spilled in mid January 1979 near the 325 Building. This spill was used to demonstrate the use of the MMT transport model as a test case scenario.

The radioactive isotopes and their initial inventories were identified from a sample of the waste material. The total inventories used in the model were calculated from an estimate that approximately 4,000 gallons (15,140 l) of fluid were accidentally discharged from the transporting pipe. The isotopes contained in the waste, initial inventories,

half-lives, retardation coefficients, and uncontrolled water radiation standards are shown in Table 9.1. For all cases a beta of 4.3 g/ml and a dispersion length of 25 ft (7.62 m) were used. Only the isotopes that would have a measurable inventory (as determined from their retardation coefficient to half-life relationship) were actually run in the transport simulation.

The transient hydrologic model was used to predict a water travel time from the 325 Building to the Columbia River of approximately 6 weeks. This travel time was calculated starting from the last week in January with the 1978 hydrologic model. A comparison of the Columbia River flow measurements and the discharge to the process water trenches for January 1979 versus January 1978 showed the levels to be very similar. Since all other model input parameters are identical for both, the 1978 model was used to simulate the flow in 1979. A conservative estimate was made that the water moved through the partially saturated zone in 10 days and entered the ground water according to a nearly normal distribution.

9.3.1 MMT Transport Simulation Results

In order to properly represent the transport, the model should be run until all isotopes have either reached the Columbia River or have decayed to zero mass. For this scenario, a simulation time of 500 years was sufficient.

A lower limit for concentration of 10^{-10} $\mu\text{Ci/ml}$ was selected for display of results on the basis that this value is at least 100 times smaller than the maximum permissible concentration for water (U.S. ERDA, 1975) in uncontrolled areas for all the radioactive isotopes released by this spill.

The results of the transport simulation are summarized in Table 9.2. The table shows the arrival times at the river boundary of the peak concentrations for each isotope exiting. The table also shows maximum isotopic concentration in the ground water, ICRP maximum permissible drinking water concentration (MPC) for each isotope, and the ratio of model-predicted maximum concentration to MPC. A plot of the maximum

TABLE 9.1. Transport Model Input Parameters

<u>Isotope</u>	<u>Half-Life (Years)</u>	<u>Kd* (ml/g)</u>	<u>Uncontrolled Water Radiation Standard (CG)** (μCi/ml)</u>	<u>Initial Inventory (μCi/4000 gal Spill)</u>
Sb-125	2.73	1 (Ames and Rai, 1978)	1.0 E-4	9.5 E 4
Pu-238	86.4	$10^2 - 10^5$ (Ames and Rai, 1978)	5.0 E-6	3.3 E 5
Pu-239	24,390	$10^2 - 10^5$ (Ames and Rai, 1978)	5.0 E-6	1.4 E 5
Sr-90	27.7	10^2 (Platt, 1978)	3.0 E-7	1.0 E 6
Eu-154	16	5×10^2 (Serne and Others, 1976)	2.0 E-5	8.9 E 5
Eu-155	1.8	5×10^2 (Serne and Others, 1976)	2.0 E-4	1.7 E 6
Pm-147	2.62	$10^3 - 10^4$ (Benson, 1960)	2.0 E-4	7.2 E 7
Am-241	458	10^3 (Hajek, 1966)	4.0 E-6	2.0 E 6
Cs-134	2.05	2×10^3 (Platt, 1978)	9.0 E-6	9.2 E 3
Cs-137	30	2×10^3 (Platt, 1978)	2.0 E-5	2.0 E 5
Ce-Pr-144	0.78	2×10^3 (Benson, 1960)	1.0 E-5	2.0 E 5

*The most conservative values (underlined) were used where a range of values is given.

**U. S. Energy Research and Development Administration, 1975

TABLE 9.2. Summary of the Transport Model

Isotope	Uncontrolled Water Radiation Standard (CG)* ($\mu\text{Ci/ml}$)	Peak Arrival Time (years) (blank means isotope decayed before it reached the river)	Model Predicted Maximum Ground-Water Concentration ($\mu\text{Ci/ml}$)	Ratio of Model Predicted Maximum Concentration to CG
Sb-125	1.0 E-4	0.54	1.5 E-6	1.5 E-2
Pu-238	5.0 E-6	43	5.4 E-8	1.1 E-2
Pu-239	5.0 E-6	43	3.0 E-8	6.0 E-3
Sr-90	3.0 E-7	43	7.7 E-8	2.6 E-1
Eu-154	2.0 E-5	--	--	--
Eu-155	2.0 E-4	--	--	--
Pm-147	2.0 E-4	--	--	--
Am-241	4.0 E-6	440	2.5 E-8	6.3 E-3
Cs-134	9.0 E-6	--	--	--
Cs-137	2.0 E-5	--	--	--
Ce-144	1.0 E-5	--	--	--

* U. S. Energy Research and Development Administration, 1975

concentration ($\mu\text{Ci/ml}$) in the ground water versus time for each exiting nuclide is shown in Figures 9.1 through 9.5. Only 5 of the isotopes reached the river via the ground water with any reportable concentration. Of these 5, only the Strontium-90 is close to MPC, its concentration being 25% of MPC. All remaining isotopes are all at least 65 times smaller than MPC. In general, the transport model results indicate that due to either a short half-life or a high retardation coefficient, this accidental spill poses little or no threat to the environment.

KD= 1.00 ML/G HALF-LIFE=2.7000E+00 YEARS BETA= 4.3 G/ML
INITIAL INVENTORY=9.4897E-02 CURIES. PRESENT INVENTORY=8.2983E-02 CURIES.
ISOTOPE SB125 TIME VS CONCENTRATION

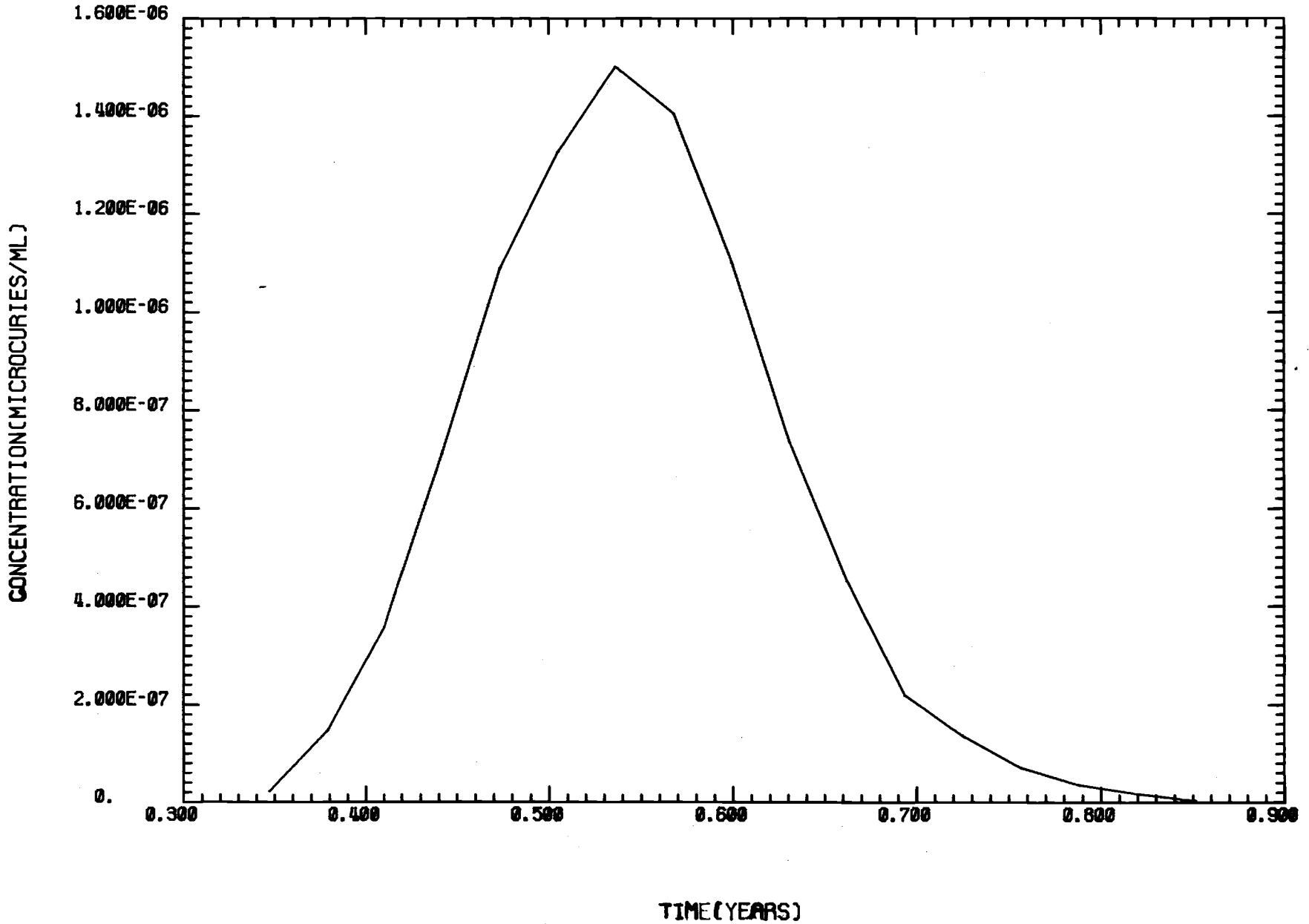


FIGURE 9.1. SB-125 Concentration Versus Time Plot

KD= 100.00 ML/G HALF-LIFE=8.6400E+01 YEARS BETA= 4.3 G/ML
INITIAL INVENTORY=3.3453E-01 CURIES. PRESENT INVENTORY=2.3591E-01 CURIES.
ISOTOPE PU238 TIME VS CONCENTRATION

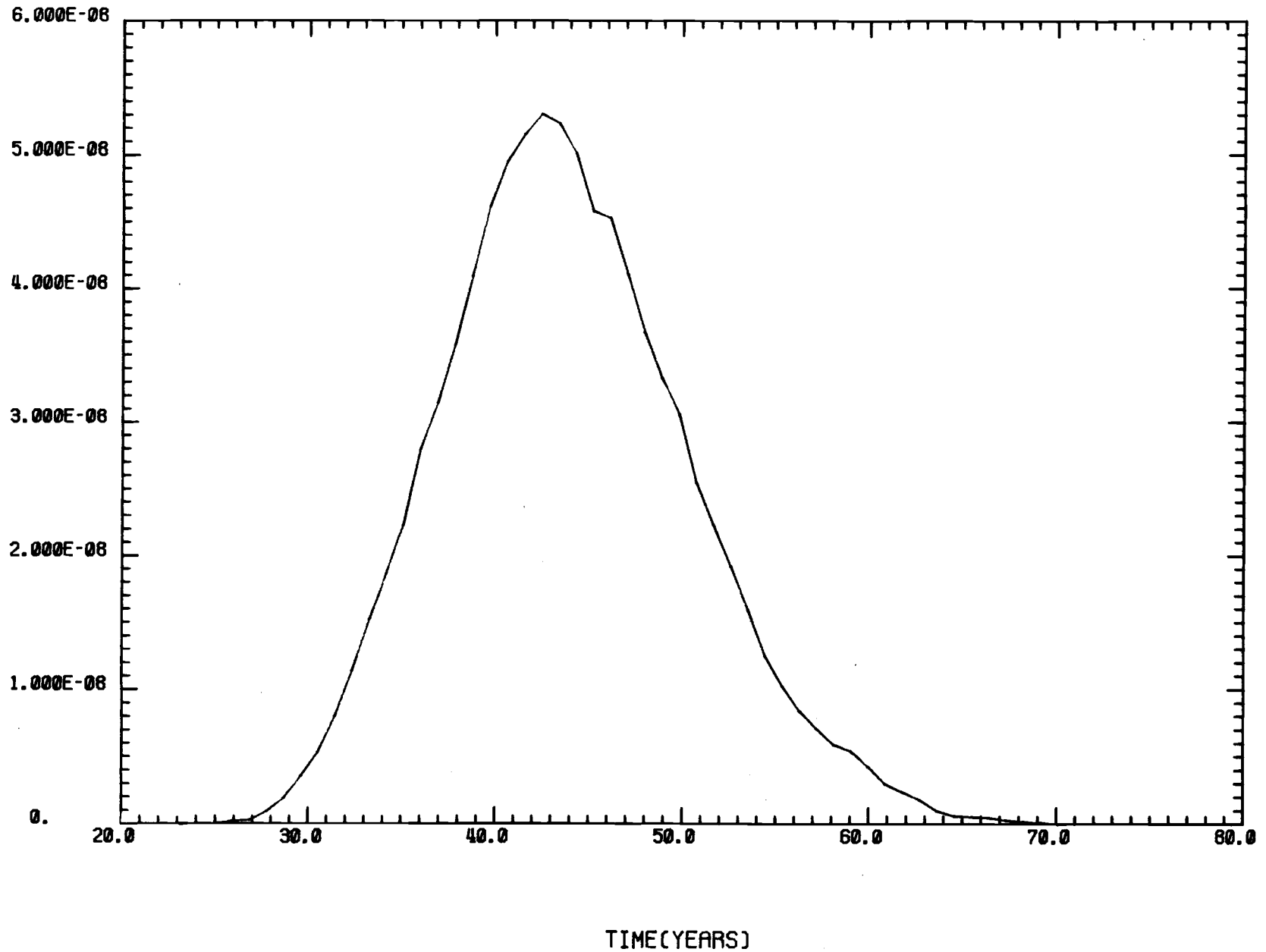


FIGURE 9.2. PU-238 Concentration Versus Time Plot

KD= 100.00 ML/G HALF-LIFE=2.4390E+04 YEARS BETA= 4.3 G/ML
INITIAL INVENTORY=1.3640E-01 CURIES. PRESENT INVENTORY=1.3618E-01 CURIES.
ISOTOPE PU239 TIME VS CONCENTRATION

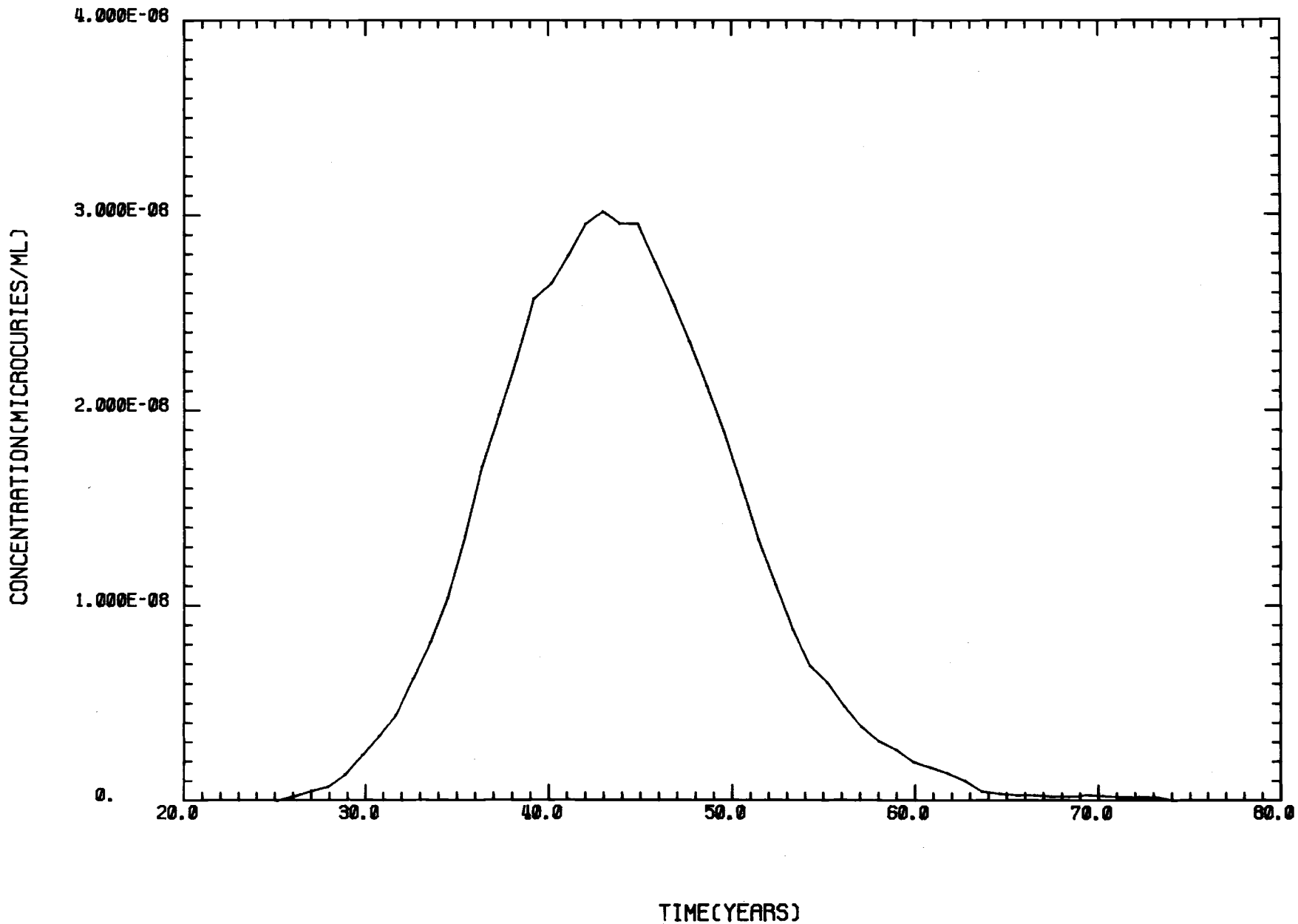


FIGURE 9.3. PU-239 Concentration Versus Time Plot

KD= 100.00 ML/G HALF-LIFE=2.7700E+01 YEARS BETA= 4.3 G/ML
INITIAL INVENTORY=1.0214E+00 CURIES. PRESENT INVENTORY=3.4865E-01 CURIES.
ISOTOPE SR90 TIME VS CONCENTRATION

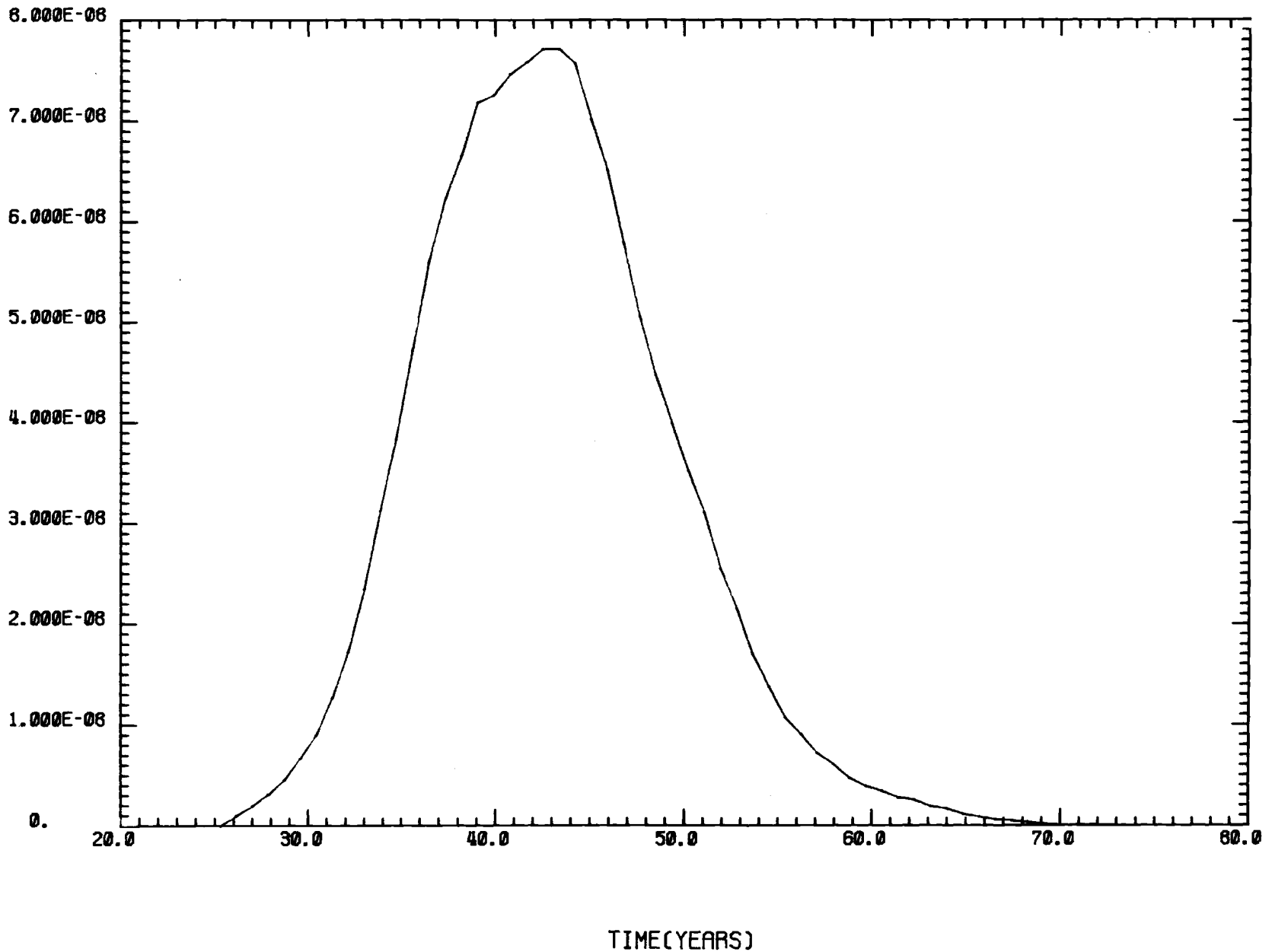


FIGURE 9.4. SR-90 Concentration Versus Time Plot

KD= 1000.00 ML/G HALF-LIFE=4.5800E+02 YEARS BETA= 4.3 G/ML
INITIAL INVENTORY=1.9499E+06 CURIES. PESENT INVENTORY=1.9151E+06 CURIES.
ISOTOPE AM241 TIME VS CONCENTRATION

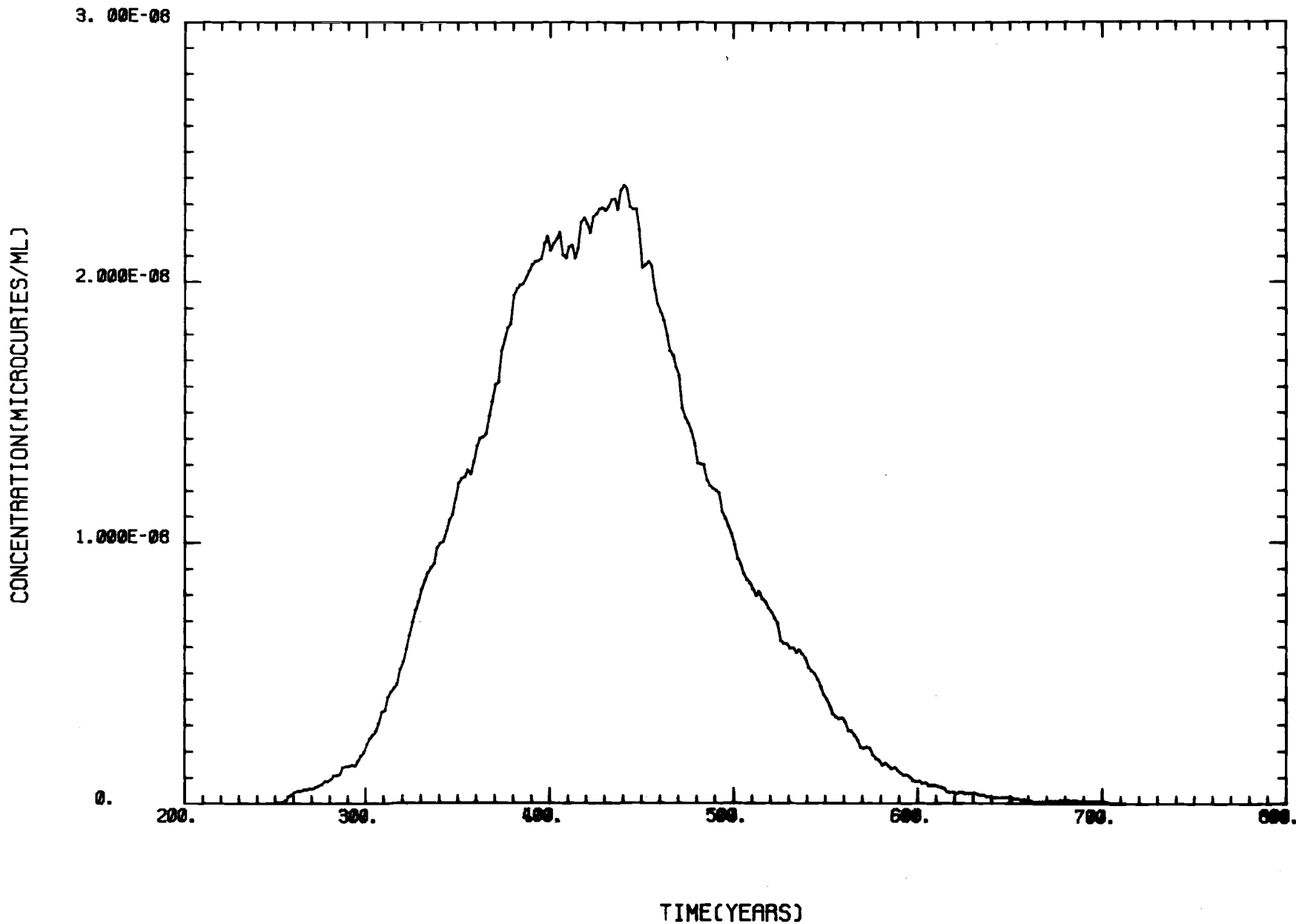


FIGURE 9.5. AM-241 Concentration Versus Time Plot

Additional References

- 1) L. L. Ames and D. Rai, 1978, Radionuclide Interactions with Soil and Rock Media, EPA 520/6-78-007.
- 2) A. M. Platt, 1978, Nuclear Waste Management Quarterly Report October through December, 1977: PNL-2377-4, Pacific Northwest Laboratory, Richland, Washington.
- 3) R. J. Serne, D. Rai, M. J. Mason and M. A. Molecke, 1976, Batch Kd Measurements of Nuclides to Estimate Migration Potential at the Proposed Waste Isolation Pilot Plant in New Mexico: PNL-2448, Pacific Northwest Laboratory, Richland, Washington.
- 4) D. W. Benson, 1960, Review of Soil Chemistry Research at Hanford: HW-67201, General Electric Company, Richland, Washington.
- 5) B. F. Hajek, 1966, Plutonium and Americium Mobility in Soils: BNWL-CC-925, Pacific Northwest Laboratory, Richland, Washington.

10.0 REFERENCES

- Allison, I. S., 1933, New version of the Spokane flood: Geol. Soc. America. Bull., v. 44, no. 4, p. 675-722.
- Atlantic Richfield Hanford Company, 1976, Preliminary feasibility study of radioactive wastes in Columbia River basalts: ARH-ST-137, Atlantic Richfield Hanford Company. V.1, 2.
- Baker, V. R., 1973, Paleohydrology and sedimentology of Lake Missoula flooding in eastern Washington: Geol. Soc. America, Special Paper 144, 79 p.
- Bear, J., 1972, Dynamics of fluids in porous media: American Elsevier Publishing Co., New York.
- Boussinesq, J. J. 1903, 1904, Recherches Theoriques sur l'ecoulement des nappes d'Eau Infiltrées dans le Sol et sur Debit des Sources: Jour. de Mathematiques Pures et Appliquees, Series 5, 10:5-78, p. 363-394.
- Bretz, J. H., 1959, Washington's channeled scablands: Washington Division Mines and Geology Bull, 57 p.
- Brown, R. E., 1960, An introduction to the surface of the Ringold Formation beneath the Hanford Works area: HW-66289, General Electric Company, Richland, Washington.
- _____, 1969 Some suggested rates of deformation of the basalts in the Pasco Basin, and their implications: Proceedings of the Second Columbia River Basalt Symposium, Northwest Scientific Association, Cheney, WA, p. 179-187.
- _____, 1975, The Ringold Formation and its setting in time (abst): Proc. of Northwest Scientific Assoc. Annual Meeting, Central Washington State College, Ellensburg.
- _____, and Brown, D. J., 1961, The Ringold Formation and its relationship to other formations: HW-SA-2319, General Electric Company, Hanford Atomic Products Operation Paper, 17 p.
- _____, and McConiga, M. W., 1969, Some contributions to the stratigraphy and indicated deformation of the Ringold Formation: Northwest Science, v. 34, no. 2, p. 43-45.

_____, Pearce, D. W., de Laguna, W., Struxness, E. G., Horton, J. H. Jr., and Patterson, C. M., 1958, Experience in the disposal of radioactive wastes to the ground: Proc. 1958 Geneva Conference on Peaceful Uses of Atomic Energy.

Carslaw, H. S., and Jaeger, J. C., 1959, Conduction of heat in solids: Oxford University Press, London.

Chandrasekhar, S., 1943, Stochastic problems in physics and astronomy: Rev. Mod. Phys., 15.

Crank, J., 1956, The mathematics of diffusion: Oxford University Press, London.

Csanady, G. T., 1973, Turbulent diffusion in the environment: D. Reidel Publishing Co., Boston, Mass.

Denham, D. J., 1970, Failure of 307 Basin transfer line and resultant ground contamination: BNWL-CC-2617m, Pacific Northwest Laboratory, 16 p, Appendices A & B.

Eddy, P. A., Myers, D. A., and Raymond, J. R. 1978. Vertical contamination in the unconfined groundwater at the Hanford Site, Washington: PNL-2724, Pacific Northwest Laboratory, 22 p.

Feller, W., 1957, An introduction to probability theory and its applications: John Wiley and Sons, New York.

Flint, R. F., 1938, Summary of Late-Cenozoic geology of southeastern Washington: Am. Jour. Sci., 5th section, v. 35, no. 27, p. 223-230.

Gustafson, E. P., 1973, The Ringold Formation, age and a new vertebrate faunal list: M.S. Thesis, University of Washington, Seattle

Haney, W. A., 1957, Dilution of 300 Area uranium wastes entering the Columbia River: HW-52401, General Electric Company, Richland, Washington, 8 p, 7 pls.

Kellogg, O. D., 1954, Foundations of potential theory: Dover Pub. Co., New York.

Kipp, K. L., Reisenauer, A. E., Cole, C. R., and Bryan, C. A., 1972 (updated 1976), Variable thickness transient groundwater flow model-theory and numerical implementation: BNWL-1703, Pacific Northwest Laboratory.

Ledgerwood, R. K., Brown, D. J., Waters, A. C., Myers, C. W., 1973, Identification of Yakima Basalt flows in the Pasco Basin: ARH-2768, Atlantic Richfield Hanford Company.

- Lindberg, J. W., 1976, Geologic survey of the spray pond excavation, Washington Nuclear Project No. 4: Pacific Testing Laboratories, Transmittal 262, Richland, Washington, 14 p.
- Lohman, S. W., 1972, Ground-water hydraulics: U.S. Geol. Survey Prof. Paper 708, 70 p.
- Mackin, J. H., 1961, A stratigraphic section in the Yakima Basalt and the Ellensburg Formation in south-central Washington: Washington Division Mines and Geology Rept. Inv. 19, 45 p.
- Mason, G. W., 1953, Interbasalt sediments of south-central Washington: M.S. Thesis, Washington State University, 16 p.
- McGhan, V. L., and Damschen, D. W., 1977, Hanford wells: BNWL-2296, Pacific Northwest Laboratory, Richland, Washington.
- Merriam, J. D. and Buwalda, J. P., 1917. Age of strata referred to the Ellensburg Formation in the White Bluffs of the Columbia River: California University Pub. Bull. 15, p. 255-266.
- Myers, D. A., 1978, Environmental monitoring report on the status of ground water beneath the Hanford Site, January-December 1977: PNL-2624, Pacific Northwest Laboratory, Richland, Washington.
- Newcomb, R. C., 1958, Ringold Formation of Pleistocene Age in type locality, the White Bluffs, Washington: Am. Jour. Sci., v. 256, p. 328-340.
- _____, Strand, R. C., and Frank, 1972, Geology and ground water characteristics of the Hanford Reservation of the U.S. Atomic Energy Commission, Washington: U.S. Geol. Survey Prof. Paper 716, 78 p.
- Occurrence Report, 1976, Unexpected release of uranyl nitrate solution: 76-BNW-14, Pacific Northwest Laboratory, Richland, Washington.
- Raymond, J. R., Myers, D. A., Fix, J. J., McGhan, V. L., and Schrotke, P.M., 1976, Environmental monitoring report on radiological status of the ground water beneath the Hanford Site, January-December, 1974: BNWL-1970, Pacific Northwest Laboratory, Richland, Washington.
- Scheidegger, A. E., 1954. Statistical hydrodynamics in porous media: Jour. Appl. Phys., No. 25.
- Schmincke, H. U., 1964, Petrology, paleocurrents and stratigraphy of the Ellensburg Formation and interbedded Yakima Basalt flows, south-central Washington: Ph.D. thesis, Johns Hopkins University, 426 p.

_____, 1967, Flow directions in Columbia River Basalt flows and paleocurrents of interbedded sedimentary rocks, south-central Washington Geologischen Rundschau Band 56, p. 992-1010.

Strand, J. R., and Hough, M. J., 1952, Age of the Ringold Formation: Northwest Sci., v. 26, no. 4, p. 152-154.

Swanson, D. A., Grolier, M. J. Higgins, M. W., Isidore, Z., 1972, Feeder dikes for Yakima Basalt near Pasco, Washington: Proc. 1972 Cordilleran Section Meeting, Geol. Soc. America, Honolulu, Hawaii, March 29-April 1.

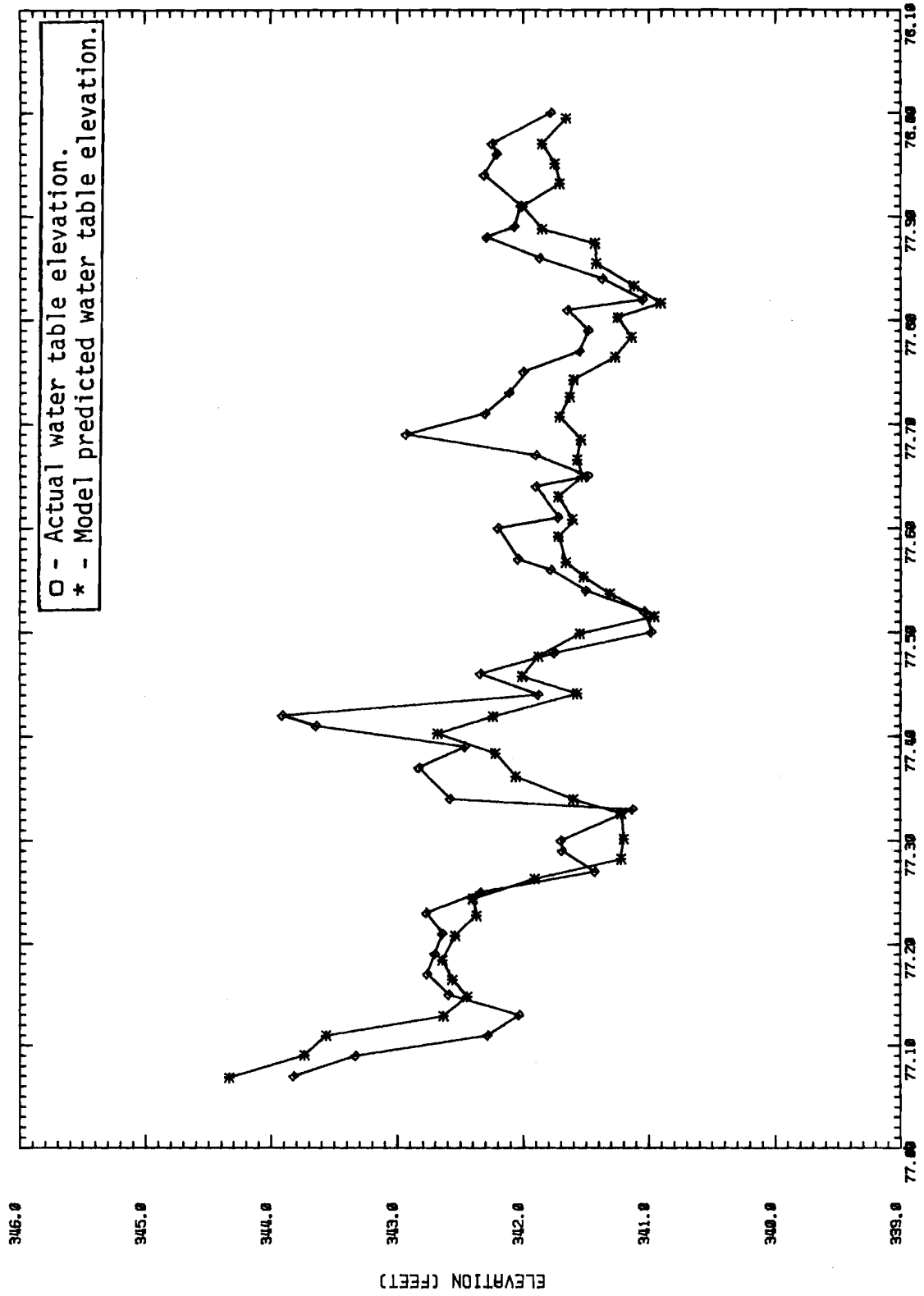
U.S. Energy Research and Development Administration, 1975, Standards for Radiation Proection: ERDA Manual, Chapter 0524, (Appendix) Annex A, Table II, Column 2.

Wallace, R. W., 1978, A comparison of evapotranspiration estimates using DOE Hanford climatological data: PNL-2698, Pacific Northwest Laboratory, Richland, Washington.

APPENDIX

WATER-TABLE ELEVATION-VERSUS-TIME HYDROGRAPH PLOTS
FOR THE 29 OBSERVATION WELLS IN THE 300 AREA

WELL NAME = 399-1-1 FILE NAME = HYGR.301

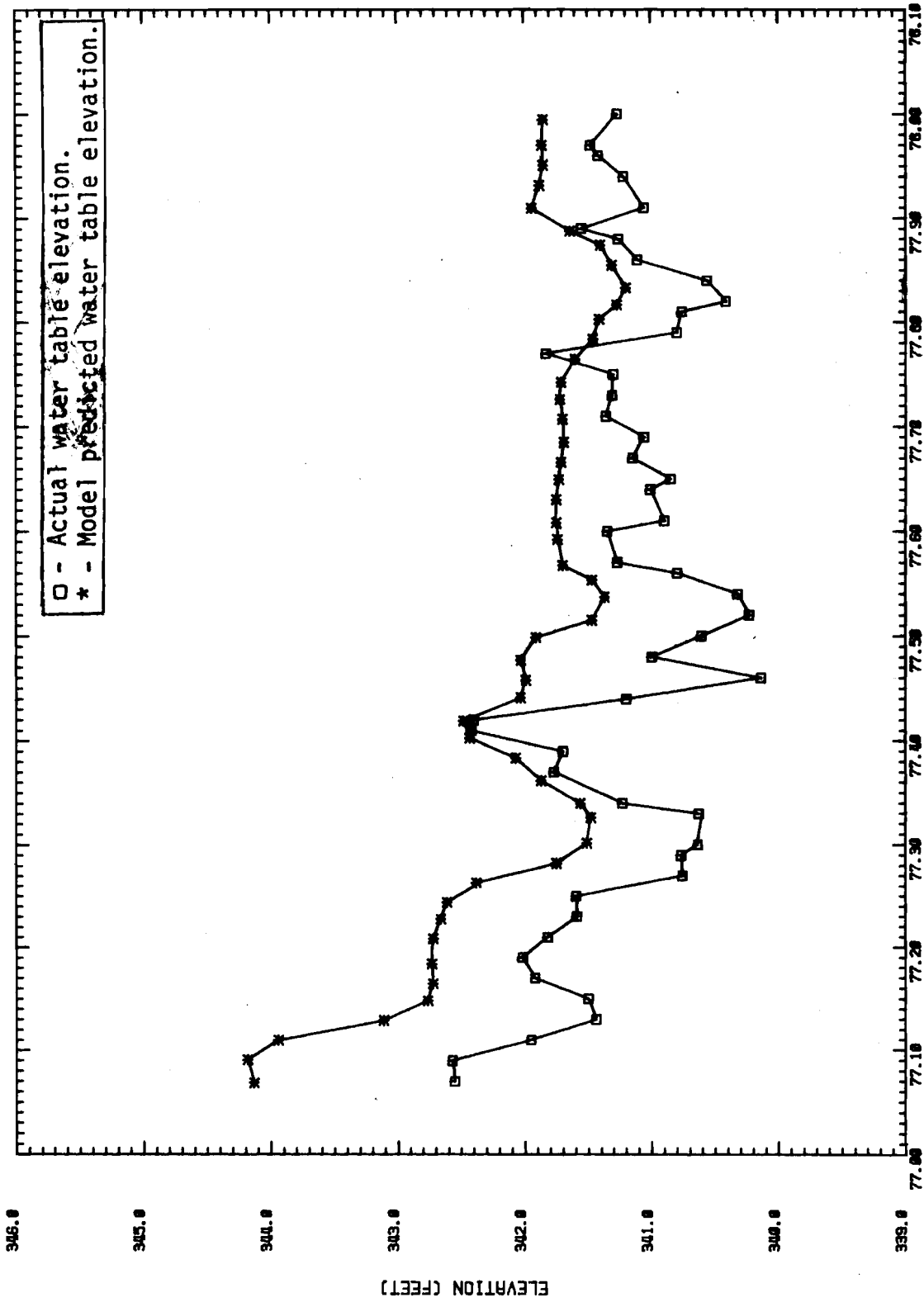


TIME (YEARS)

TIME= 11:57:01 DATE= 25-JAN-79

FIGURE A.1.

WELL NAME = 399-1-2 FILE NAME = HYGR.302

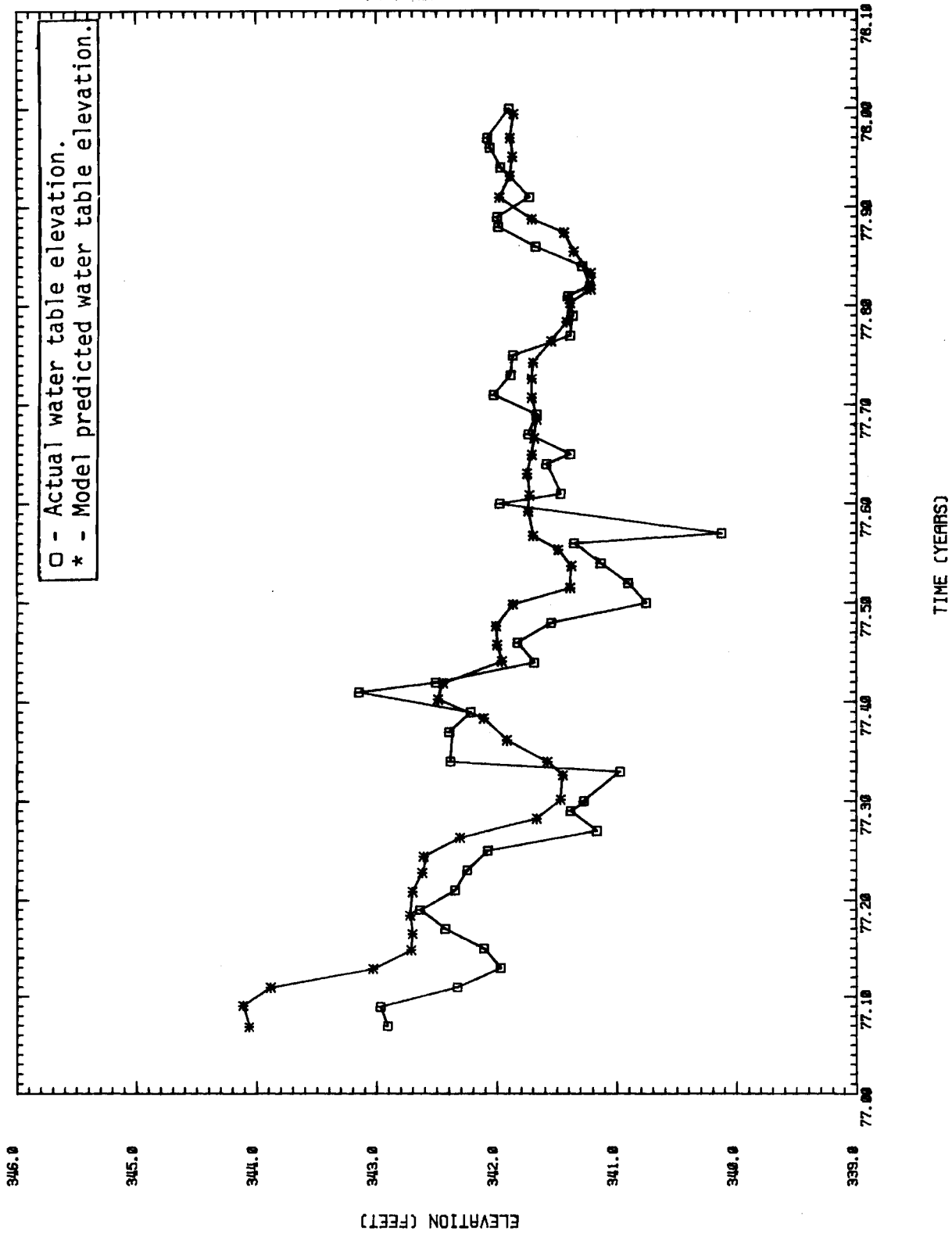


TIME (YEARS)

TIME: 11:59:03 DATE: 25-JUN-79

FIGURE A.2.

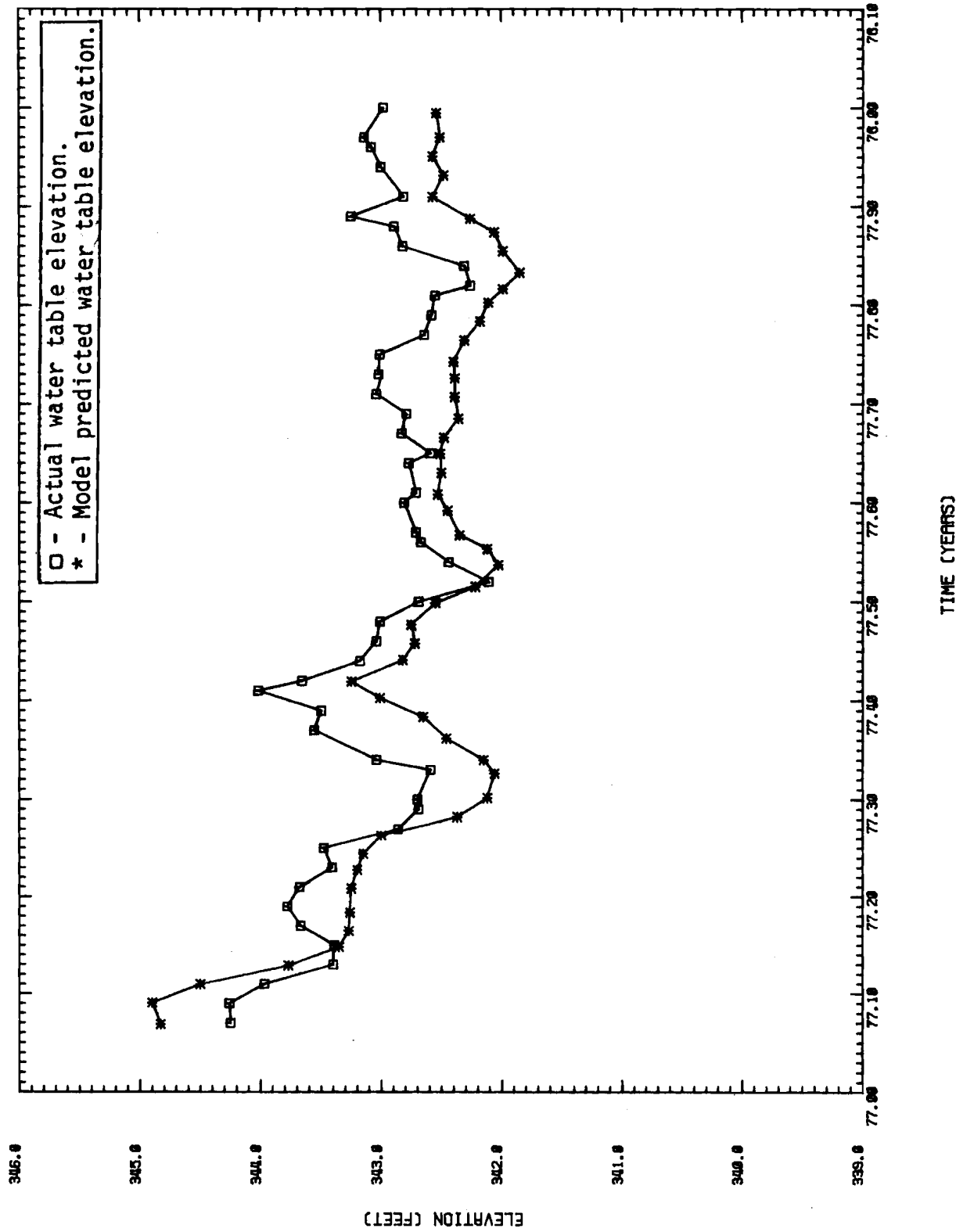
WELL NAME = 399-1-3 FILE NAME = HYGR.303



TIME = 12:01:42 DATE = 25-JAN-79

FIGURE A.3.

WELL NAME = 399-1-4 FILE NAME = HYGR.304

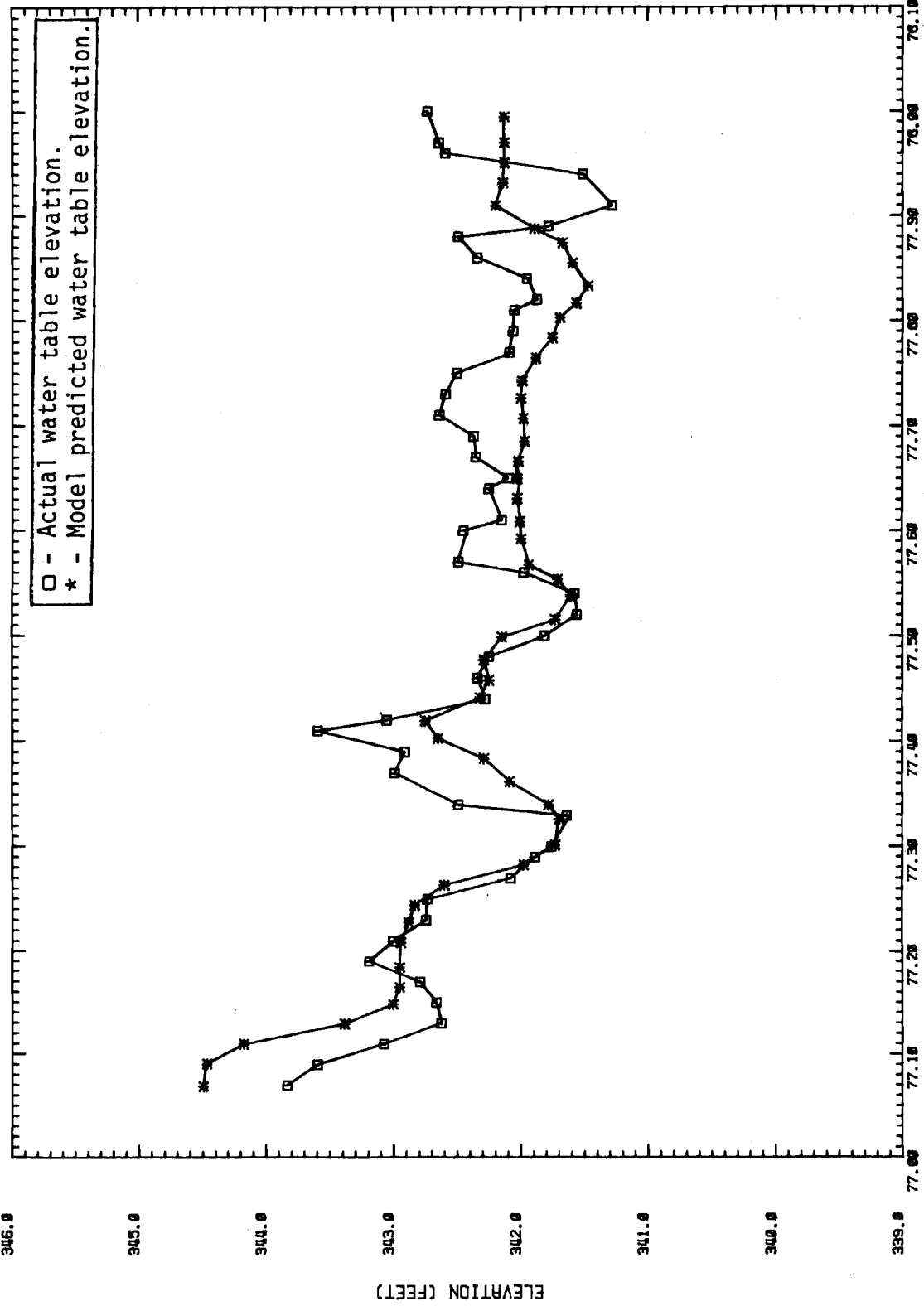


TIME= 12:05:02 DATE= 25-JUN-79

TIME (YEARS)

FIGURE A.4.

WELL NAME = 399-1-5 FILE NAME = HYGR.305

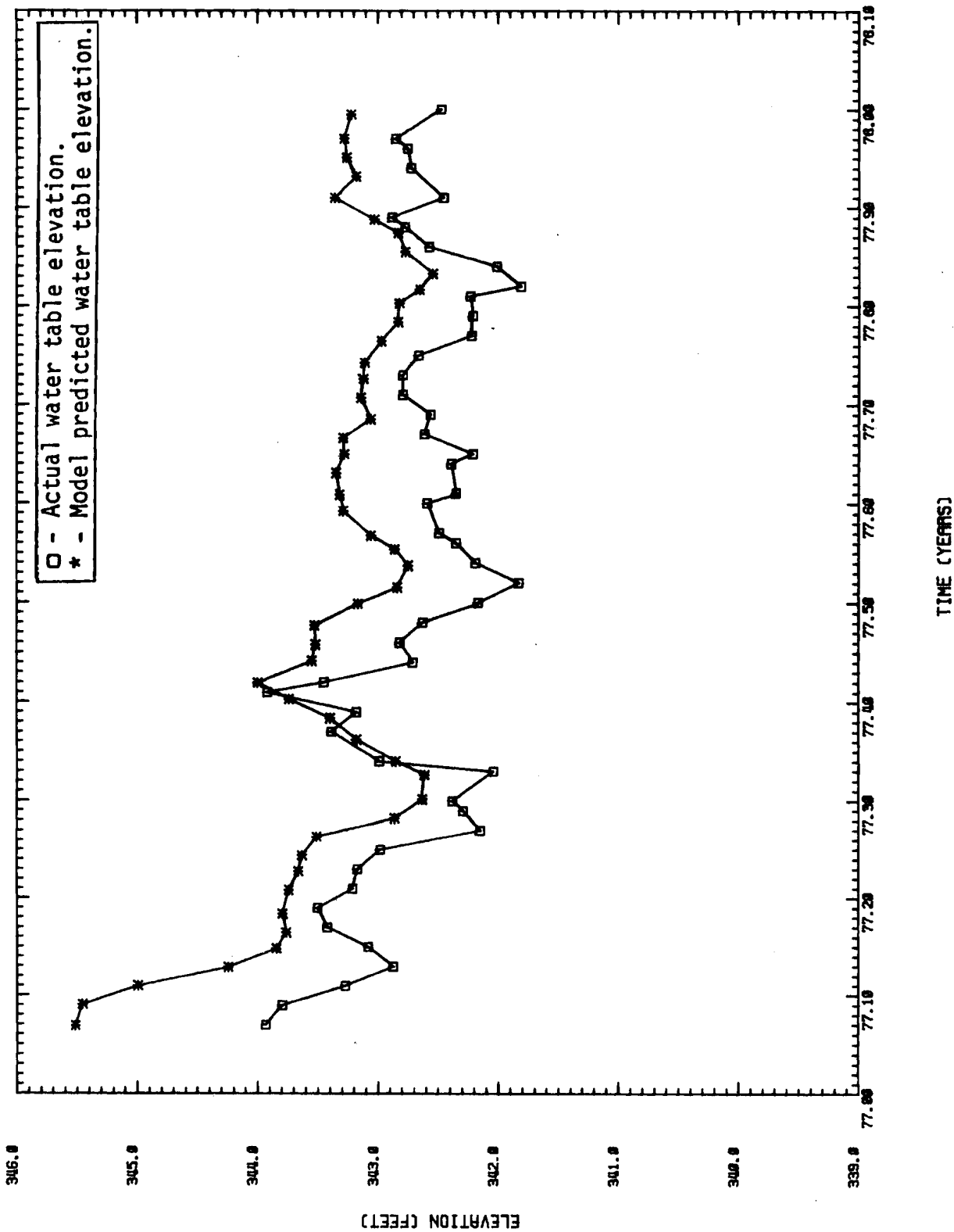


TIME (YEARS)

TIME= 12:07:37 DATE= 25-JAN-79

FIGURE A.5.

WELL NAME = 399-1-6 FILE NAME = HYGR.306

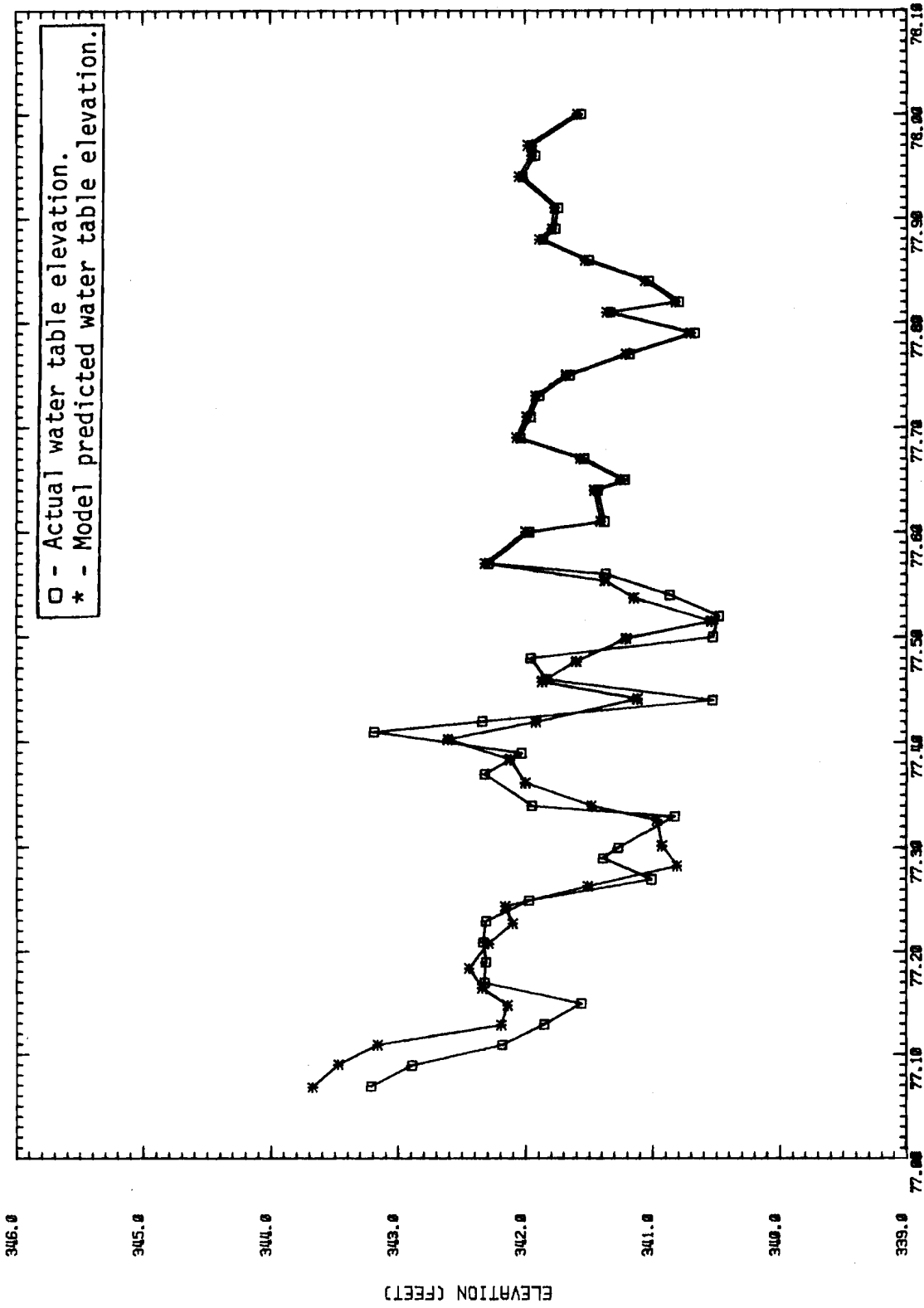


TIME: 12:10:55 DATE: 25-JUN-79

TIME (YEARS)

FIGURE A.6.

WELL NAME = 399-2-1 FILE NAME = HYGR.307

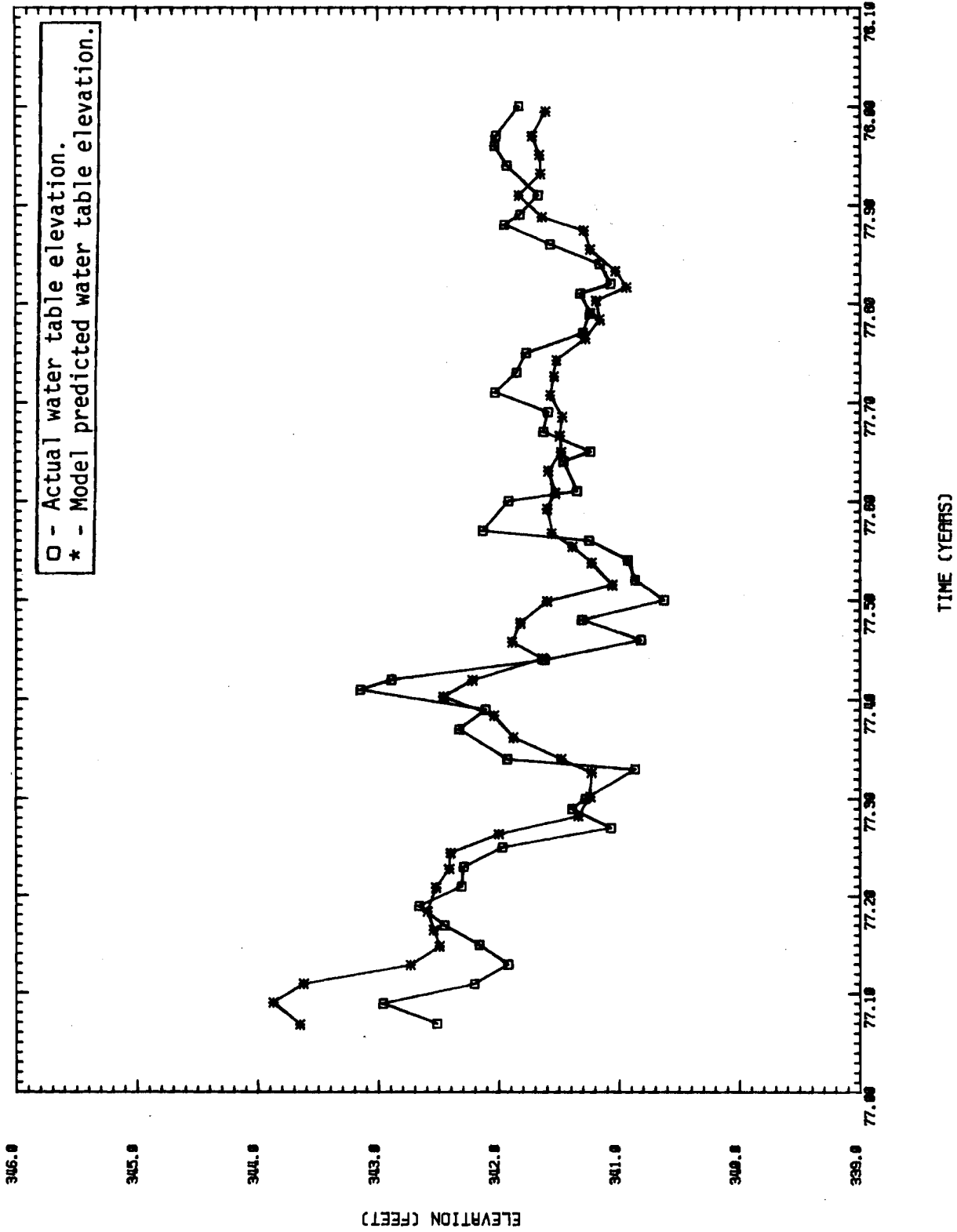


TIME (YEARS)

TIME= 12:13:15 DATE= 25-JAN-79

FIGURE A.7.

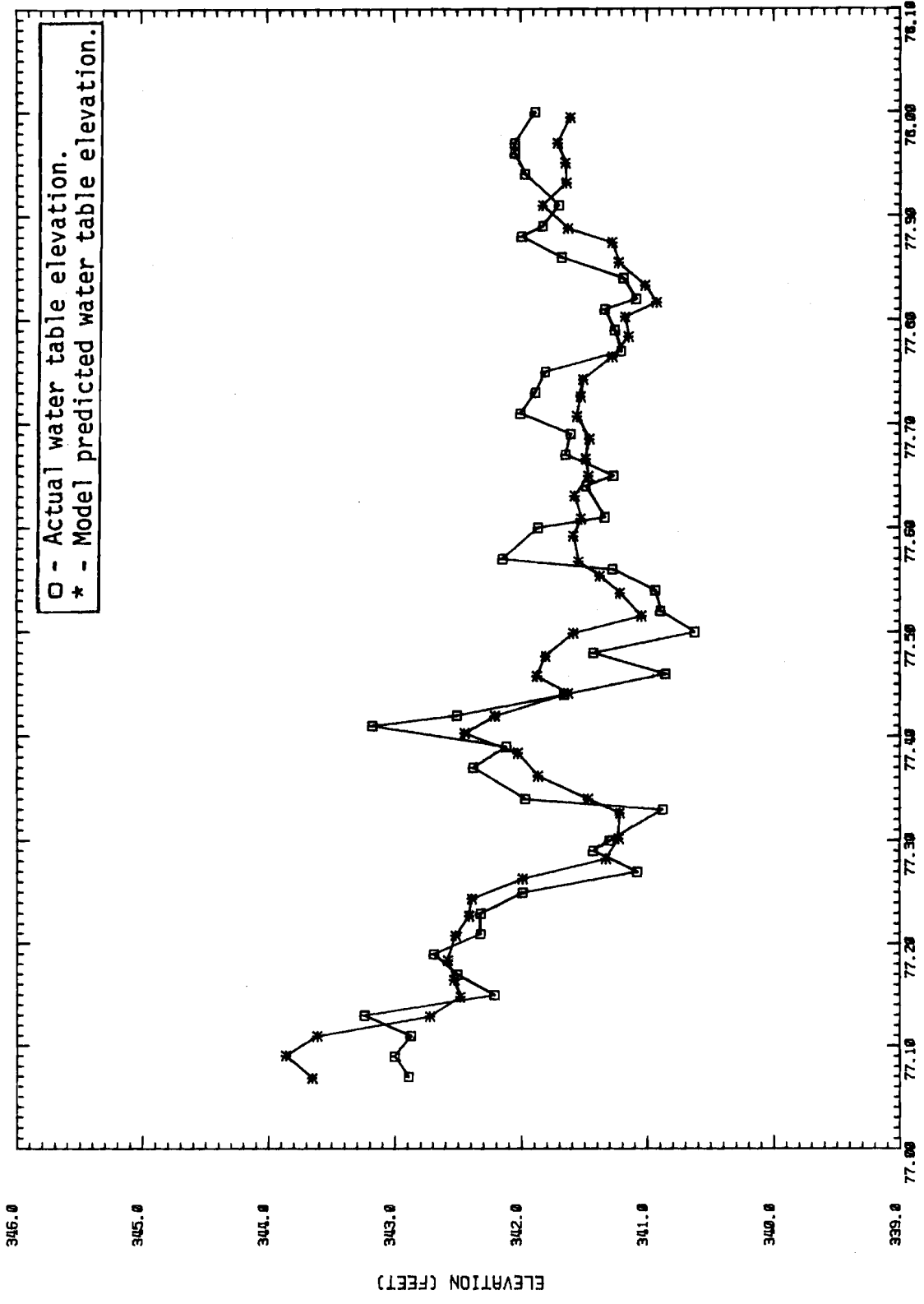
WELL NAME = 399-2-2 FILE NAME = HYGR.308



TIME = 12:16:08 DATE = 25-JAN-79

FIGURE A.8.

WELL NAME = 399-2-3 FILE NAME = HYGR.309

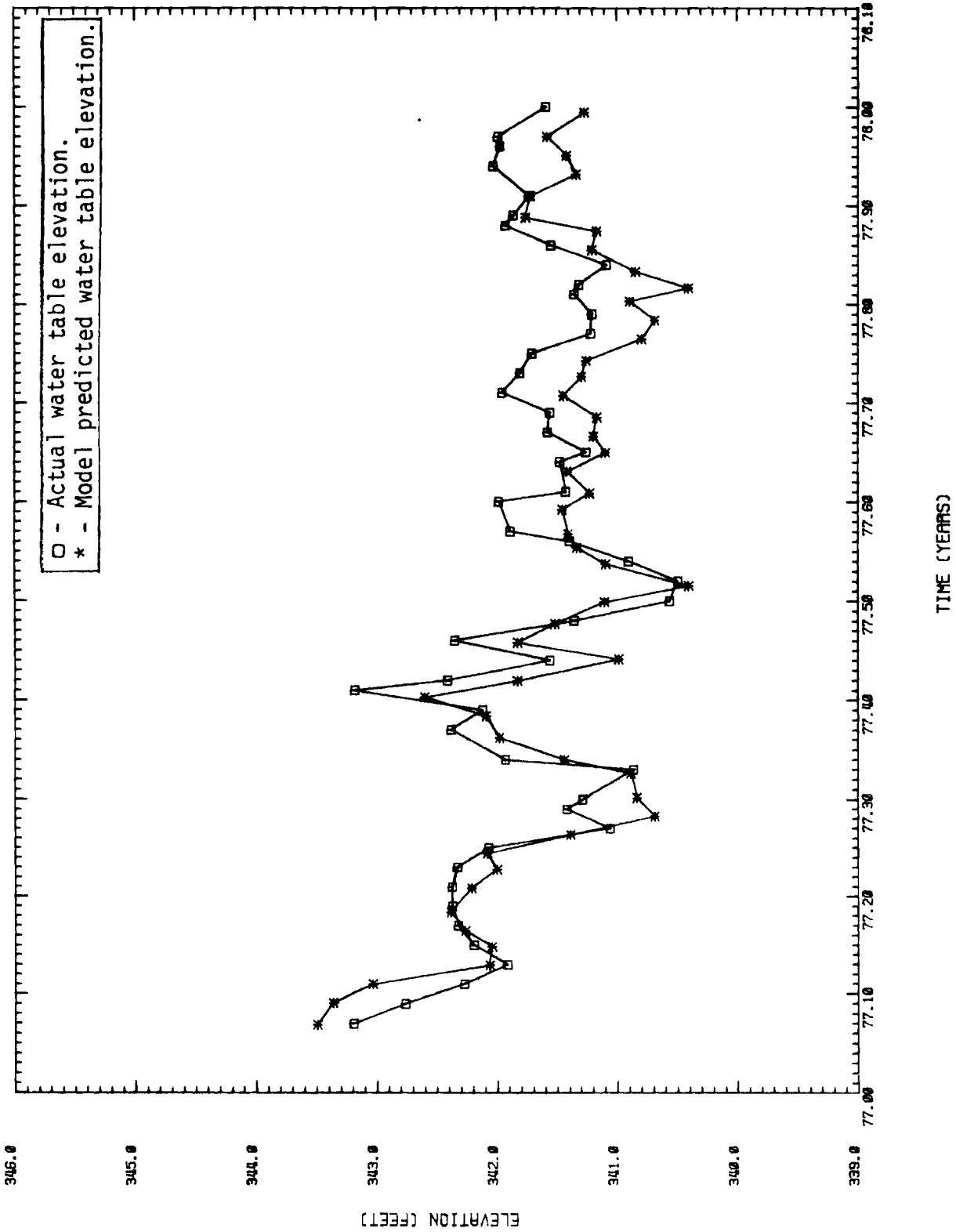


TIME (YEARS)

TIME: 12-16-79 DATE: 25-JAN-79

FIGURE A.9.

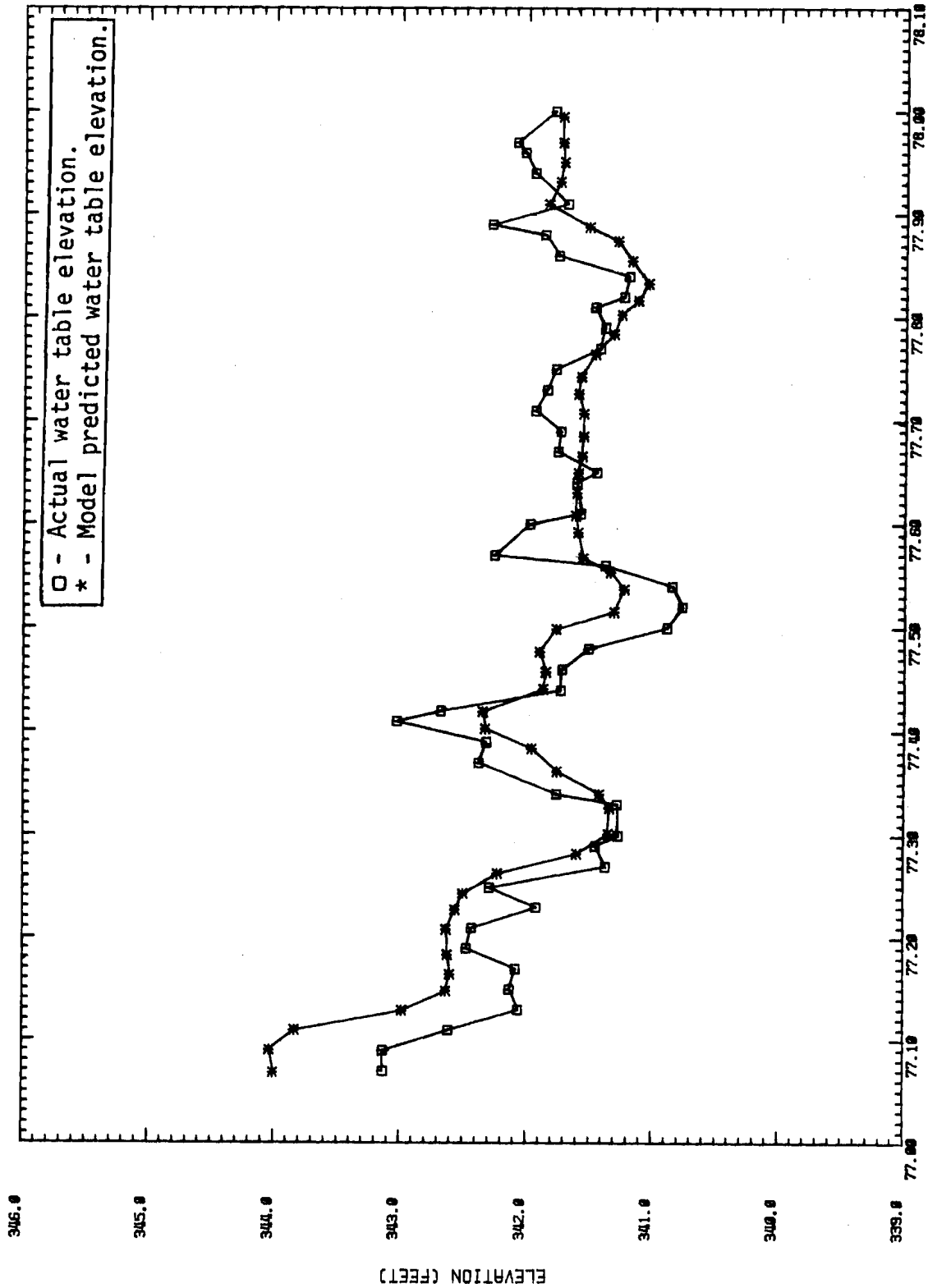
WELL NAME = 399-3-1 FILE NAME = HYGR.310



TIME = 12:20:33 DATE = 25-JAN-79

FIGURE A.10.

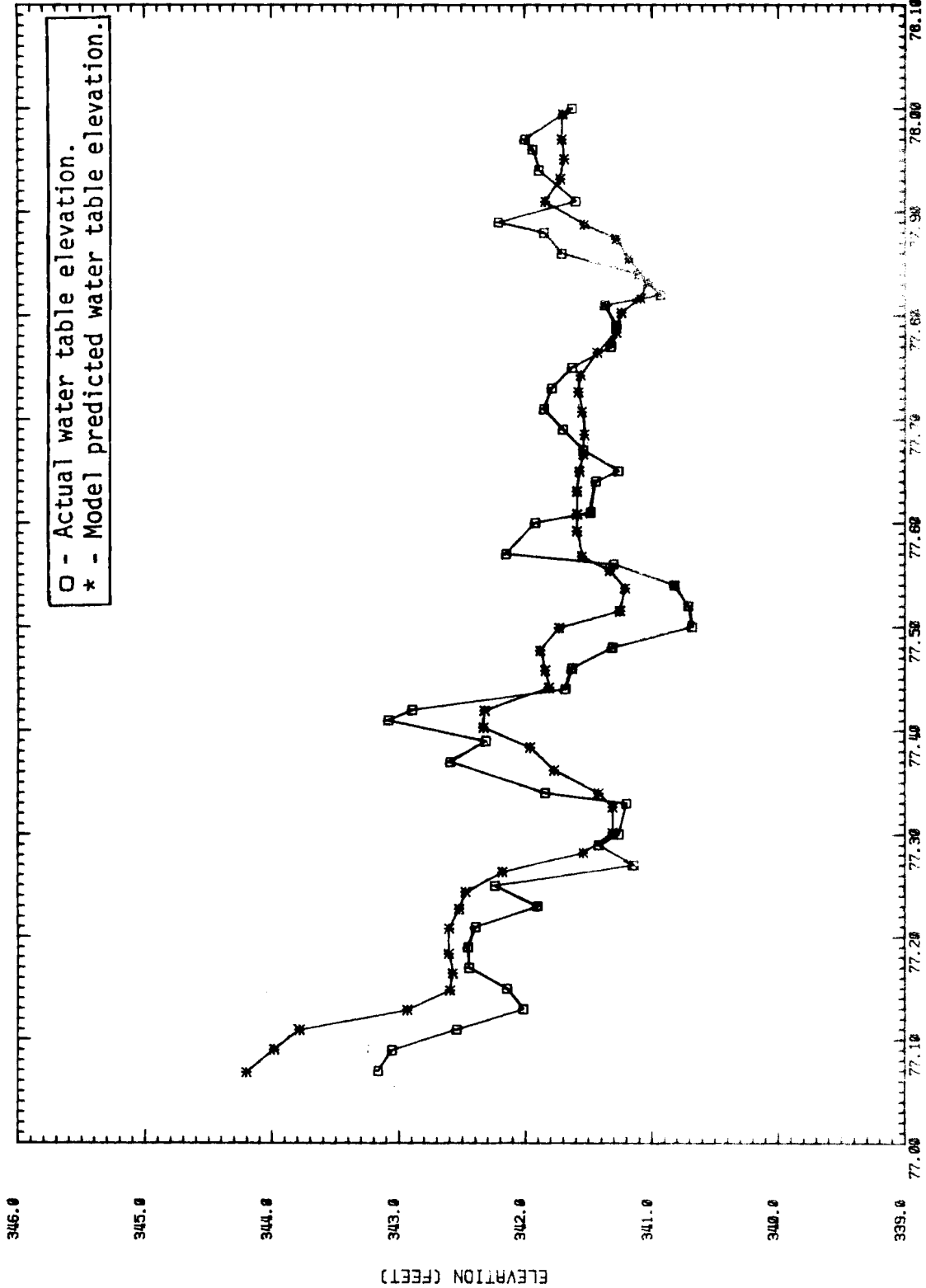
WELL NAME = 399-3-2 FILE NAME = HYGR.311



TIME (YEARS)

TIME= 12-22-85 DATE= 25-JAN-79

FIGURE A.11.

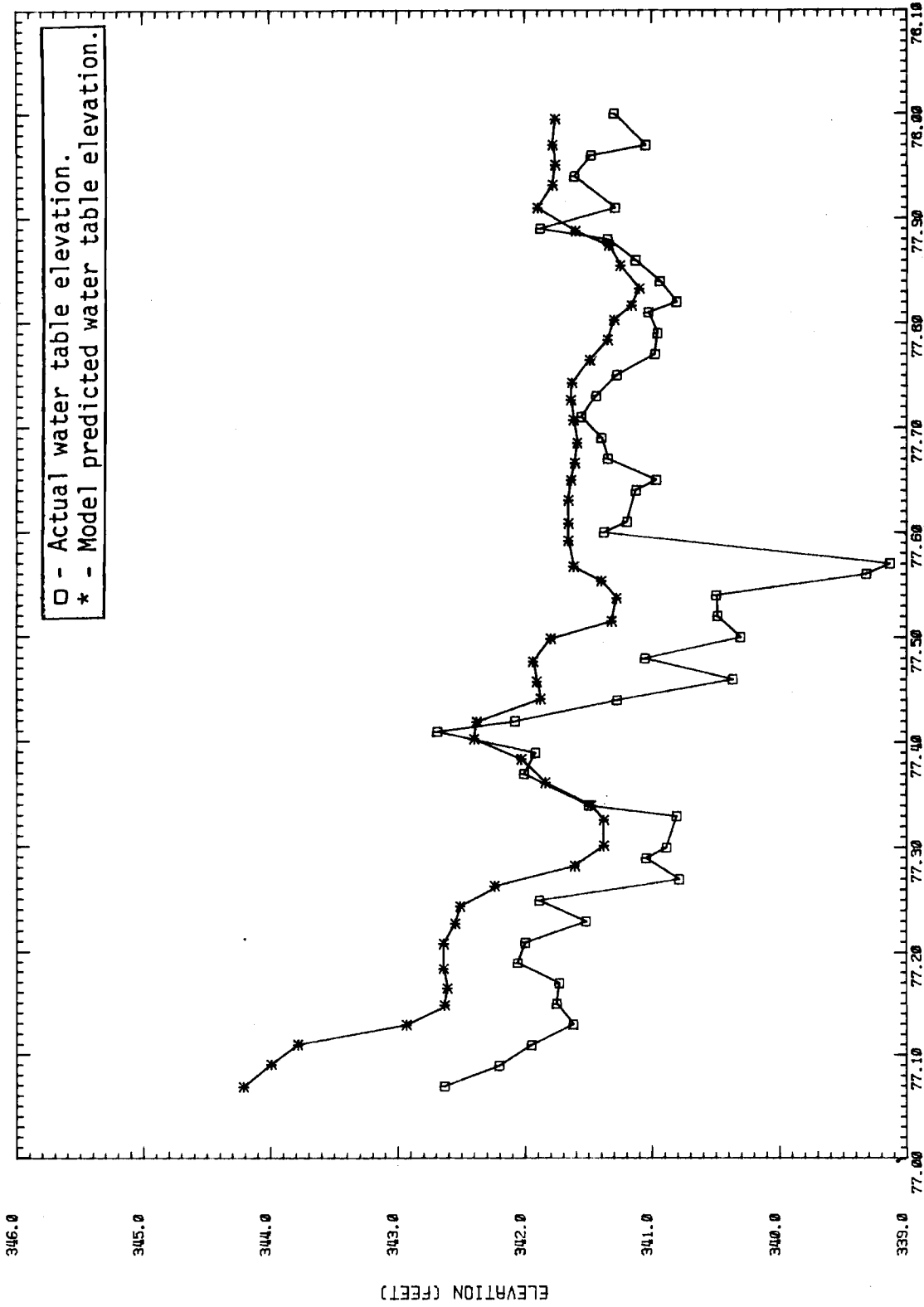


TIME (YEARS)

TIME = 12:24:40 DATE = 25-JAN-79

FIGURE A.12.

WELL NAME = 399-3-8 FILE NAME = HYGR.313

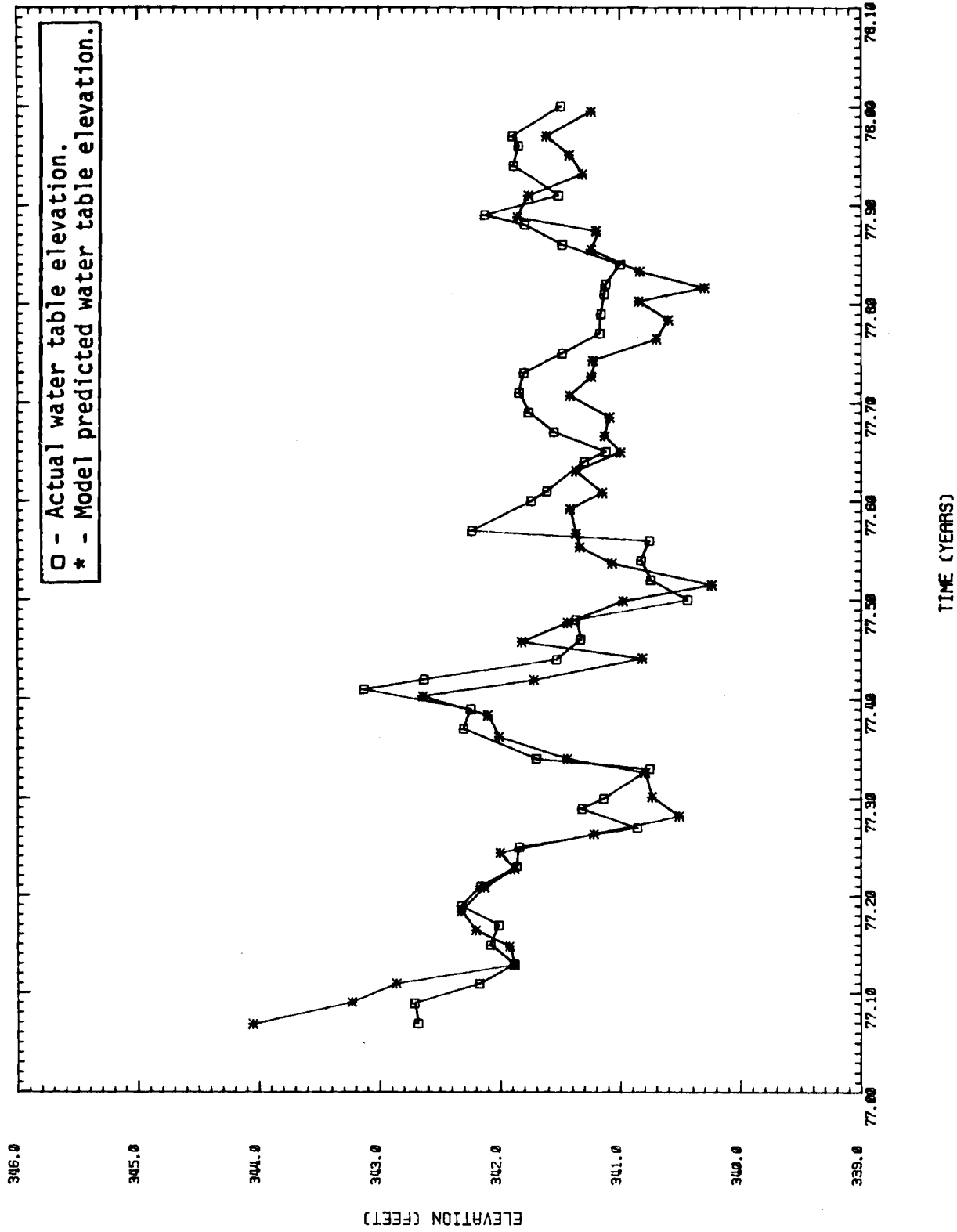


TIME (YEARS)

TIME = 12:54:05 DATE = 25-JAN-79

FIGURE A.13.

WELL NAME = 399-3-9 FILE NAME = HYGR.314

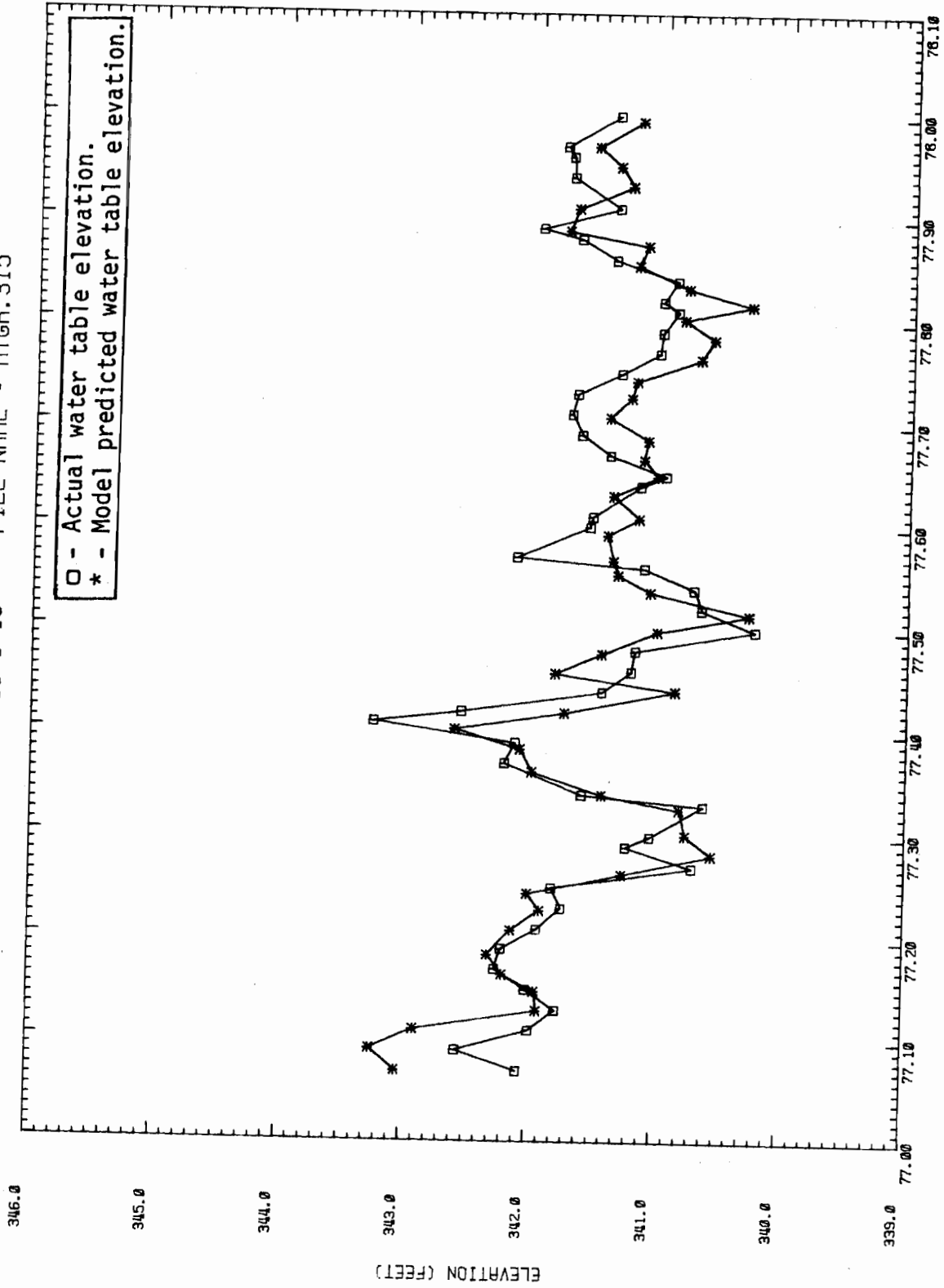


TIME = 12:56:04 DATE = 25-JUN-79

TIME (YEARS)

FIGURE A.14.

WELL NAME = 399-3-10 FILE NAME = HYGR.315

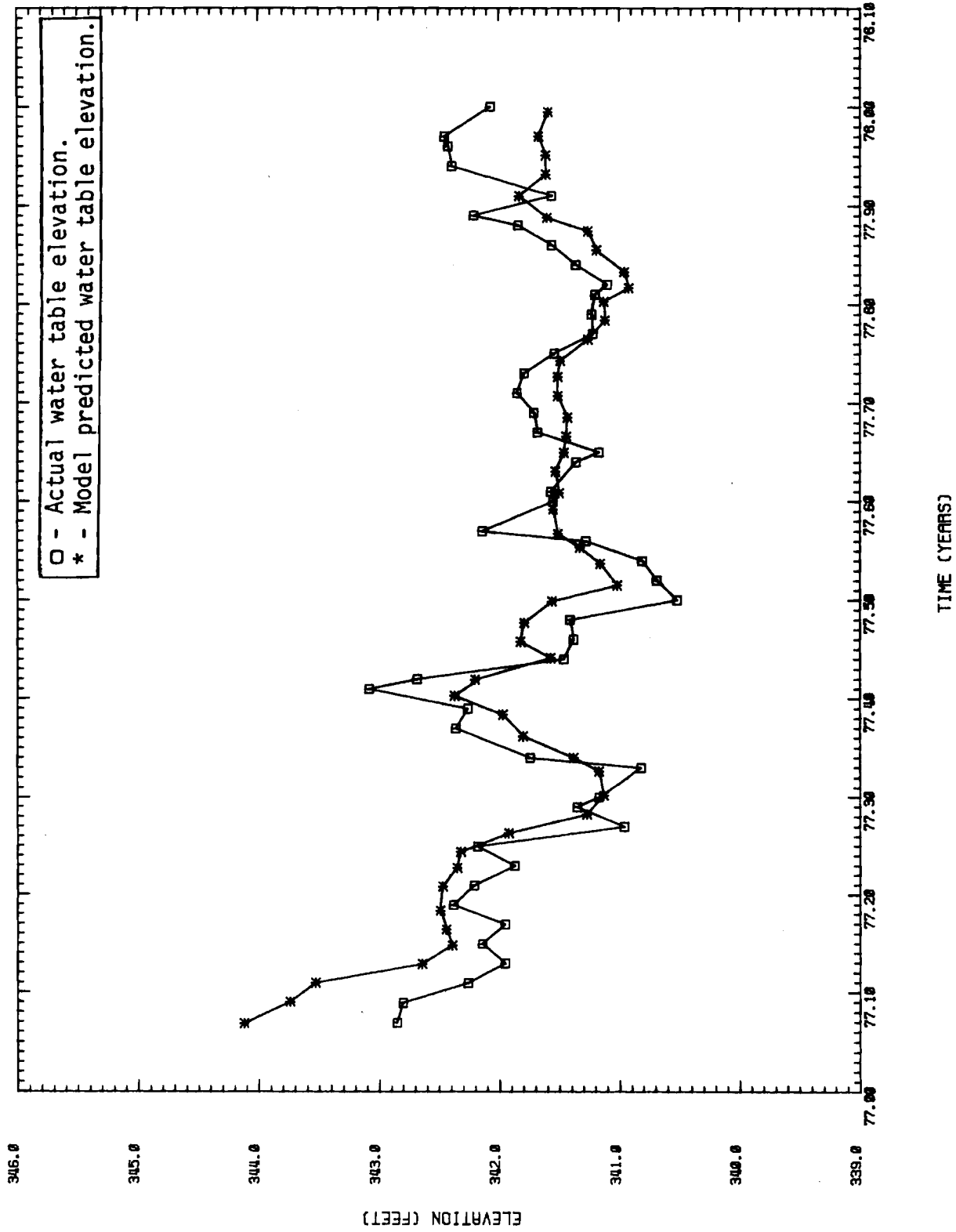


TIME (YEARS)

TIME= 12+56+04 DATE= 25-JAN-79

FIGURE A.15.

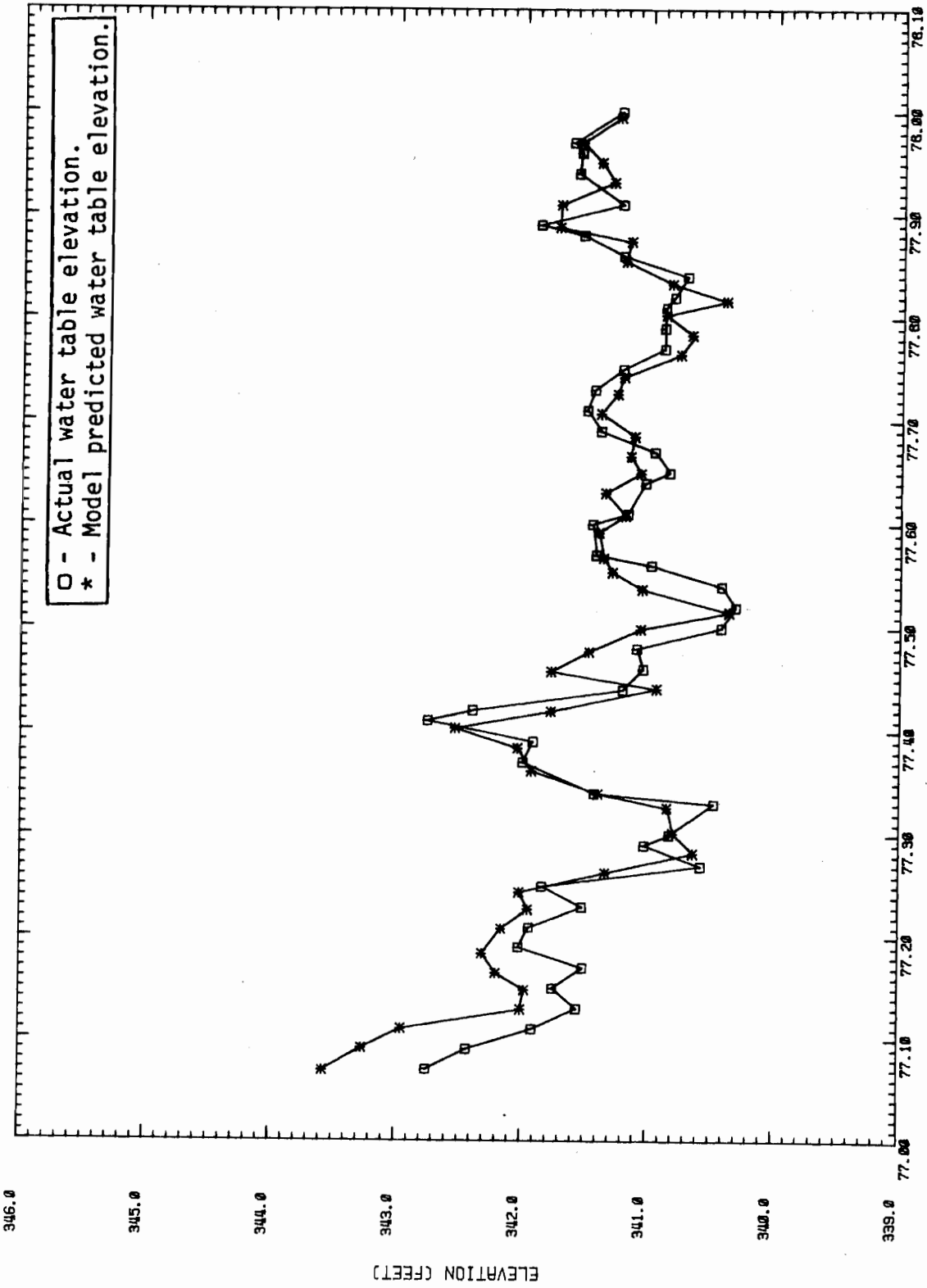
WELL NAME = 399-3-11 FILE NAME = HYGR.316



TIME = 13:00:21 DATE = 25-JAN-79

FIGURE A.16.

WELL NAME = 399-4-1 FILE NAME = HYGR.317

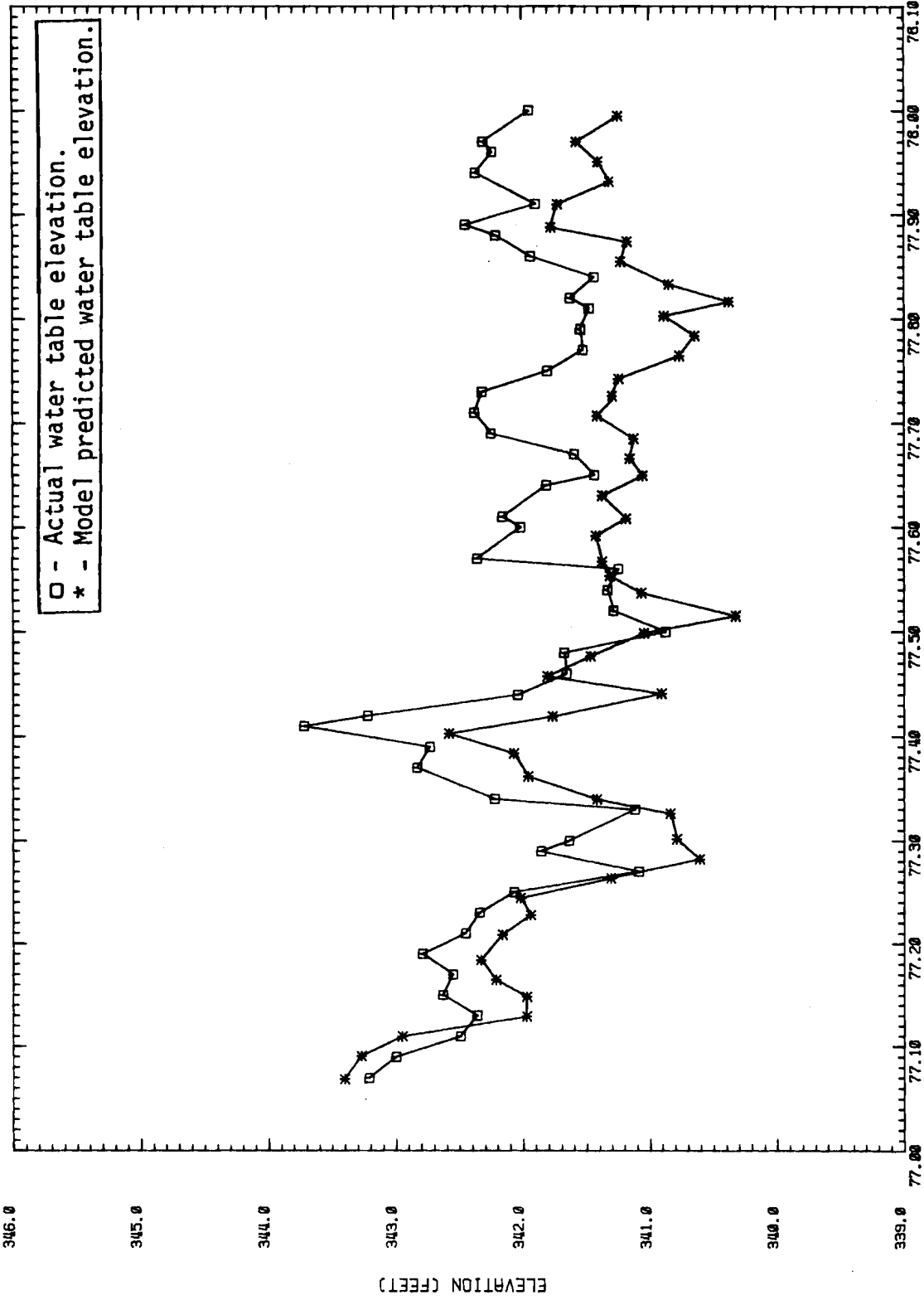


TIME (YEARS)

TIME= 14:58:12 DATE= 25-JAN-79

FIGURE A.17.

WELL NAME = 399-4-7 FILE NAME = HYGR.318

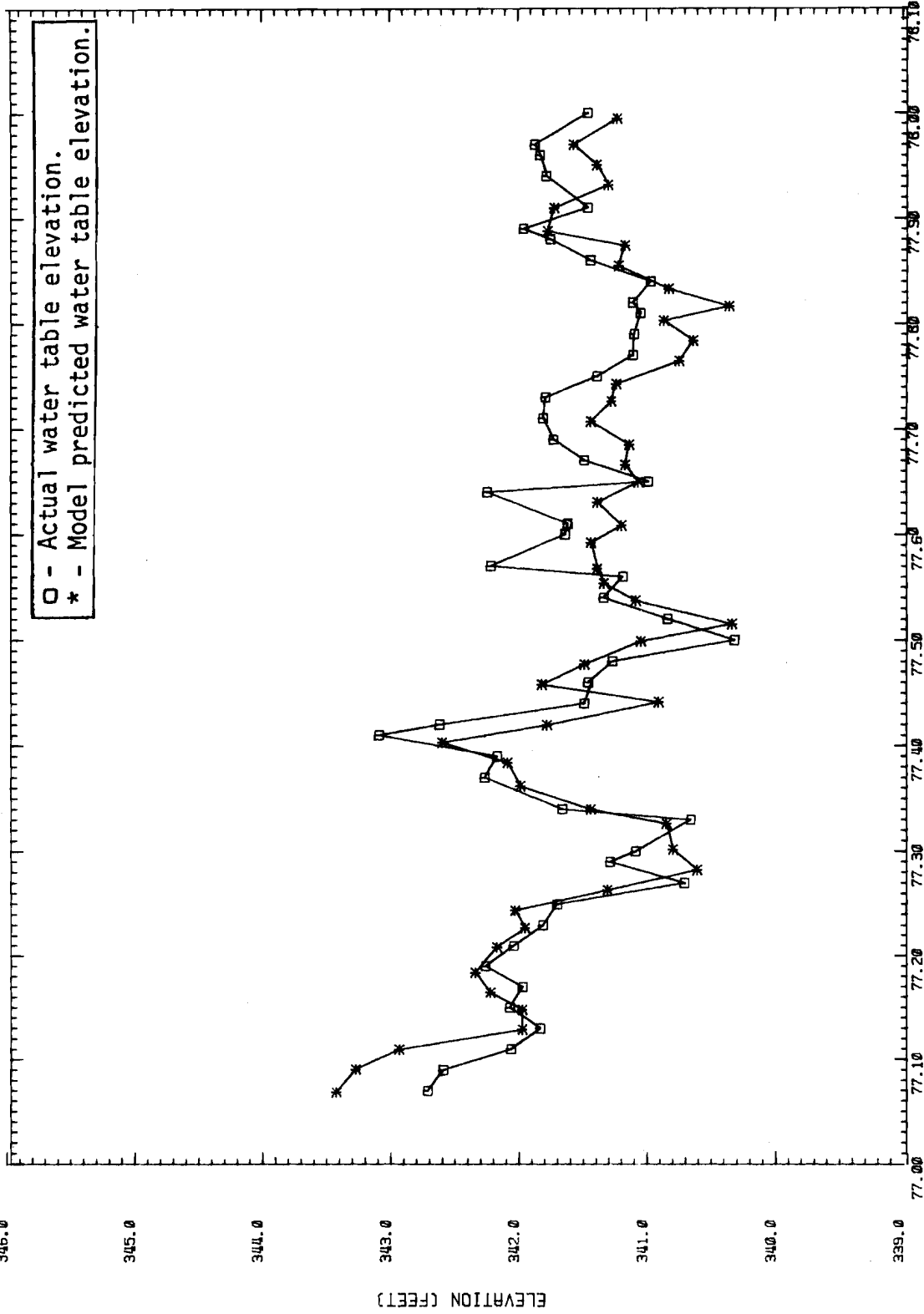


TIME (YEARS)

TIME = 15:00:14 DATE = 25-JAN-79

FIGURE A.18.

WELL NAME = 399-4-9 FILE NAME = HYGR.319

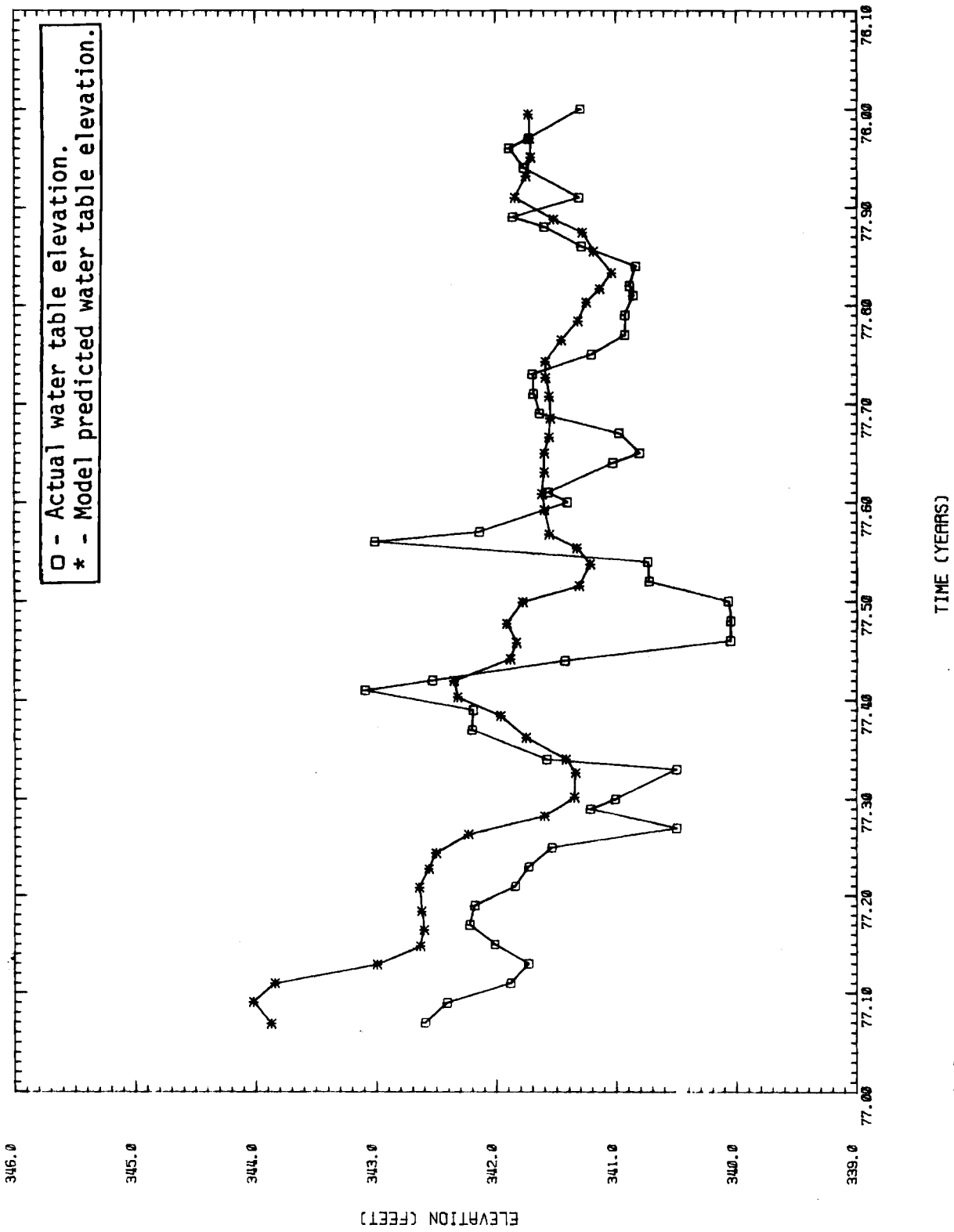


TIME (YEARS)

TIME = 15:02:31 DATE = 25-JAN-79

FIGURE A.19.

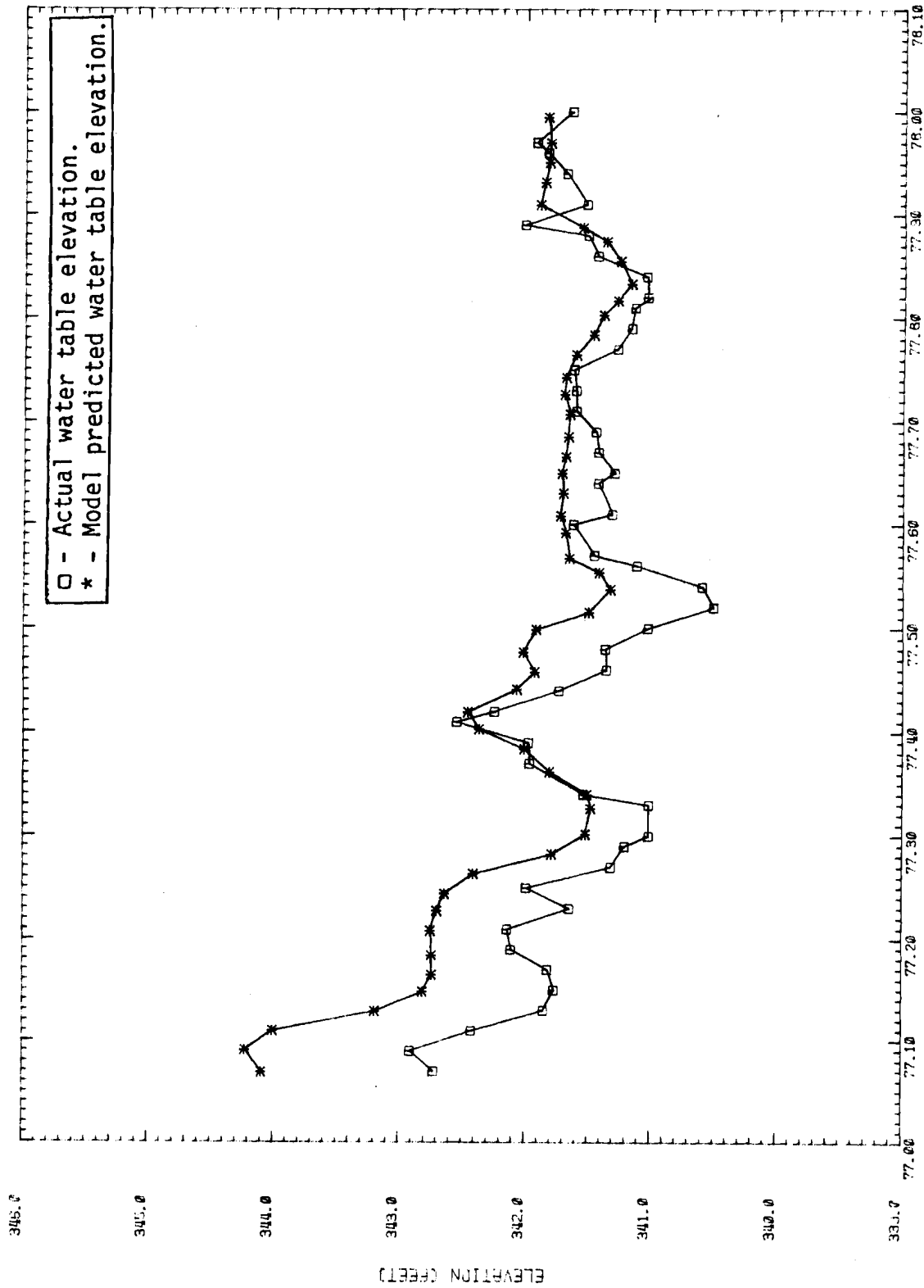
WELL NAME = 399-4-10 FILE NAME = HYGR.320



TIME = 15:04:36 DATE = 25-JAN-79

FIGURE A.20.

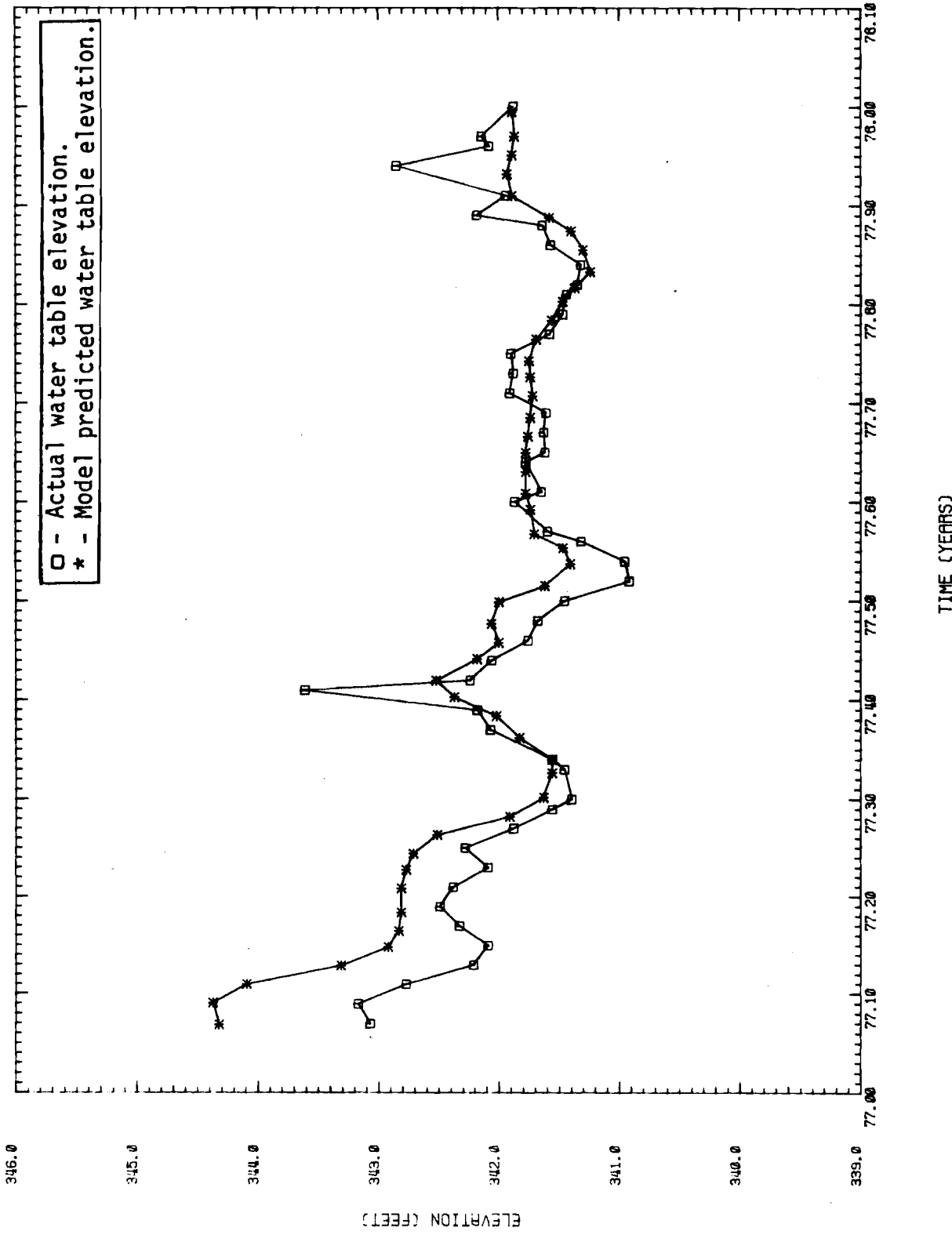
WELL NAME = 399-5-1 FILE NAME = HYGR.321



TIME (YEARS)

TIME = 15:06:40 DATE = 25-JAN-79

FIGURE A.21.

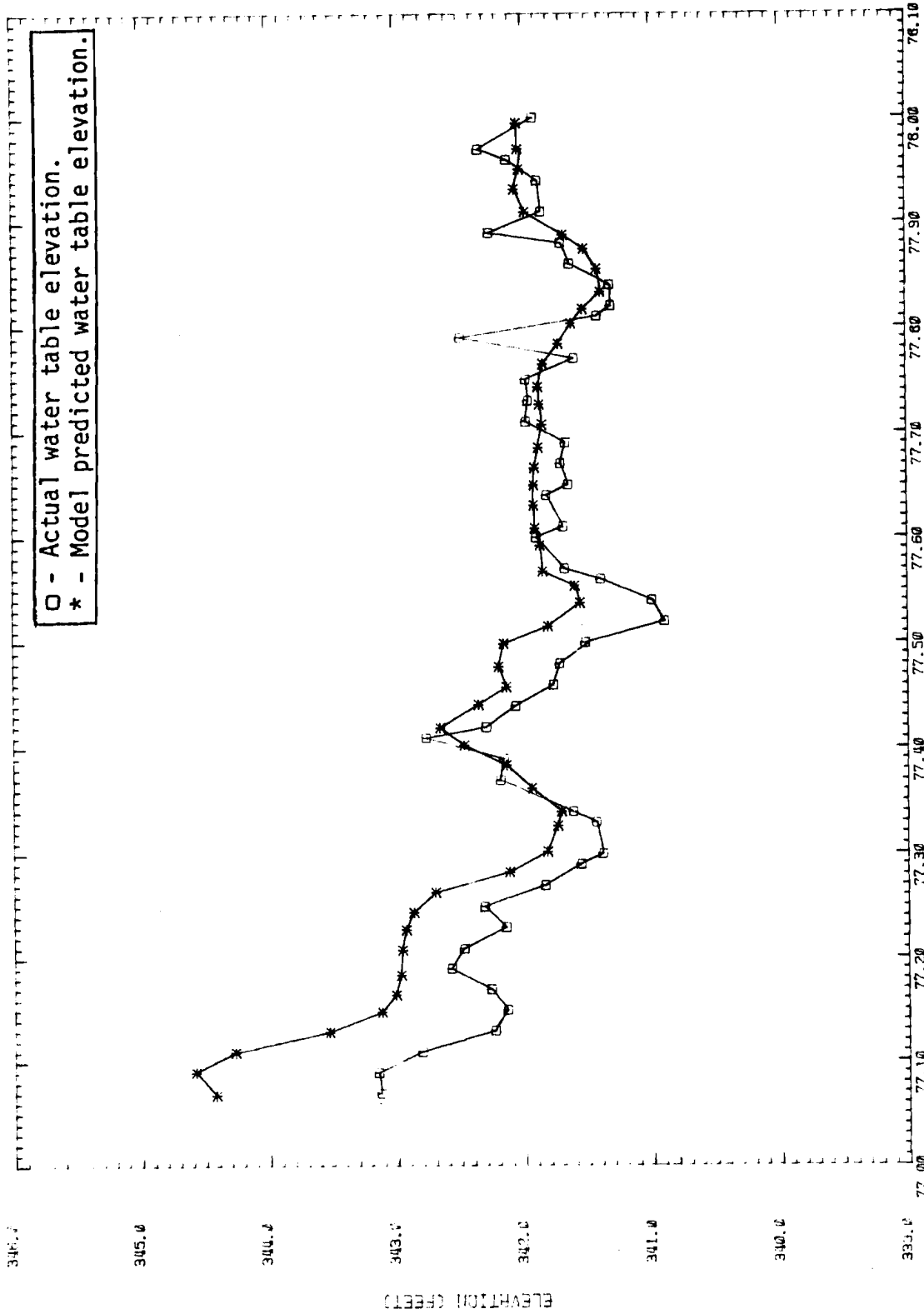


TIME = 15:08:55 DATE = 25-JAN-79

TIME (YEARS)

FIGURE A.22.

WELL NAME = 399-8-1 FILE NAME = HYDR.323

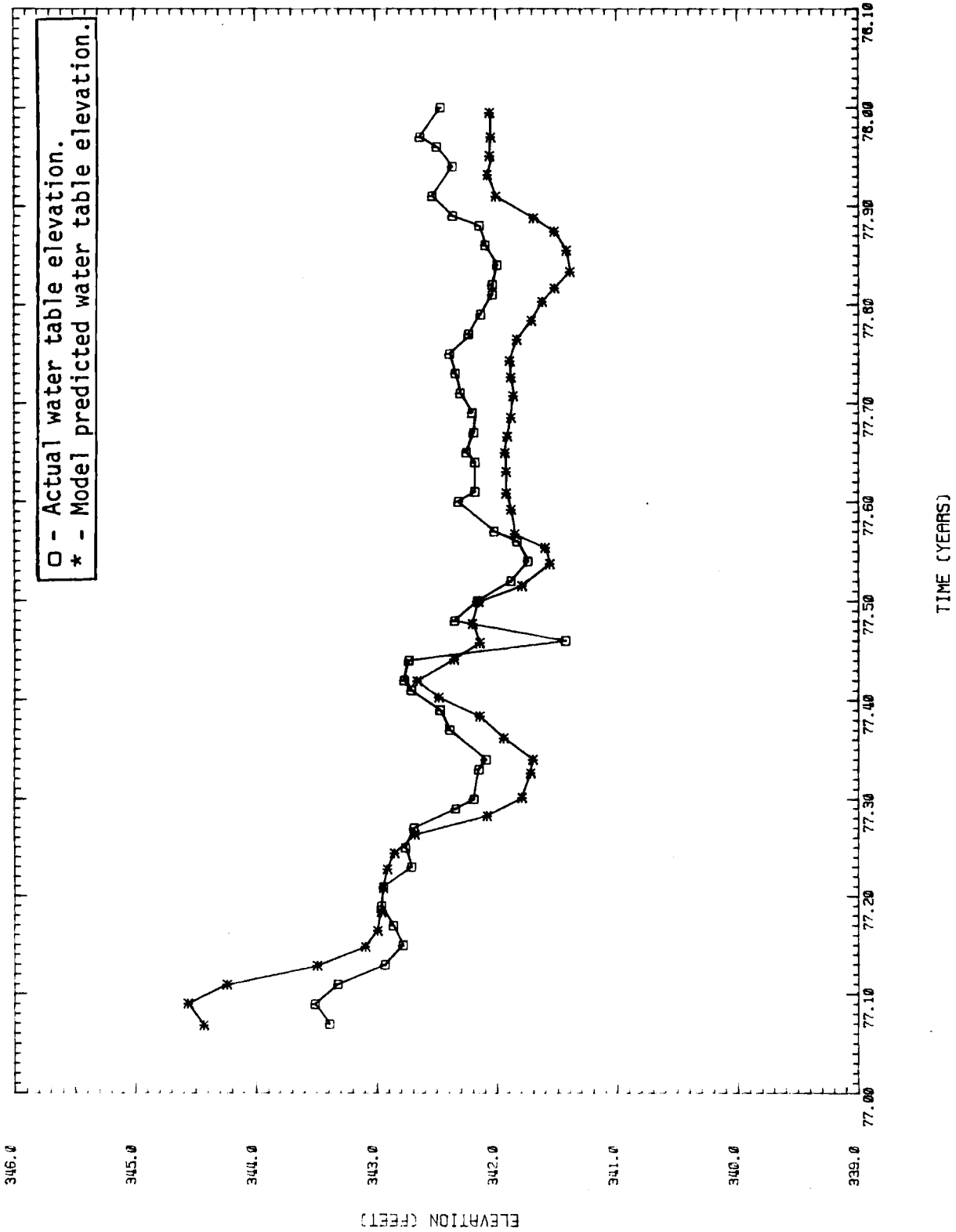


TIME (YEARS)

TIME= 15.11.10 DATE= 25-JAN-79

FIGURE A.23.

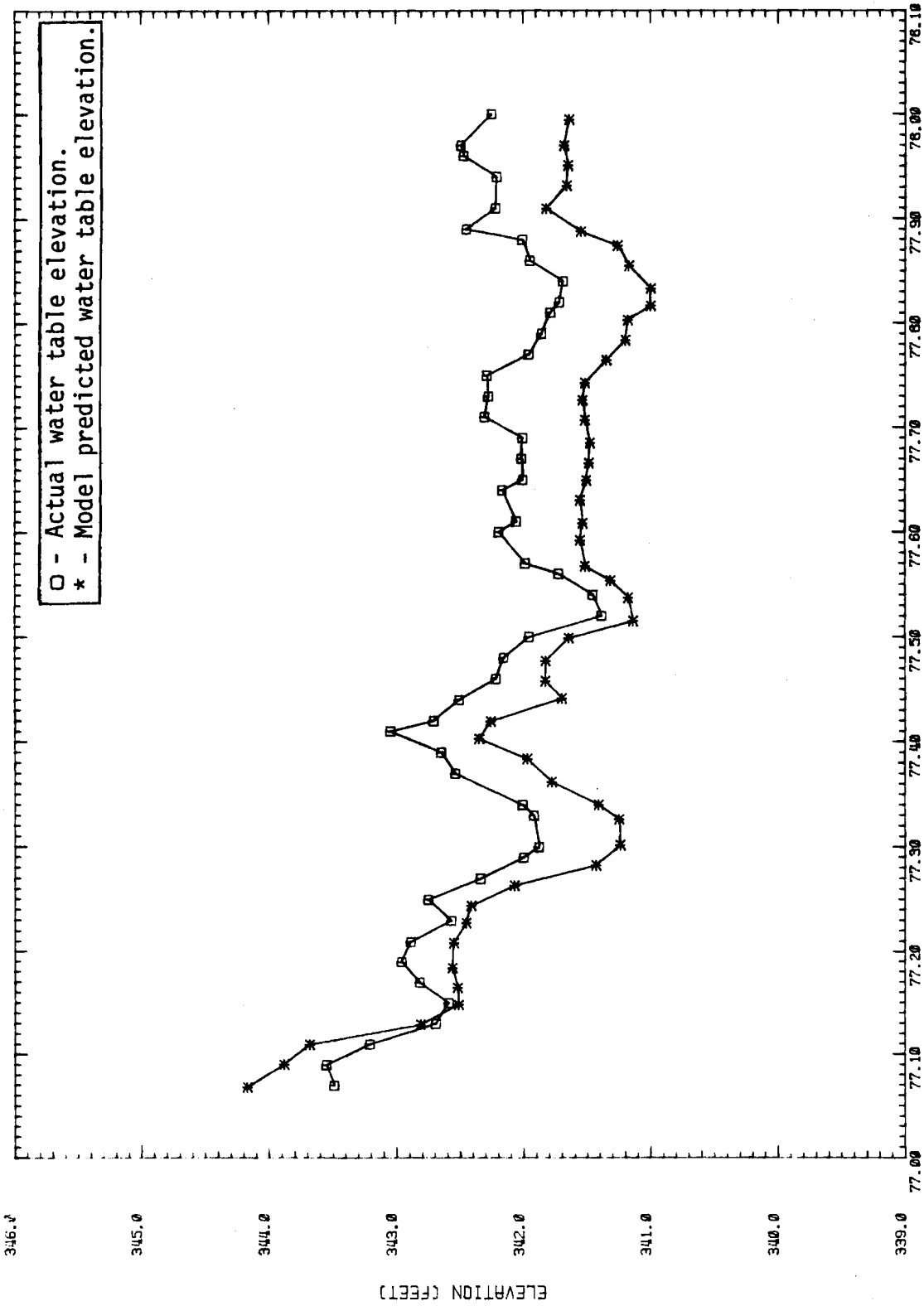
WELL NAME = 399-8-2 FILE NAME = HYGR.324



TIME= 15*13*15 DATE= 25-JAN-79

FIGURE A.24.

WELL NAME = 399-8-3 FILE NAME = HYGR.325

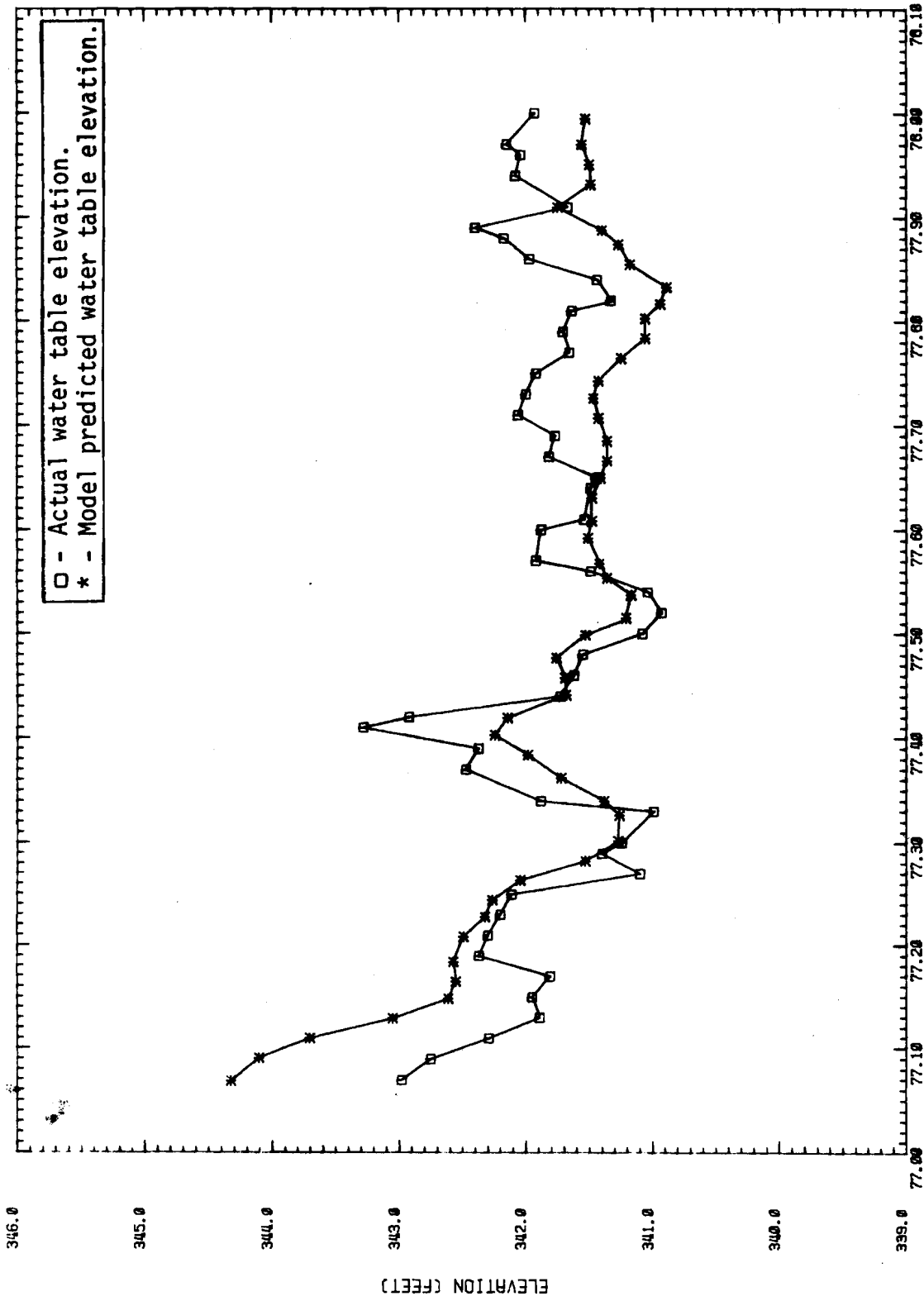


TIME (YEARS)

TIME= 15:15:21 DATE= 25-JAN-79

FIGURE A.25.

WELL NAME = 99-E15 FILE NAME = HYGR.326



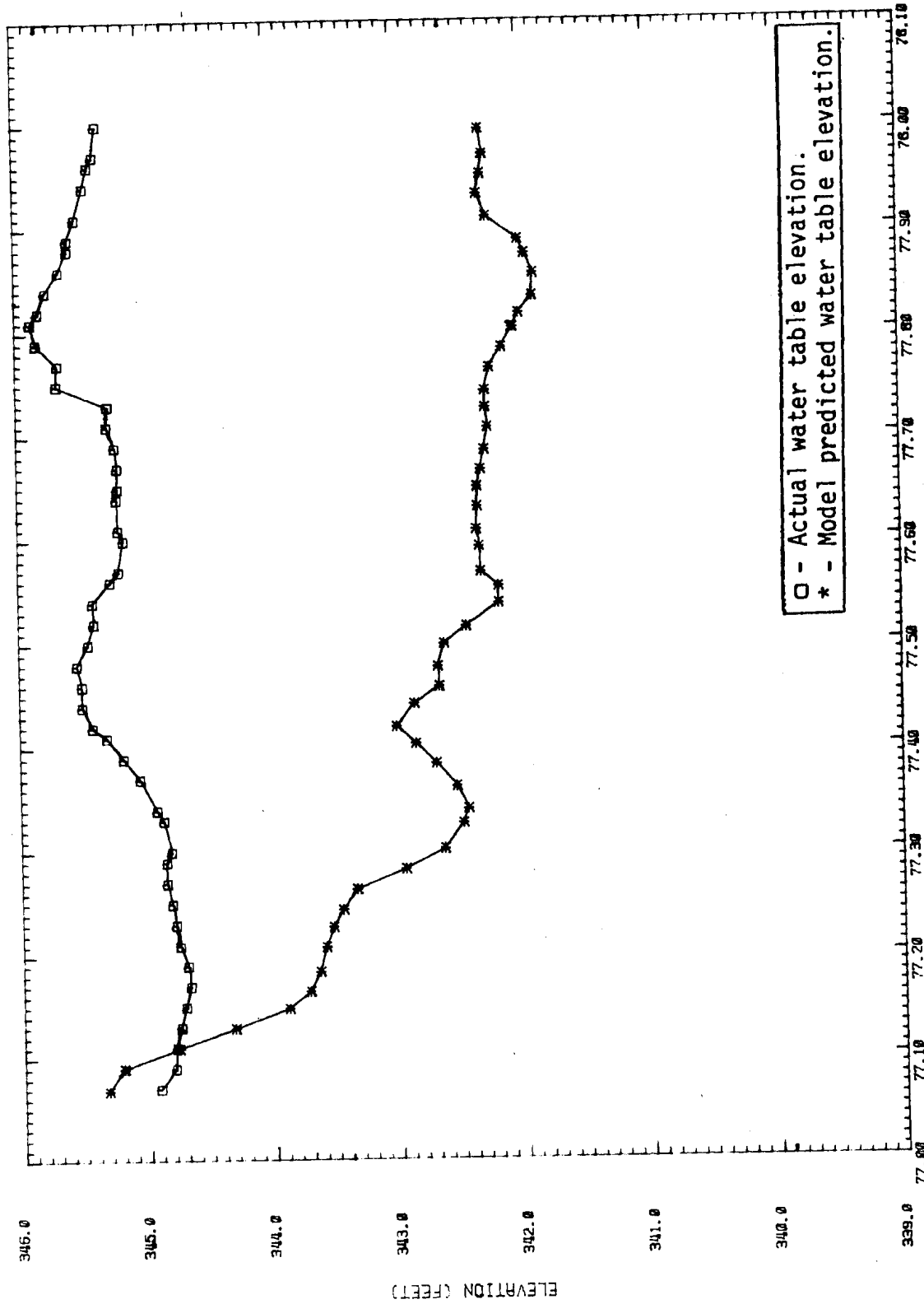
□ - Actual water table elevation.
* - Model predicted water table elevation.

TIME (YEARS)

TIME= 15.17.28 DATE= 25-JAN-79

FIGURE A.26.

WELL NAME = 399-E12 FILE NAME = HYGR.327

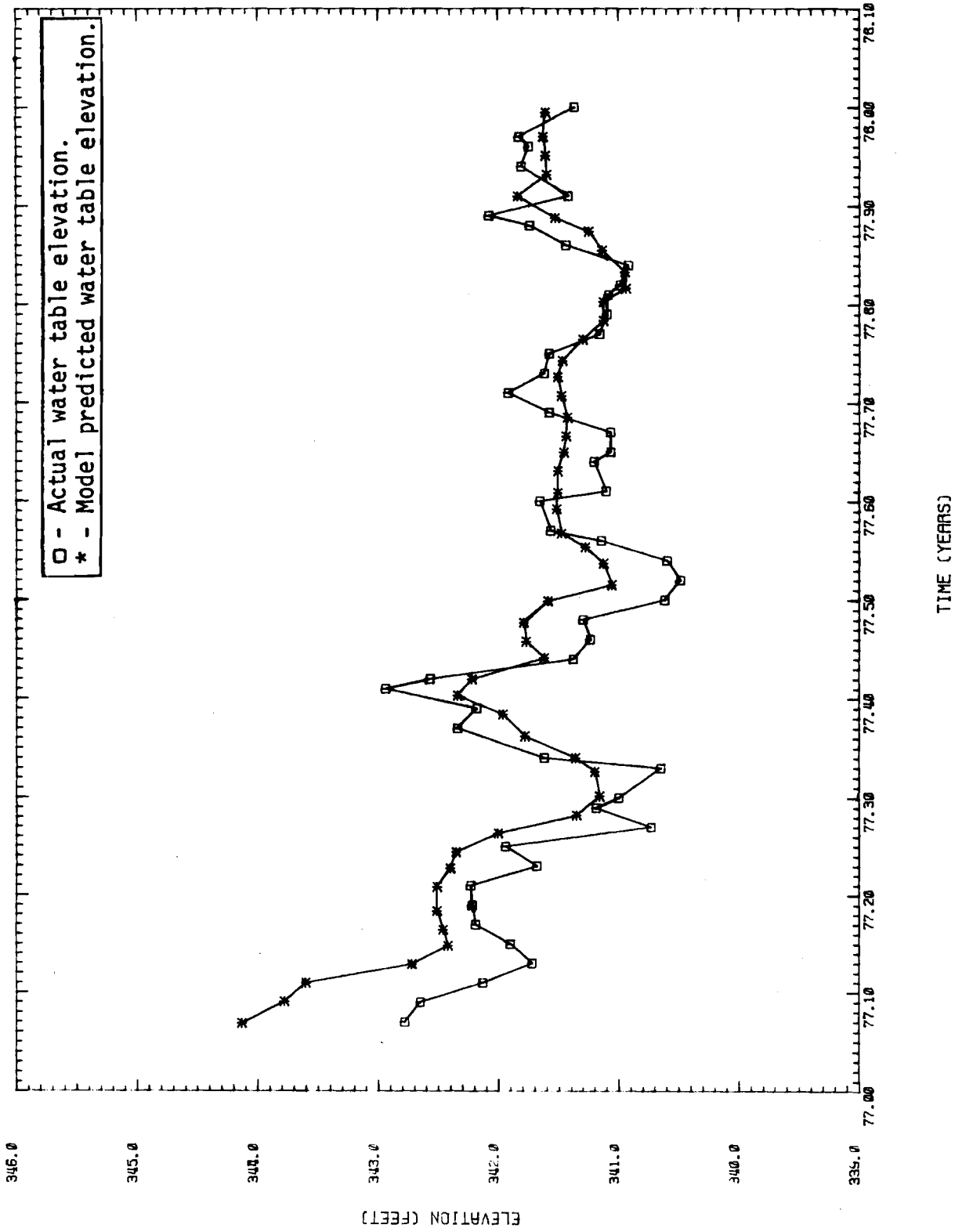


TIME (YEARS)

TIME = 15:20:00 DATE = 25-JAN-79

FIGURE A.27.

WELL NAME = 399-E14 FILE NAME = HYGR.328

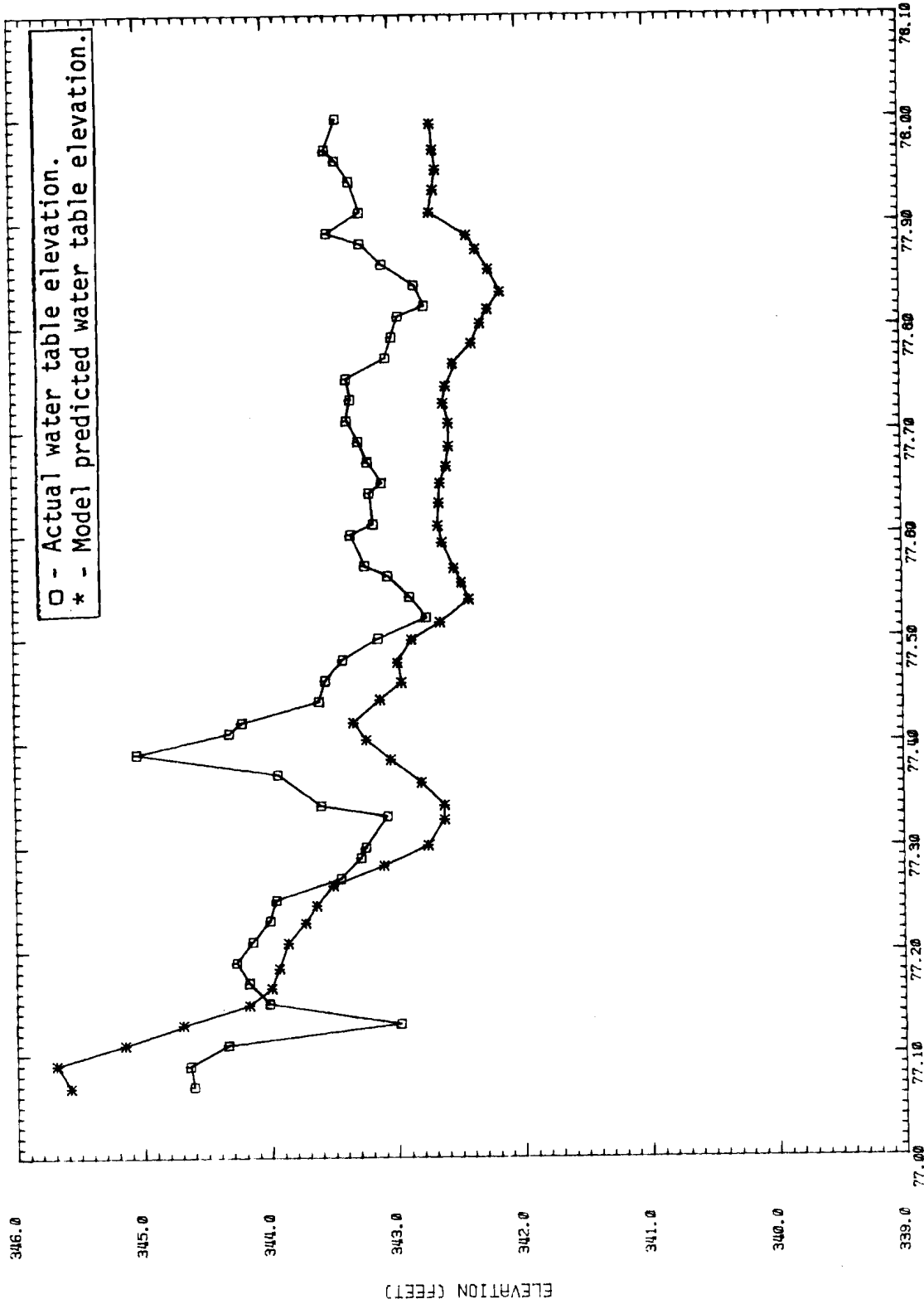


TIME= 15:24:26 DATE= 25-JUN-79

TIME (YEARS)

FIGURE A.28.

WELL NAME = 399-E13 FILE NAME = HYGR.329

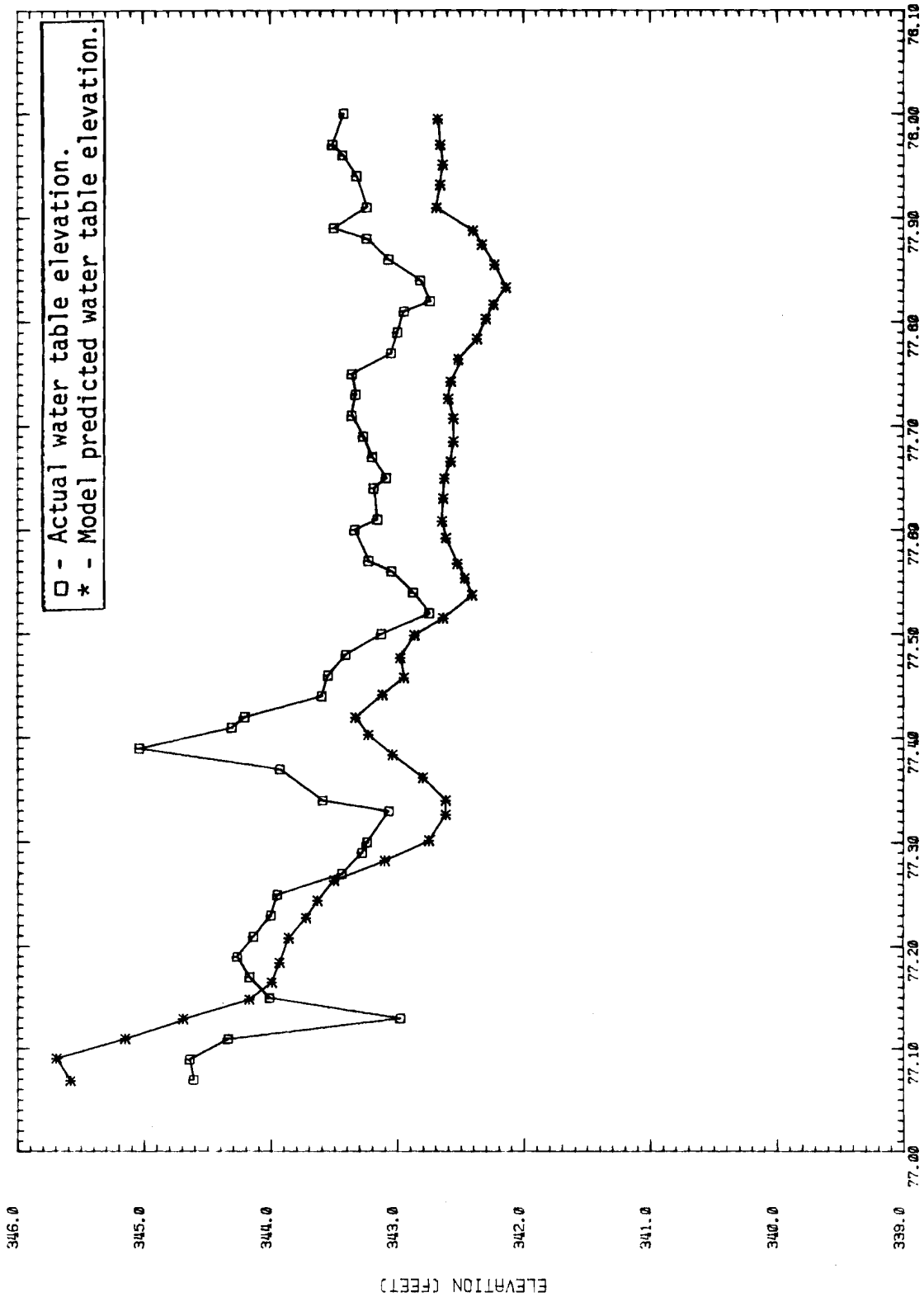


TIME (YEARS)

TIME = 15:28:01 DATE = 25-JAN-79

FIGURE A.29.

WELL NAME = 399-E13 FILE NAME = HYGR.329



TIME (YEARS)

TIME = 15:28:01 DATE = 25-JAN-79

FIGURE A.29.

DISTRIBUTION

No. of
Copies

No. of
Copies

OFFSITE

	A.A. Churm DOE Chicago Patent Group 9800 South Cass Avenue Argonne, IL 60439	4	G. Dix DOE Division of Operational and Environmental Safety Washington, DC 20545
27	<u>DOE Technical Information Center</u> D.H. Slade DOE Division of Biomedical and Environmental Research Washington, DC 20545		A.A. Schoen DOE Division of Operational and Environmental Safety Washington, DC 20545
2	G.W. Cunningham DOE Div. of Waste Management, Production & Reprocessing Washington, DC 20545		G. Facer DOE Div. of Military Applications Washington, DC 20545
	R.H. Engleken NRC Directorate of Regional Operations, Region V 1990 N. California Blvd., Suite 202 Walnut Creek, CA 94596		W.J. Larkin DOE Nevada Operations Office Office of Safety P.O. Box 14100 Las Vegas, NV 89114
	J.D. Griffith Asst. Dir. of Reactor Safety DOE Div. of Reactor Develop- ment and Technology Washington, DC 20545	5	E. Cowan Environmental Protection Agency Region X Seattle, WA 98101
	R.E. Tiller DOE Idaho Operations Operational Safety Division Idaho Falls, ID 83401		H.S. Jordon Los Alamos Scientific Laboratory Los Alamos, NM 87544
	C. Sherman DOE Headquarters Library Mail Station G-043 Washington, DC 20545		L.B. Day, Director Oregon State Department of Environmental Quality 1234 SW Morrison Portland, OR 97205
			G. Toombs Oregon State Health Division P.O. Box 231 Portland, OR 97207

No. of
Copies

M.W. Parratt
Oregon State Health Division
P.O. Box 231
Portland, OR 97207

R.R. Mooney
Washington State Department
of Social & Health Services
1514 Smith Tower
Seattle, WA 98104

R.C. Will
Washington State Department
of Social & Health Services
P.O. Box 1788, MS 56-1
Olympia, WA 98504

W.G. Hallauer
Washington State Department
of Ecology
Olympia, WA 98504

J.C. Ebert
U.S. Geological Survey
1201 Pacific Ave., Suite 600
Tacoma, WA 98402

V.E. Michael
Benton-Franklin Health Center
Pasco, WA 99301

D.D. Tillson
Washington Public Power
Supply System
3000 George Washington Way
Richland, WA 99352

City of Richland
Water and Sewer Department
505 Swift Blvd.
Richland, WA 99352

Battelle Memorial Institute
Office of Nuclear Waste Isolation
Attn: Beverly Rawles
505 King Avenue
Columbus, Ohio 43201

No. of
Copies

R. H. Poirier
Battelle Memorial Institute
505 King Avenue
Columbus, OH 43201

R.C. Scott
EPA Office of Water Programs
760 Market Street
San Francisco, CA 94102

M.O. Fretwell
U.S. Geological Survey
345 Middlefield Rd.
Menlo Park, CA 94025

J.B. Robertson
U.S. Geological Survey
345 Middlefield Rd.
Menlo Park, CA 94025

R.D. Paris
Oregon State Health Division
1400 S.W. Fifth Avenue
Portland, OR 97201

ONSITE

16 DOE Richland Operations
Office

O.J. Elgert (2)
D.R. Elle (5)
R.L. Ferguson
H.E. Ransom
R.E. Gerton
M.W. Tiernan
M.G. White (5)

No. of
Copies

No. of
Copies

ONSITE

55 Pacific Northwest Laboratory

6 Rockwell Hanford Operations

R.C. Arnett
D.J. Brown
F.A. Spane
J.V. Panesko
W.H. Price
RHO File

G.E. Backman
P.J. Blumer
F.W. Bond (5)
P.E. Bramson
R.E. Brown
D.B. Cearlock
C.R. Cole
J.P. Corley
P.A. Eddy (5)
J.R. Eliason
E.L. Hilty
J.R. Houston
H.V. Larson
J.W. Lindberg (5)
V.L. McGhan
T.J. McLaughlin
D.A. Myers (5)
R.W. Nelson
S.J. Phillips
J.R. Raymond
J. Sobotka
C.M. Unruh
J.F. Washburn (5)
Technical Information (5)
Publishing Coordination (2)
Water and Land Resources
Library (5)
Ro

2 Hanford Environmental Health
Foundation

L.J. Maas
B.D. Reinert

4 United Nuclear Industries, Inc.

T.E. Dabrowski
E.A. Weakley (2)
UNI File

7 Westinghouse Hanford Company

R.O. Budd
G. Carpenter
D. Gray
R.B. Hall (2)
L.J. Lucas
K.G. Togode